ABSTRACT

RASTOGI, VINAYAK. Microdroplet Engineering for Microbioassay and Synthesis of Functional Structured Porous Particles. (Under the direction of Dr. Orlin D. Velev).

We present methods where sessile or suspended microdroplets are used to develop applications in the areas of bio-detection, photonics, drug delivery and catalysis. The first technique we report is for droplet-on-a-chip microbioassays. The assays are performed in droplet micro-containers suspended on the surface of high density fluorinated oil and are based on the process of agglutination of antibody-coated particles. Droplet microbioassays for the detection of Ricin were designed and their performance was compared to the standard handheld field assays. These droplet microbioassays were found to be 10 times more sensitive in terms of analyte concentration while requiring 100 times smaller volumes. We developed a model for the agglutination kinetics and mass transfer processes inside the droplets, which correlates well with the experimental data.

The second technique that we developed uses droplet templates dispensed on superhydrophobic substrates for the fabrication of a new class of three dimensional hierarchical microsphere assemblies. The technique is termed Dry Self Assembly (DSA) since the fabricated supraparticles are easily detached from the substrate and collected unlike methods where assembled structures are suspended in liquid environment. The sessile droplet templates cast the final supraparticles into light diffracting near-spherical assemblies. When illuminated with a collimated beam of light, the structures exhibit unique ring shaped color diffraction patterns on their surface. The experimental observations for the angular

position and wavelength corresponding to a spot on the rings are interpreted using a surface diffraction grating model.

We also tailored the DSA method to produce both shape-anisotropic and composition-anisotropic supraparticles. The shape anisotropy was demonstrated by fabricating "doughnut" assemblies using droplets of both pure silica suspensions and silica mixed with gold nanoparticles. The composition anisotropy was realized by redistribution of magnetic nanoparticles in droplets containing mixtures of latex and magnetic particle suspensions. The redistribution is dictated by the pattern of magnetic field to which the droplet templates are introduced during drying. We developed new types of patchy magnetic particles that can find application in targeted drug delivery. The latex matrix can be infused with a drug and the magnetic patch(es) facilitate remote manipulation of the carrier. A new microfluidic chip was developed for the in-vitro characterization of drug/material release rate from the porous latex network in a live environment. The release rate of dye (drug simulant) from the porous supports is quantified and interpreted on the basis of diffusion/dissolution based mass transfer models. The technique has the potential to perform simultaneous screening of multiple samples and replace the conventional bulk laboratory setup needed for determining the release profiles in drug development process.

Microdroplet Engineering for Microbioassay and Synthesis of Functional Structured Porous Particles

by
Vinayak Rastogi

A dissertation submitted to the Graduate Faculty of
North Carolina State University
in partial fulfillment of the
requirements for the degree of
Doctor of Philosophy

Chemical Engineering

Raleigh, North Carolina

2010

APPROVED BY:

_____	_____
Peter K. Kilpatrick	Jan Genzer
_____	_____
Glen M. Walker	Orlin D. Velev Chair of Advisory Committee

DEDICATION

this dissertation is dedicated to

my parents Urmila & Vinod Kumar Rastogi,

my brother Raghav

and

my fiancé Monica,

for their endless love, encouragement, support, and sacrifices

BIOGRAPHY

Vinayak Rastogi was born to Urmila & Vinod Kumar Rastogi on 20 October 1978 in the city of Moradabad, 100 KM southeast of INDIA's capital New Delhi. Moradabad is famous for its brassware and metalwork all over the world. He was raised in Moradabad and graduated from Parker College with high school diploma in 1997. His father Vinod (agriculture and spice businessman) and mother Urmila (a vocal music teacher) always encouraged him to follow his own interests and pursue a career in science and engineering. Always performing at the top of his class, Vinayak worked hard with dedication and determination to compete successfully with more than hundred thousand in the prestigious Joint Entrance Examination held by the Indian Institute of Technology (IIT). He joined the Chemical Engineering program at IIT Roorkee and received his Bachelor of Technology in May 2002. After his graduation he gained two valuable years of professional experience at Infosys Technologies Limited before beginning his doctoral studies in the area of 'Colloidal Science & Nanoscale Engineering' under the guidance of Professor Orlin Velev at North Carolina State University in August 2004.

ACKNOWLEDGMENTS

The journey of my graduate research would not have been successful without the support, guidance, affection and love of all the individuals who have influenced my life in one way or another. First and foremost I would like to thank my parents Urmila and Vinod Kumar Rastogi, for their unconditional love and support. They have always encouraged me to pursue my interests in science and engineering and provided me with all possible resources to excel in those endeavors. I am also grateful to my brother Raghav who has always been my best friend and provided me with moral support and enthusiasm. I will always owe my fiancé and sweetheart Monica for giving me the much needed comforting hand and gentle nudges to successfully write my thesis. I am also thankful to my sister Kiran Mathur and my brother-in-law Vivek Mathur for being my support system.

I thank Professors Peter K. Kilpatrick, Jan Genzer and Glen M. Walker for serving on my dissertation committee. I am thankful to Dr. Krassimir P. Velikov, Dr. Antonio A. García and Dr. Manuel Marquez for their collaboration, guidance and support throughout my research. I want to thank Professor Khan for advising me in making the right decision to join NC State for my graduate studies. I am also thankful to the CBE faculty members, who have let me use their lab facilities and equipment during my research. All the staff members of the CBE department have in one way or another helped me during my five years here at State and I thank every one of them for that.

I greatly value the company of all former and current members of Velev Research Group. The research publications, conference presentations I made during my graduate studies would not have been as good without their valuable feedback. All of them have been very helpful in and outside the lab and I enjoyed every bit of our lunches, dinners and outings together. I especially want to thank Dr. Brian G. Prevo, Dr. Ketan H. Bhatt, Dr. Bridgette M. Budhlall, Dr. Olivier J. Cayre, Dr. Sejong Kim, Dr. Stoyan Smoukov, Dr. Shalini Gupta, and Dr. Suk Tai Chang for their advice, numerous research discussions and all the laughter moments. I especially want to thank my buddy Dr. Suk Tai Chang for his assistance during my first year in the lab and all late night company and breaks in between work. I am also thankful to Sumit Gangwal for sharing his research experiences and providing with valuable feedbacks. I like to express my thanks to Ahmet Burak Uçar and Hyung-Jun Koo for their jokes and fun times in the lab. I also owe a debt to my friends Deepankar Nayak, Dr. Amit K. Sahu, Roja Ergun, Dr. Tushar R. Mahale, Dr. Rakesh Ranjan, Nathaniel A. Cain, Dr. Prabhat Kumar, Dr. Prashant Mudgal, Kiran Kumar Goli, Shivaram Keelara, Aswini Kumar Singh Jasrotia, Shashank Shekhar, Rameshwar Yadav and Joshua Manasco for their constant support throughout my good and bad days.

Finally, but most importantly, I would like to express my gratitude to my advisor Dr. Orlin D. Velev for being an exceptional mentor and a great boss. His work ethic and his amazing ability to come up with ingenious ideas have been a real source of inspiration to me. His ever enthusiastic nature has provided me with immense energy during my graduate

research. He has groomed me beyond the realms of scientific research into becoming a professional. For all his efforts I thank him and wish him the very best for his future career.

TABLE OF CONTENTS

List of Figures……ix

List of Tables……xiii

Chapter 1. Introduction and Dissertation Goals 1

1.1 Introduction 2
1.2. Droplet Microfluidics 4
1.2.1. Droplet Generation and Manipulation 5
1.3. Droplets as sites for biodetection 9
1.3.1. Dielectrophoresis 9
1.3.2. Conventional Immunoassays Methods 11
1.4. Droplets as templates for hierarchical materials assembly 17
1.5. Layout of this dissertation 19
1.6. References 21

Chapter 2. Development and Evaluation of Realistic Microbioassays in Freely Suspended Droplets on a Chip 35

2.1 Introduction 36
2.1.1. Principles of the immunological bioassays in microdroplets 40
2.1.2 Formats of immunoagglutination bioassays studied 41
2.2. Experimental Procedures 43
2.2.1. Materials 43
2.2.2. Experimental Setup 44
2.2.3. Methodolgy 45
2.3. Results and Discussion 47
2.3.1. Gold Only Agglutination Microbioassay (GOAgg) 47
2.3.2. Gold and Latex Agglutination Microbioassay (GLAgg) 53
2.3.3. Gold Only Agglutination Microbioassay (GOAgg) with Ricin Antibody 55
2.3.4. Factors affecting evaporation rate of droplets. 57
2.4. Model of Particle Agglutination Dynamics 60
2.5. Concluding remarks 68
2.6. Acknowledgements 70
2.7. References 71

Chapter 3. Synthesis of Light-Diffracting Assemblies from Microspheres and Nanoparticles in Droplets on a Superhydrophobic Surface 75

3.1 Introduction 76
3.2. Experimental Section 77
3.3. Results and Discussion 79
3.4. Conclusions 91
3.5. Acknowledgements 93
3.6. References 94

Chapter 4. Anisotropic Particle Synthesis inside Droplet Templates on Superhydrophobic Surface 98

4.1 Introduction 99
4.2. Experimental Section 100
4.3. Results and Discussion 103
4.4. Conclusions 114
4.5. Acknowledgements 115
4.6. References 116

Chapter 5. Microfluidic Characterization of Sustained Release from Porous Supraparticles 119

5.1 Introduction 120
5.2. Experimental Section 122
5.2.1. Fabrication of 'Dye Pellet' and 'Dye Infused Latex Supraparticle' 123
5.2.2. Fabrication of microfluidic channel network for release monitoring 123
5.2.3. Dye intensity measurements 124
5.3. Results and Discussion 125
5.4. Conclusions 136
5.5. Acknowledgements 137
5.6. References 138

Chapter 6. Summary and Outlook 142

6.1 Summary 143
6.2 Outlook 145

LIST OF FIGURES

Figure 1.1. (a) Formation of water-in-oil droplets at a T-junction. (b) Flow focusing channel geometry. (c) Microcapillary geometry for generating double emulsions from coaxial jets. (d) Droplet formation in a coplanar DEP electrode setting. (e) Droplet formation from an on chip reservoir by electrowetting effect. 6

Figure 1.2. (a) Actuation of a droplet of Electrowetting based chip. (b) DEP manipulation of aqueous suspension droplets of microparticles freely suspended on the surface of high density oil. (c) Mixing in droplets enhanced by introducing a scheme of smooth and sharp turns in the channels. (d) Sequential fission of droplets in a T-junction series. (e) Electric field assisted fusion of droplets. (f) Setup for droplet generation from two incoming streams with ratio control by changing the flow rates. 8

Figure 1.3. Dielectrophoretic force is induced by the presence of an electric field gradient ∇E^2. The particle is either attracted to or repelled from the high field intensity region depending on the sign of Re $|K(\omega)|$ 10

Figure 1.4. Conventional latex agglutination test and techniques to determine aggregation state 14

Figure 1.5. Schematics of lateral flow device for immunoagglutination test 16

Figure 1.6. (a, d) Schematics for self assembly of microparticles at the two phase interface and in bulk of the droplets. Anisotropic and functional supraparticle synthesis (b, c) around emulsion droplet templates and (e, f) inside freely suspended droplet templates. (g, h) Self assembly inside droplets templates dispensed on solid surface..... 18

Figure 2.1. (a) Experimental setup with evaporating droplets on a DEP chip. (b) Schematics and optical micrograph from above of evaporating droplet without antigen. (c) Schematics and micrograph of gold nanoparticle aggregation in a droplet containing antigen. 39

Figure 2.2. Schematics of the immunorecognition and agglutination processes taking place in the two microbioassay formats studied. 41

Figure 2.3. Optical micrographs of droplets in a Gold Only Agglutination (GOAgg) assay. 1.0 μg/mL antigen concentration shows the least amount of gold nanoparticles collection on top for 30 min incubation time. The white areas in the top of the droplets are the dense latex particle phases. The gold nanoparticles reaching the top are easily observed because of their intensively red color. 48

Figure 2.4. Scanning electron micrograph showing cluster of aggregated gold nanoparticles trapped in the interstices between latex particles in the bottom portion of droplet cap. 50

Figure 2.5. Optical micrographs of GOAgg microbioassay for varying incubation times (vertical direction) and varying concentration (horizontal direction)..... 51

Figure 2.6. Optical micrographs of droplets with GLAgg assays at increasing antigen concentrations. 54

Figure 2.7. Comparison between optical micrographs of droplet GOAgg assay with Ricin as an antigen (top) and conventional Hand Held Assay for Ricin. 30 min incubation. 56

Figure 2.8. Micrographs of typical droplets, illustrating the effect of presence of gold nanoparticles and Tween-20 on the drying rate of droplets. (a) Latex only, (b) Latex and gold nanoparticles, (c) Latex and Tween-20, (d) Latex, gold nanoparticles and Tween-20. All droplets were allowed to evaporate for 65 minutes. 58

Figure 2.9. Droplet diameter variation with evaporation time for droplets containing different ingredients. 59

Figure 2.10. Schematics of two step model for aggregation of gold nanoparticles in the presence of antigen. 63

Figure 2.11. Concentration profiles of different types of aggregates relative to initial gold nanoparticle concentration (equations 2.10 and 2.13). 67

Figure 3.1. Schematics of the process for making spherical colloidal assemblies on superhydrophobic surface, (a) latex opal ball and (b) latex and gold opal ball. The inset is a SEM image displaying hexagonal close-packed structure of latex spheres inside an opal ball from 540 nm latex..... 81

Figure 3.2. Timeline of formation of spherical opal assemblies on superhydrophobic Si-NW substrate. (a) latex, (b) latex and 0.1 wt% Au nanoparticles, and (c) latex and 1.0 wt% Au nanoparticles. The latex microsphere diameter is 540 nm in each droplet. The Au nanoparticle diameter is 22 nm. Scale bar is 500 μm. 83

Figure 3.3. Scanning electron micrograph of the surface of a supraparticle made from a mixture of 540 nm latex and 22 nm gold nanoparticles. Dark spheres are latex and bright regions are clusters of gold nanoparticles. Scale bar is 5 μm. The inset is a SEM of the whole supraparticle with patches of gold scattered all over the surface. The scale bar in the inset is 200 μm. 83

Figure 3.4. Optical micrographs of latex opal balls made of microspheres with varying sizes taken under identical illumination conditions..... 85

Figure 3.5. Optical micrographs of latex and gold nanoparticle opal balls containing microspheres of varying sizes as in Fig. 3.4. 85

Figure 3.6. (a) Colored rings in the top view of a 540 nm latex opal ball; (b) Side view schematics of the angles used in the theoretical calculation of wavelength for a particular color ring..... 86

Figure 3.7. Normalized path difference versus the normalized wavelength for colored rings patterns in latex opal balls and latex/gold opal balls. 90

Figure 4.1. (a) Schematic of supraparticle formation by evaporating a droplet containing suspension of silica and gold nanoparticles. (b) Top and angled view of "golden doughnut" supraparticles fabricated from a droplet containing 330 nm diameter silica and 22 nm gold particles. The scale bars in both images correspond to 500 μm. 105

Figure 4.2. Evolution of dimensions recorded for a drying a droplet with 10% initial volume fraction of 330 nm diameter silica particles. Normalized diameter was calculated using the original dimension values at the time of dispensing the droplet. The parameters shown are as follows: B is the droplet base, R is meridian radius and H is the height. The inset shows an overlay of experimental images for the side-view profile of a drying droplet with silica particles over time..... 107

Figure 4.3. Top view optical micrographs of silica supraparticles fabricated from droplets with varying initial particle volume fractions. The scale bars in all images are 500 μm. ... 109

Figure 4.4. Schematics of the assembly configuration, optical micrographs and simulation patterns of applied external magnetic fields for (a) Single patch magnetic supraparticles, (b) bi-patch magnetic supraparticles, and (c) tri-patch or so-called "Mickey Mouse" magnetic supraparticles. The scale bars are 500 μm in length. The magnetic simulation pattern is drawn to scale; one square on the grid represents an area of 1 mm^2. 111

Figure 4.5. (a) Scanning electron micrograph on the surface of a supraparticle illustrating the junction of magnetic nanoparticle rich patch (right) with the bulk constituting of close packed latex microsphere arrays (left). (b) Close-packed array of multiple single-patch supraparticles on solid surface assembled by using remote magnetic manipulation..... 112

Figure 5.1. Schematics (not drawn to scale) of the formation process of DIL-Supraparticle and D-Pellet. The optical micrographs on the right show the side profile of D-Supraparticle and top profile of D-Pellet. All scale bars are 500 μm. 127

Figure 5.2. Schematic representation of soft lithography based microfluidic channel network employed to characterize the release rate of dye from porous microsphere network matrices. 127

Figure 5.3. Snapshots of microfluidic network taken during the dye release characterization experiments. The first and second series shows the comparison of dye dissolution from the D-Pellet and DIL-Supraparticle respectively. 128

Figure 5.4. Release rate of dye measured for D-Pellet and DIL-Supraparticle in the novel microfluidic characterization system. 129

Figure 5.5. Schematics of the system parameters and streamline flow around the spherical particle inside the loading chamber. 131

Figure 5.6. Comparison between dye release rates from dye pellet and the predictions of theoretical model. 133

Figure 5.7. Comparison between dye release rates from DIL-Supraparticle and the predictions of the model. 135

LIST OF TABLES

Table 2.1	Summary comparison between HHAs and droplet based microbioassays	57
Table 2.2	Comparison between experimental results and theoretical values for droplet microbioassays	68
Table 2.3	List of constants and variables used in the theoretical calculations	68

Chapter 1.

Introduction and Dissertation Goals

1.1 Introduction

Microfluidics is the study and development of systems that deal with control, manipulation and processing of fluids at micron and submicron volume scales to perform large scale laboratory operations in an efficient and high throughput fashion. Performing laboratory operations on a small scale has drawn much attention from researchers in the last couple of decades due to the inherent fundamental features that accompany system miniaturization. These features include processing and handling miniscule volumes of fluids, increased analytical power as compared to conventional laboratory methods, reduced infrastructural footprint, inexpensive fabrication and setup procedures and ability to simultaneously process multiple samples.

Small sample volumes reduce the time needed for synthesis or analysis of a sample. This has led to the miniaturization of laboratory operations to micro and nano scale devices known as lab-on-a-chip or micro total analysis systems (μ-TAS) where multiple laboratory processes can be performed efficiently.[1-7] μ-TAS devices are portable, easy to operate and reduce the reagent costs and amount of waste produced.[2,8,9] μ-TAS can be integrated with other microanalysis systems, thus creating immense potential for automated operations, which can be used in biochemical detection[10-14], drug discovery and design[15-17], proteomic and genomic analysis[18-20], clinical and forensic applications[9,21-23], materials synthesis[24-26]. Micro devices are cost effective and prevent the need for big investments in setting up laboratories with large sophisticated equipment.

Microfluidic devices and methods can be also used for manipulation of colloidal particles,[27-29] fluids,[5,30-33] and biomolecules.[34-37] The development of microscale devices gives rise to several challenges such as design, fabrication and integration into automated systems. Reduction of the length scales of devices makes the surface forces more dominant in comparison to the volume forces. Hence, the induction of flow in microchannels calls for the usage of non conventional techniques. Several methods such as pressure gradients and electroosmosis[37] have been used to induce fluid flow in microchannels.[38-40] Alternatively, application of an electric field can be used to manipulate colloidal particles, fluids or biomolecules in suspension form. Potentials of small magnitude can produce high electric field intensity through usage of microscale electrodes [1,41]. Electrically induced forces like dielectrophoresis (DEP)[42-45] can be exploited to manipulate particles suspended in the media. During electrophoretic motion of particles, forces like electrohydrodynamics[46] and gravity also act on the particles which need to be considered while calculating the net force.

The primary focus of my graduate research is to explore, understand and exploit the fundamentals of microdroplet engineering for the development of new biodetection techniques and synthesis of hierarchical anisotropic porous assemblies. This chapter overviews the field of droplet microfluidics and presents a comprehensive outlook of the recent developments in droplet based research and applications. Typically most lab-on-a-chip systems are operated under single phase fluid flow conditions wherein the dispersion of reacting volumes takes place due to the velocity profile variation from channel center towards walls[32]. Such behavior leads to varying residence time distributions for different

fluid volume elements, thus causing changes in product distribution and yield efficiency of a reaction run[47]. Close channel microfluidic chips also poses drawbacks and challenges including high pressure heads; undesired channel clogging due to adhesion of proteins, particles or cells[7,24] and long result read out times. Research fields like bio-defense also call for extremely economical usage of limited sample volumes which is not always possible with conventional microfluidic techniques.

1.2. Droplet Microfluidics

Compartmentalization of fluid elements in the form of discrete droplets provides alternative to overcome or bypass a few problem occurring in closed channel microfluidics[5,24,48-51]. Droplets are generated by the use of immiscible phases, which avoids lateral dispersion of reactants. Restricting the reactive elements within droplet containers works as an effective way of eliminating differences in residence times and provides uniformity in incubation times for simultaneous processing and analysis of multiple biological samples.[52] The high surface area to volume ratio for microscale droplets facilitates immense reduction of time scales required for heat and mass transfer thus aiding in rapid quantitative result output. Droplet based microfluidics provides precise control in terms of generating monodisperse droplet microreactors, which can be individually processed for transportation, mixing and analysis[53,54] of reagents.

Multiple identical droplets can be formed on a single microfluidic chip in a short time wherein parallel processing of reactants and experimentation can be done to efficiently

generate large data sets. Such versatility of droplet systems extends the potential for scalability and handling high throughput requirements as compared to continuous flow systems[55]. Researchers have exploited droplet based microfluidic systems to develop a variety of applications like fabricating anisotropic particles[56-63], double emulsions[64,65], nanoparticle synthesis[66], light diffracting supraparticles[67], photonic crystals[68] and biodetection[69-72].

1.2.1. Droplet Generation and Manipulation

The requirements of the applications and system geometry define the method to be used for generation and manipulation of droplets[51,73] in microdevices[74]. The two most common methods used to generate droplets in bulk within microfluidic channels are T-junction[75-80] and flow focusing geometries[81-85]. Thorsen et al. in 2001 demonstrated the continuous formation of water droplets at the T-junction of two microchannels containing water and oil surfactant mixture[80]. The droplets were formed by injecting the dispersed phase (aqueous) stream perpendicular to continuous phase (oil) stream (Fig 1.1(a)). The droplet formation results from induced shear forces at the interface between two phases. A T-junction setup has been employed for continuous synthesis of polymer particles by solidifying the droplets, resulting in highly monodisperse[84,86], anisotropic[58,87,88] and mesoporous[89] microparticles.

In the flow focusing method the dispersed phase flows through the central channel and continuous phase in two outside channels (Fig 1.1(b)). The outer fluid applies pressure

and shear on the inner fluid which then breaks into droplets at or beyond the downstream narrow orifice at a position defined by the capillary number.[91] Weitz and coworkers have created monodisperse double or multiple emulsions using the flow focusing technique by interleaved glass capillary arrangements and demonstrated uniform microencapsulations, functional microgels, and nanoparticle colloidosomes with selective permeability (Fig 1.1(c)).[65,92,93] Ismagilov et al. have demonstrated crystallization of proteins in nano-droplets transported inside glass capillaries.[94] Such methods provide the flexibility of precise control over droplet size by changing the fluid flow rates and channel geometry.

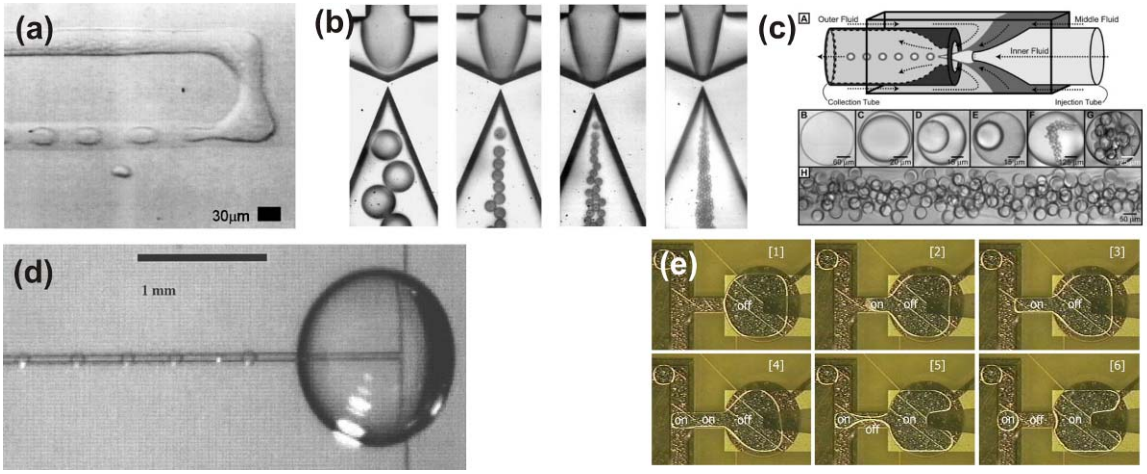

Figure 1.1. (a) Formation of water-in-oil droplets at a T-junction.[80] (b) Flow focusing channel geometry.[85] (c) Microcapillary geometry for generating double emulsions from coaxial jets.[65] (d) Droplet formation in a coplanar DEP electrode setting.[90] (e) Droplet formation from an on chip reservoir by electrowetting effect.[72]

Selective generation and manipulation of droplets at the micro and nanoscale can be done in planar surface-based systems by two electric field based methods, namely

dielectrophoresis (DEP) and electro wetting on dielectric (EWOD). These kinds of systems eliminate the need for external pumps and channels and at the same time allow independent control of droplets. DEP is used to generate uniform droplets by drawing a long stream of fluid from the parent reservoir droplet and then allowing it to break into smaller droplets due to capillary instability (Fig 1.1(d)). The drawing of rivulet from the parent droplet is based on the phenomenon that fluids which are more polarizable than the surrounding media are drawn into the high electric field region created by a system of coplanar electrodes.[44,90,95-97]

EWOD, on the other hand, is based on the principle of using an electric field to alter the interfacial energy and thus the contact angle between the fluid and the surface with which it is in contact[98-102] Srinivasan et al. demonstrate an integrated and reconfigurable lab-on-a-chip device where droplets are used as containers for performing bioassays on human physiological fluids. The droplets are generated and manipulated using the EWOD effect (Fig 1.1(e), Fig 1.2(a)).[72] Biodetection on a chip requires minimal contact of droplets containing sample with solid surfaces. To meet this criterion Velev et al. developed a novel DEP-based lab-on-a-chip system (Fig 1.2(b)) wherein freely suspended droplets can be manipulated by applying AC electric fields through electrode arrays submerged under high density fluorinated oil.[7,56] Mixing of samples has been performed by fusion of droplets on programmable EWOD based chips[72,103] or transportation through winding channels (Fig 1.2(c)).[104] Division of a droplet into one or more daughter droplets can be executed with a T-junction channel network (Fig 1.2(d)).[105,106] Fusion of droplets of different materials has also been demonstrated on a T-junction chip (Fig 1.2(e, f)).

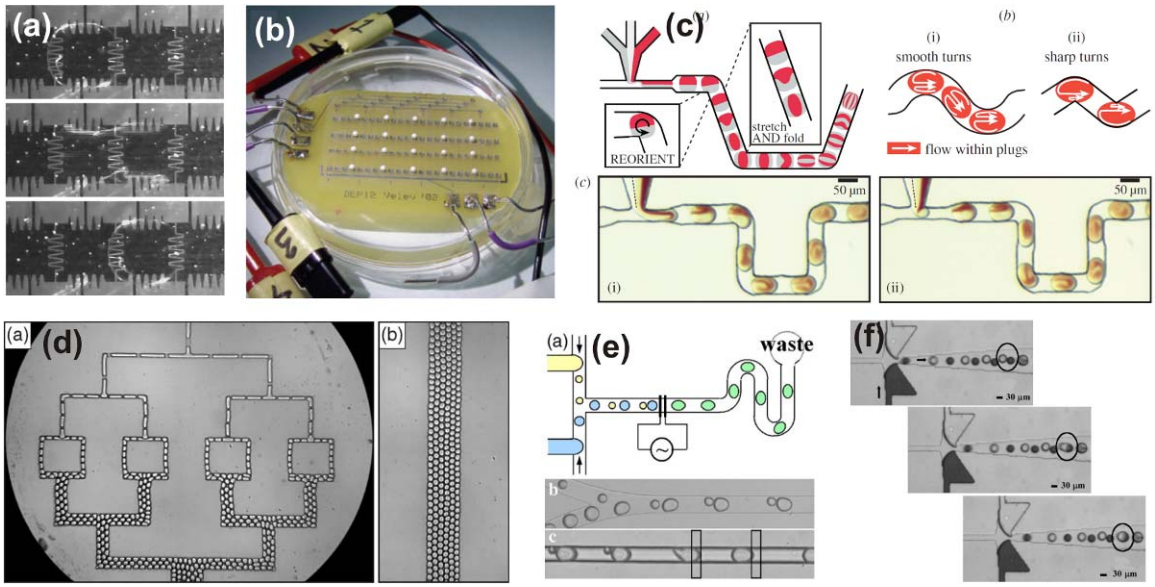

Figure 1.2. (a) Actuation of a droplet of Electrowetting based chip.[103] (b) DEP manipulation of aqueous suspension droplets of microparticles freely suspended on the surface of high density oil.[56] (c) Mixing in droplets enhanced by introducing a scheme of smooth and sharp turns in the channels.[104] (d) Sequential fission of droplets in a T-junction series.[105] (e) Electric field assisted fusion of droplets.[107] (f) Setup for droplet generation from two incoming streams with ratio control by changing the flow rates.[106]

1.3. Droplets as sites for biodetection

Microdroplets have also been deployed as reactors for simultaneous execution of multiple reactions on a single chip.[35,73,108,109] Biodetection is a specific case of this application where one or all the reactants are biological entities. Performing biological reactions inside droplets separated by immiscible fluid environment allows easy isolation of reactants from the surrounding environment, thus avoiding contamination. Also the mixing of reactants is more convenient, no high liquid pressure is required and sample usage is minimized.[1,72,110,111] We use the DEP based droplet chip to perform biodetection in microliter size droplets. The following section explains the physical phenomena responsible for holding the freely suspended droplet containers in place while the microbioassays are performed. The next section explains the immunoagglutination principle on which conventional bioassays are based.

1.3.1. Dielectrophoresis

Dielectrophoresis is the term used to explain the motion of a particle in the presence of non-uniform electric field. When a polarizable particle is subjected to non-uniform electric field, a dipole is induced. The particle is attracted to or repelled from the region of high electric field intensity, depending on its polarizability compared to the medium (Fig 1). The DEP force does not depend on the polarity of electric field and is observed with alternating current fields (AC) as well as direct current fields (DC)[112]. In the AC electric field the particles exhibit a net displacement due to the non-zero time average of the

field[112,113]. Unlike DC field, use of AC field allows application of high electric field strength without creating electrolysis and electroosmotic flows. The time average DEP force (Fig. 1.3), F_{DEP}, is given by

$$F_{DEP} = 2\pi\varepsilon_m r^3 \,\mathrm{Re}\left|K(\omega)\right|\nabla E^2 \tag{1-1}$$

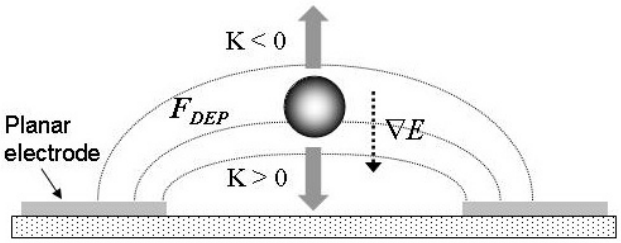

Figure 1.3. Dielectrophoretic force is induced by the presence of an electric field gradient ∇E^2. The particle is either attracted to or repelled from the high field intensity region depending on the sign of Re $|K(\omega)|$

where ε_m is the dielectric permittivity of the medium, r is the radius of the particle, E is the electric field intensity, and $K(\omega)$ is the Clausius-Mossotti factor, the particle's effective polarizability in media. The direction of the force on the particle depends on the real part of $K(\omega)$[114],

$$\mathrm{Re}\left|K(\omega)\right| = \frac{\varepsilon_p - \varepsilon_m}{\varepsilon_p + 2\varepsilon_m} + \frac{3(\varepsilon_m\sigma_p - \varepsilon_p\sigma_m)}{\tau_{MW}(\sigma_p + 2\sigma_m)^2(1 + \omega^2\tau_{MW}{}^2)} \tag{1-2}$$

where σ_m is the conductivity of the medium, ε_p and σ_p are the dielectric permittivity and the conductivity of the particle, ω is the applied field frequency, and τ_{MW} is the Maxwell-Wagner charge relaxation time

$$\tau_{MW} = (\varepsilon_p + \varepsilon_m)/(\sigma_p + 2\sigma_m) \quad (1\text{-}3)$$

Therefore, the direction in which the particle moves is not only determined by the properties of the particle and the medium but also the frequency of the applied field. For dielectric particles, the sign of the real part of $K(\omega)$ is changed at a crossover frequency of $\omega_c = (\tau_{MW})^{-1}$. When $\mathrm{Re}|K(\omega)| > 0$, the particle is attracted toward the electric field maxima (positive DEP). When $\mathrm{Re}|K(\omega)| < 0$, the force on the particle drives it toward the region of lower field (negative DEP).

Recently it has been shown that microwires can be assembled from a suspension of metallic nanoparticles[42,115,116] by DEP. The DEP force has also been applied to prepare colloidal crystals and induce the separation and concentration of dielectric particles[117-119]. Apart from this DEP has found many useful applications in biosensors[120], separation and manipulation of biological particles such as yeast cells, viruses, and DNA[121-123].

1.3.2. Conventional Immunoassays Methods

Last five decades have seen immense development in the immunoagglutination techniques[124,125] for detection and identification of biological molecules. Microfluidic devices have been commonly used[124,126-131] in conjunction with immunoagglutination

techniques for applications such as detection of proteins like toxins, immunoglobulin, and hormones present in blood samples, immunoassays[132], nucleic acid amplification tests, flow cytometry[133], clinical diagnostics and detection of chemical and biological agents.

The latex agglutination assay[134] is one of the popular methods to detect the presence of analyte (biological or other chemical species) in a sample (Fig. 1.4)[135]. It was first described in 1956 by Singer and Plotz[136] and applied to rheumatoid factor. In this case latex refers to aqueous dispersion of antibody-coated polymeric microspheres which aggregate in the presence of an analyte of interest. The polymer microspheres are usually composed of a large number of polystyrene molecules held together by van der Waals forces. The surface properties of the polystyrene spheres depend on the type of end group attached to each individual polystyrene molecule[137]. A large selection of end groups can be incorporated onto the surface of microspheres to covalently attach a specific protein and at the same time provide colloidal stability. The spheres are electrostatically stabilized in aqueous solution because of the surface charge imparted by the functional groups. Because of the hydrophobic nature of the constituent polymeric material, the particles easily adsorb more hydrophobic molecules like antibodies and act as a base for the immunoagglutination process.

Typical immunoagglutination assays use polystyrene microspheres with antibody molecules attached to their surfaces. The aqueous suspension of these microspheres is in turn mixed with a sample containing antigen molecules which is the analyte in immunological tests. Samples can be whole blood, serum, urine, etc. The antigen molecules

attach two antibody molecules situated on different microspheres and cause the agglutination of latex microspheres. The agglutination process can be used in several different modes depending on the functionalization of latex with antigen or antibody, to detect the analyte (antigen or an antibody, whichever is of interest), but each mode has its own application and limitations which is illustrated elsewhere[130]. Several different techniques such as nephelometry and spectrophotometry (Fig. 1.4) are employed to determine and quantify the aggregation state of the latex particles.

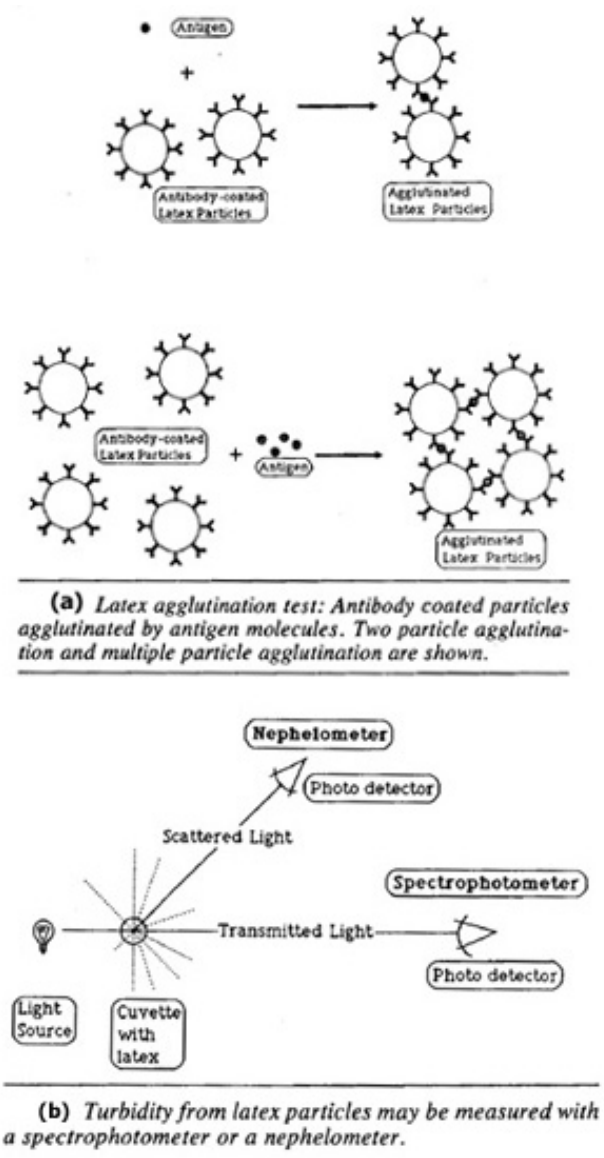

Figure 1.4. Conventional latex agglutination test and techniques to determine aggregation state[135]

One of the variations of immunoagglutination assays is the lateral flow device. These membrane based assays rely on immunochromatography principle[125,138-140]. These devices are commonly used to detect the presence of drugs of abuse, viruses and other agents of disease present in samples of blood, urine, hormones etc. The most common of these devices is the pregnancy test. A lateral flow device typically comprises of a porous membrane, usually nitrocellulose. The capture protein for the target analyte is immobilized onto the membrane. Once the sample is applied to the sample pad, the liquid migrates by capillary diffusion through the conjugate pad and re-hydrates the conjugate. Specific interaction between the conjugate and the analyte occurs, resulting in the formation of the complex. This complex proceeds to move onto the membrane and migrate towards the capture binding protein, where it becomes immobilized. The functioning of the device is shown in the Figure 1.5[141]. The process depends on the flow rate of the fluid through the membrane and typically takes 15-20 min for many commercial devices. The device requires at least 100 μL of antigen (or antibody) sample which is critical in areas such as biodefense where every drop of the sample is precious. This problem can be overcome using our DEP technique which requires less than a microliter of sample.

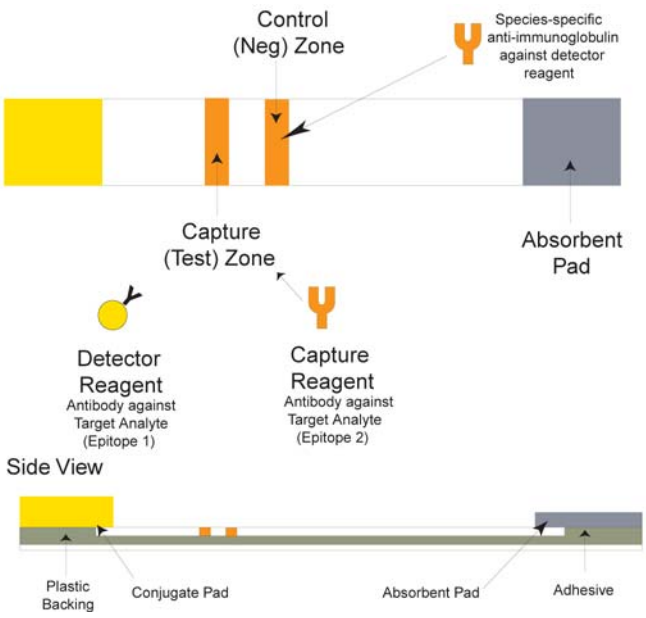

Figure 1.5. Schematics of lateral flow device for immunoagglutination test[141]

1.4. Droplets as templates for hierarchical materials assembly

Droplet engineering has emerged as a versatile tool for developing multiple microscale applications in the last two decades. The droplets also work as sites for fabrication of hierarchical and responsive materials which can further find applications in photonics, [84,86,87]microfluidics and sustained and targeted delivery of materials.[142] Emulsion droplets have been exploited as templates for fabricating three-dimensional shell like assemblies.[59,60,62,89,143-147] However, the initial aim for such processes was to use colloidal particles as an alternative to surface active agents in stabilizing emulsion droplets.[148] Velev et al. demonstrated the use of emulsion droplet as templates to fabricate hollow "supraparticles".[59,60,62] (Fig. 1.6 (a, b) Similar hollow microstructures ("colloidosomes") were fabricated by Weitz et al. where the interstitial porosity is easily controlled by changing the size of constituent colloidal particle stabilizers (Fig. 1.6 (c). Researchers have also exploited the droplets in microchannels as sites to design, synthesize and self assemble polymeric or Janus particles.[88,92,149]

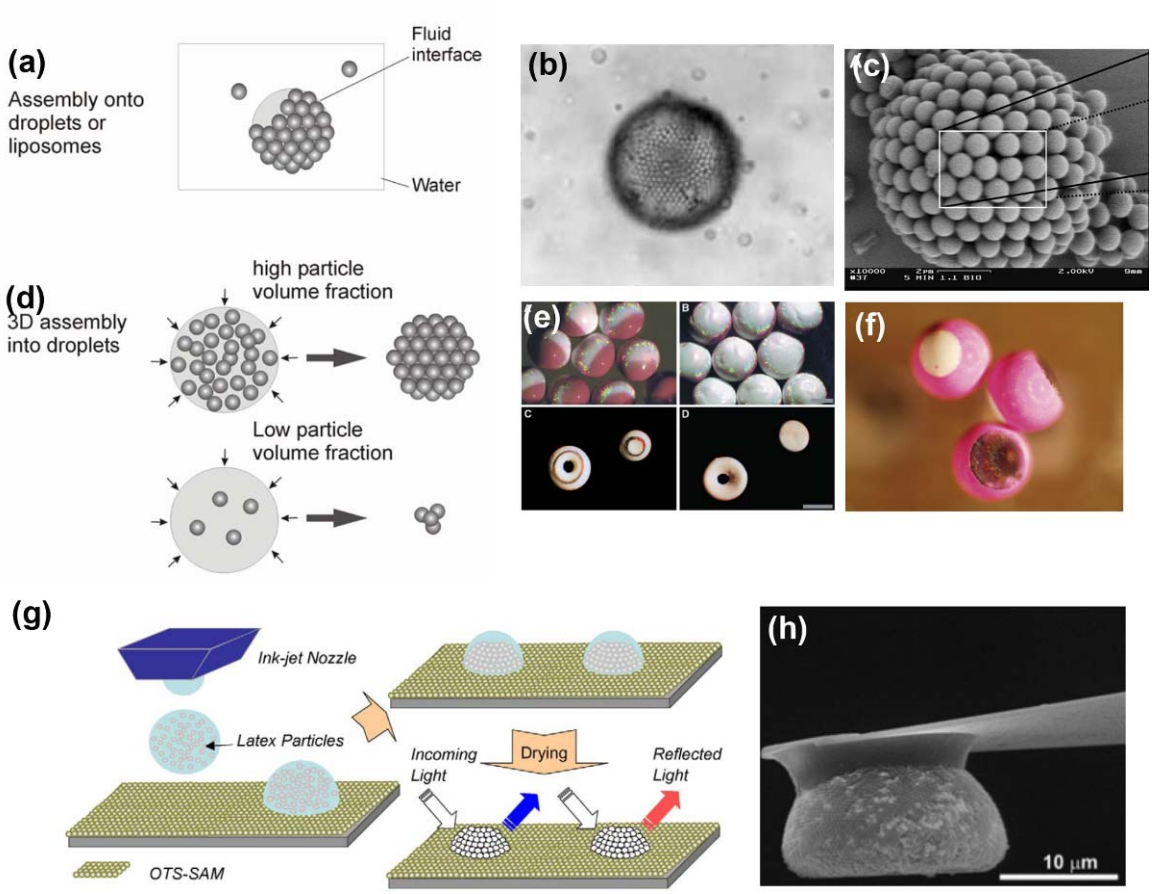

Figure 1.6. (a, d) Schematics for self assembly of microparticles at the two phase interface and in bulk of the droplets.[142] Anisotropic and functional supraparticle synthesis (b, c) around emulsion droplet templates[59,145] and (e, f) inside freely suspended droplet templates[56,61]. (g, h) Self assembly inside droplets templates dispensed on solid surface.[68,155]

Self assembly process of microparticles is not just limited to the two phase interface of droplets. Velev et al. developed a technique where microparticles self assemble within the droplets freely suspended on the surface of an immiscible fluid (high density fluorinated oil).[29,56,61,150,151] By varying the initial composition of the suspended droplets and application

of external fields, a variety of shape-anisotropic and composition-anisotropic supraparticles were fabricated (Fig. 1.6 (e, f).[61] Aerosol liquid droplet methods and spray drying have also been used to fabricate hierarchical assemblies.[152-154] A major issue in performing self assembly in droplets suspended in liquid environment is to get rid of the liquid/organic solvent entrained in the pores of particle matrices. To overcome this issue, researchers have dispensed droplets containing microparticle suspensions on hydrophobic solid substrates (Fig. 1.6 (g, h) which allow the final structures to assume hemispherical shapes.[68,155,156] However, this method does not provide the flexibility of precise control over final shape and anisotropy development in the supraparticles. The challenge of shape control can be met by the usage of substrates which possess extremely high contact angles akin to the superhydrophobic surfaces found in nature.[157,158]

1.5. Layout of this dissertation

We have presented the versatile nature of microliter droplets in synthesizing novel materials and as sites for high throughput screening of multiple samples. My graduate research is focused on microdroplet engineering for performing bioassays and synthesis of functional structured porous assemblies. The work described in Chapter 2 illustrates the immunoagglutination assays performed inside droplet containers that need only a few nanoliters of analyte for biomolecular detection. The work is based on the method for electric field manipulation of microdroplets suspended on the surface of high density oil in

new liquid-liquid microfluidic chips[7]. The quantification is done based on particle aggregation dynamics theory, which was found to correlate well with experimental results. The physical parameters affecting the performance of microbioassays are discussed. The study is performed with antibodies and antigens supplied by the Department of Defense (DOD) Critical Reagents Program (CRP). The performance of the microbioassays is also compared to the Hand Held Assays (HHA) available through this program.

Chapter 3 presents the synthesis of light diffracting near spherical supraparticles using droplet templates dispensed on superhydrophobic substrates. The physical phenomena responsible for the appearance of colorful ring patterns and a theoretical model (without fitting parameter) for the prediction of the angular position pertaining to any colored spot are also presented. Chapter 4 illustrates the application of spherical sessile droplet templates to fabricate shape-anisotropic ('doughnut') and composition-anisotropic ('patchy magnetic') hierarchical assemblies. Chapter 5 presents an investigation of the use of porous supraparticle assemblies in sustained release of dye (drug simulant). The novel microfluidic chip technique for the characterization of materials release from functional porous particles is presented. The release kinetics is explained on the basis of diffusion and dissolution based mass transfer model. Finally we summarize our findings in Chapter 6 and provide an outlook on future extension of the work.

1.6. References

1. S. T. Chang, O. D. Velev. Evaporation-induced particle microseparations inside droplets floating on a chip. *Langmuir*, (2006), **22** (4), 1459-1468.

2. R. Daw, J. Finkelstein. Lab on a chip. *Nature*, (2006), **442** (7101), 367-367.

3. J. El-Ali, P. K. Sorger, K. F. Jensen. Cells on chips. *Nature*, (2006), **442** (7101), 403-411.

4. G. Medoro, N. Manaresi, A. Leonardi, L. Altomare, M. Tartagni, R. Guerrieri. A lab-on-a-chip for cell detection and manipulation. *Ieee Sensors Journal*, (2003), **3** (3), 317-325.

5. H. A. Stone, A. D. Stroock, A. Ajdari. Engineering flows in small devices: Microfluidics toward a lab-on-a-chip. *Annual Review of Fluid Mechanics*, (2004), **36** 381-411.

6. F. Su, K. Chakrabarty, R. B. Fair. Microfluidics-based biochips: Technology issues, implementation platforms, and design-automation challenges. *IEEE Transactions on Computer-Aided Design of Integrated Circuits and Systems*, (2006), **25** (2), 211-223.

7. O. D. Velev, B. G. Prevo, K. H. Bhatt. On-chip manipulation of free droplets. *Nature*, (2003), **426** (6966), 515-516.

8. A. J. deMello. Control and detection of chemical reactions in microfluidic systems. *Nature*, (2006), **442** (7101), 394-402.

9. P. Yager, T. Edwards, E. Fu, K. Helton, K. Nelson, M. R. Tam, B. H. Weigl. Microfluidic diagnostic technologies for global public health. *Nature*, (2006), **442** (7101), 412-418.

10. E. Delamarche, D. Juncker, H. Schmid. Microfluidics for Processing Surfaces and Miniaturizing Biological Assays. *Advanced Materials*, (2005), **17** (24), 2911-2933.

11. A. Bange, H. B. Halsall, W. R. Heineman. Microfluidic immunosensor systems. *Biosensors and Bioelectronics*, (2005), **20** (12), 2488-2503.

12. H. Andersson, A. van den Berg. Microfluidic devices for cellomics: a review. *Sensors and Actuators B: Chemical*, (2003), **92** (3), 315-325.

13. J. Khandurina, A. Guttman. Bioanalysis in microfluidic devices. *Journal of Chromatography A*, (2002), **943** (2), 159-183.

14. J. Hong, J. B. Edel, A. J. deMello. Micro- and nanofluidic systems for high-throughput biological screening. *Drug Discovery Today*, (2009), **14** (3-4), 134-146.

15. P. S. Dittrich, A. Manz. Lab-on-a-chip: microfluidics in drug discovery. *Nat Rev Drug Discov*, (2006), **5** (3), 210-218.

16. L. Kang, B. G. Chung, R. Langer, A. Khademhosseini. Microfluidics for drug discovery and development: From target selection to product lifecycle management. *Drug Discovery Today*, (2008), **13** (1-2), 1-13.

17. J. Pihl, M. Karlsson, D. T. Chiu. Microfluidic technologies in drug discovery. *Drug Discovery Today*, (2005), **10** (20), 1377-1383.

18. Y. Sun, Y. C. Kwok. Polymeric microfluidic system for DNA analysis. *Analytica Chimica Acta*, (2006), **556** (1), 80-96.

19. C. Zhang, J. Xu, W. Ma, W. Zheng. PCR microfluidic devices for DNA amplification. *Biotechnology Advances*, (2006), **24** (3), 243-284.

20. S. Mouradian. Lab-on-a-chip: applications in proteomics. *Current Opinion in Chemical Biology*, (2002), **6** (1), 51-56.

21. G. A. J. Besselink, R. B. M. Schasfoort, A. J. Tüdos. Trends in miniaturized total analysis systems for point-of-care testing in clinical chemistry. *Lab on a chip*, (2001), **1** (2), 83-95.

22. M. H. Katie, M. B. Joan, R. B. Kiev, P. L. James. Forensic DNA Analysis on Microfluidic Devices: A Review. *Journal of Forensic Sciences*, (2007), **52** (4), 784-799.

23. T. H. Schulte, R. L. Bardell, B. H. Weigl. Microfluidic technologies in clinical diagnostics. *Clinica Chimica Acta*, (2002), **321** (1-2), 1-10.

24. A. Günther, K. F. Jensen. Multiphase microfluidics: from flow characteristics to chemical and materials synthesis. *Lab on a chip*, (2006), **6** (12), 1487-1503.

25. S. Yujun, H. Josef, S. S. R. K. Challa. Microfluidic Synthesis of Nanomaterials. *Small*, (2008), **4** (6), 698-711.

26. C. A. Serra, Z. Q. Chang. Microfluidic-assisted synthesis of polymer particles. *Chemical Engineering & Technology*, (2008), **31** (8), 1099-1115.

27. D. J. Bennett, B. Khusid, C. D. James, P. C. Galambos, M. Okandan, D. Jacqmin, A. Acrivos. Combined field-induced dielectrophoresis and phase separation for manipulating particles in microfluidics. *Applied Physics Letters*, (2003), **83** (23), 4866-4868.

28. W. M. Choi, O. Park. The fabrication of micropatterns of a 2D colloidal assembly by electrophoretic deposition. *Nanotechnology*, (2006), **17** (1), 325-329.

29. O. D. Velev. Self-assembly of unusual nanoparticle crystals. *Science*, (2006), **312** (5772), 376-377.

30. R. M. Lorenz, J. S. Edgar, G. D. M. Jeffries, D. T. Chiu. Microfluidic and optical systems for the on-demand generation and manipulation of single femtoliter-volume aqueous droplets. *Analytical Chemistry*, (2006), **78** (18), 6433-6439.

31. D. Psaltis, S. R. Quake, C. H. Yang. Developing optofluidic technology through the fusion of microfluidics and optics. *Nature*, (2006), **442** (7101), 381-386.

32. H. A. Stone, S. Kim. Microfluidics: Basic issues, applications, and challenges. *Aiche Journal*, (2001), **47** (6), 1250-1254.

33. G. M. Whitesides. The origins and the future of microfluidics. *Nature*, (2006), **442** (7101), 368-373.

34. V. Brisson, R. D. Tilton. Self-assembly and two-dimensional patterning of cell arrays by electrophoretic deposition. *Biotechnology and Bioengineering*, (2002), **77** (3), 290-295.

35. V. W. Cornish. Biological chemistry - Catalytic competition for cells. *Nature*, (2006), **440** (7081), 156-157.

36. S. Fiedler, S. G. Shirley, T. Schnelle, G. Fuhr. Dielectrophoretic sorting of particles and cells in a microsystem. *Analytical Chemistry*, (1998), **70** (9), 1909-1915.

37. K. Kleparnik, P. Bocek. Theoretical Background for Clinical and Biomedical Applications of Electromigration Techniques. *Journal of Chromatography-Biomedical Applications*, (1991), **569** (1-2), 3-42.

38. B. S. Gallardo, V. K. Gupta, F. D. Eagerton, L. I. Jong, V. S. Craig, R. R. Shah, N. L. Abbott. ELectrochemical principles for active control of liquids on submillimeter scales. *Science*, (1999), **283** (5398), 57-60.

39. D. E. Kataoka, S. M. Troian. Patterning liquid flow on the microscopic scale. *Nature*, (1999), **402** (6763), 794-797.

40. A. D. Stroock, R. F. Ismagilov, H. A. Stone, G. M. Whitesides. Fluidic ratchet based on Marangoni-Benard convection. *Langmuir*, (2003), **19** (10), 4358-4362.

41. R. Mukhopadhyay. Diving into droplets. *Analytical Chemistry*, (2006), **78** (5), 1401-1404.

42. K. H. Bhatt, S. Grego, O. D. Velev. An AC electrokinetic technique for collection and concentration of particles and cells on patterned electrodes. *Langmuir*, (2005), **21** (14), 6603-6612.

43. M. P. Hughes. Strategies for dielectrophoretic separation in laboratory-on-a-chip systems. *Electrophoresis*, (2002), **23** (16), 2569-2582.

44. T. B. Jones. Liquid dielectrophoresis on the microscale. *Journal of Electrostatics*, (2001), **51** 290-299.

45. H. A. Pohl. The Motion and Precipitation of Suspensoids in Divergent Electric Fields. *Journal of Applied Physics*, (1951), **22** (7), 869-871.

46. A. Castellanos, A. Ramos, A. Gonzalez, N. G. Green, H. Morgan. Electrohydrodynamics and dielectrophoresis in microsystems: scaling laws. *Journal of Physics D-Applied Physics*, (2003), **36** (20), 2584-2597.

47. S. Krishnadasan, R. J. C. Brown, A. J. deMello, J. C. deMello. Intelligent routes to the controlled synthesis of nanoparticles. *Lab on a chip*, (2007), **7** (11), 1434-1441.

48. J. Atencia, D. J. Beebe. Controlled microfluidic interfaces. *Nature*, (2005), **437** (7059), 648-655.

49. S. Haeberle, R. Zengerle. Microfluidic platforms for lab-on-a-chip applications. *Lab on a chip*, (2007), **7** (9), 1094-1110.

50. M. Joanicot, A. Ajdari. Applied physics - Droplet control for microfluidics. *Science*, (2005), **309** (5736), 887-888.

51. S. Y. Teh, R. Lin, L. H. Hung, A. P. Lee. Droplet microfluidics. *Lab on a Chip*, (2008), **8** (2), 198-220.

52. V. Rastogi, O. D. Velev. Development and evaluation of realistic microbioassays in freely suspended droplets on a chip. *Biomicrofluidics*, (2007), **1** (1), 014107-014117.

53. R. Fair. Digital microfluidics: is a true lab-on-a-chip possible? *Microfluidics and Nanofluidics*, (2007), **3** (3), 245-281.

54. D. R. Link, E. Grasland-Mongrain, A. Duri, F. Sarrazin, Z. D. Cheng, G. Cristobal, M. Marquez, D. A. Weitz. Electric Control of Droplets in Microfluidic Devices. *Angewandte Chemie International Edition*, (2006), **45** (16), 2556-2560.

55. N. Blow. Microfluidics: in search of a killer application. *Nat Meth*, (2007), **4** (8), 665-670.

56. J. R. Millman, K. H. Bhatt, B. G. Prevo, O. D. Velev. Anisotropic particle synthesis in dielectrophoretically controlled microdroplet reactors. *Nature Materials*, (2005), **4** (1), 98-102.

57. T. Nisisako, T. Torii. Formation of Biphasic Janus Droplets in a Microfabricated Channel for the Synthesis of Shape-Controlled Polymer Microparticles. *Advanced Materials*, (2007), **19** (11), 1489-1493.

58. T. Nisisako, T. Torii, T. Takahashi, Y. Takizawa. Synthesis of monodisperse bicolored janus particles with electrical anisotropy using a microfluidic co-flow system. *Advanced Materials*, (2006), **18** (9), 1152-1156.

59. O. D. Velev, K. Furusawa, K. Nagayama. Assembly of latex particles by using emulsion droplets as templates .1. Microstructured hollow spheres. *Langmuir*, (1996), **12** (10), 2374-2384.

60. O. D. Velev, K. Furusawa, K. Nagayama. Assembly of latex particles by using emulsion droplets as templates .2. Ball-like and composite aggregates. *Langmuir*, (1996), **12** (10), 2385-2391.

61. O. D. Velev, A. M. Lenhoff, E. W. Kaler. A class of microstructured particles through colloidal crystallization. *Science*, (2000), **287** (5461), 2240-2243.

62. O. D. Velev, K. Nagayama. Assembly of latex particles by using emulsion droplets .3. Reverse (water in oil) system. *Langmuir*, (1997), **13** (6), 1856-1859.

63. T. Stefaniuk, P. Wrobel, R. Dominiak, G. Gawlik, K. Bajdor, M. Zielecka, T. Szoplik. Self-assembly of arrays of micro-rings by colloidal evaporative deposition. *Surface Science*, (2007), **601** (21), 4922-4924.

64. T. Nisisako, S. Okushima, T. Torii. Controlled formulation of monodisperse double emulsions in a multiple-phase microfluidic system. *Soft Matter*, (2005), **1** (1), 23-27.

65. A. S. Utada, E. Lorenceau, D. R. Link, P. D. Kaplan, H. A. Stone, D. A. Weitz. Monodisperse Double Emulsions Generated from a Microcapillary Device. *Science*, (2005), **308** (5721), 537-541.

66. I. Shestopalov, J. D. Tice, R. F. Ismagilov. Multi-step synthesis of nanoparticles performed on millisecond time scale in a microfluidic droplet-based system. *Lab on a chip*, (2004), **4** (4), 316-321.

67. V. Rastogi, S. Melle, O. G. Calderón, A. A. García, M. Marquez, O. D. Velev. Synthesis of Light-Diffracting Assemblies from Microspheres and Nanoparticles in Droplets on a Superhydrophobic Surface. *Advanced Materials*, (2008), **20** (22), 4263-4268.

68. J. Park, J. Moon, H. Shin, D. Wang, M. Park. Direct-write fabrication of colloidal photonic crystal microarrays by ink-jet printing. *Journal of Colloid and Interface Science*, (2006), **298** (2), 713-719.

69. V. Dugas, J. Broutin, E. Souteyrand. Droplet evaporation study applied to DNA chip manufacturing. *Langmuir*, (2005), **21** (20), 9130-9136.

70. A. Egatz-Gomez, S. Melle, A. A. Garcia, S. A. Lindsay, M. Marquez, P. Dominguez-Garcia, M. A. Rubio, S. T. Picraux, J. L. Taraci, T. Clement, D. Yang, M. A. Hayes, D. Gust. Discrete magnetic microfluidics. *Applied Physics Letters*, (2006), **89** (3),

71. P. Paik, V. K. Pamula, R. B. Fair. Rapid droplet mixers for digital microfluidic systems. *Lab on a chip*, (2003), **3** (4), 253-259.

72. V. Srinivasan, V. K. Pamula, R. B. Fair. An integrated digital microfluidic lab-on-a-chip for clinical diagnostics on human physiological fluids. *Lab on a chip*, (2004), **4** (4), 310-315.

73. A. Huebner, S. Sharma, M. Srisa-Art, F. Hollfelder, J. B. Edel, A. J. Demello. Microdroplets: A sea of applications? *Lab on a Chip*, (2008), **8** (8), 1244-1254.

74. K. Jensen, A. P. Lee. The Science & Applications of Droplets in Microfluidic Devices. *Lab on a chip*, (2004), **4** (4), 31N-32N.

75. T. Nisisako, T. Torii, T. Higuchi. Droplet formation in a microchannel network. *Lab on a chip*, (2002), **2** (1), 24-26.

76. J. D. Tice, H. Song, A. D. Lyon, R. F. Ismagilov. Formation of droplets and mixing in multiphase microfluidics at low values of the Reynolds and the capillary numbers. *Langmuir*, (2003), **19** (22), 9127-9133.

77. J. H. Xu, G. S. Luo, S. W. Li, G. G. Chen. Shear force induced monodisperse droplet formation in a microfluidic device by controlling wetting properties. *Lab on a chip*, (2006), **6** (1), 131-136.

78. C. Priest, S. Herminghaus, R. Seemann. Generation of monodisperse gel emulsions in a microfluidic device. *Applied Physics Letters*, (2006), **88** (2), 024106-024103.

79. P. Garstecki, M. J. Fuerstman, H. A. Stone, G. M. Whitesides. Formation of droplets and bubbles in a microfluidic T-junction-scaling and mechanism of break-up. *Lab on a chip*, (2006), **6** (3), 437-446.

80. T. Thorsen, R. W. Roberts, F. H. Arnold, S. R. Quake. Dynamic Pattern Formation in a Vesicle-Generating Microfluidic Device. *Physical Review Letters*, (2001), **86** (18), 4163.

81. S. L. Anna, N. Bontoux, H. A. Stone. Formation of dispersions using "flow focusing" in microchannels. *Applied Physics Letters*, (2003), **82** (3), 364-366.

82. Z. T. Cygan, J. T. Cabral, K. L. Beers, E. J. Amis. Microfluidic platform for the generation of organic-phase microreactors. *Langmuir*, (2005), **21** (8), 3629-3634.

83. R. Dreyfus, P. Tabeling, H. Willaime. Ordered and disordered patterns in two-phase flows in microchannels. *Physical Review Letters*, (2003), **90** (14),

84. P. Garstecki, I. Gitlin, W. DiLuzio, G. M. Whitesides, E. Kumacheva, H. A. Stone. Formation of monodisperse bubbles in a microfluidic flow-focusing device. *Applied Physics Letters*, (2004), **85** (13), 2649-2651.

85. L. Yobas, S. Martens, W. L. Ong, N. Ranganathan. High-performance flow-focusing geometry for spontaneous generation of monodispersed droplets. *Lab on a chip*, (2006), **6** (8), 1073-1079.

86. M. Seo, Z. Nie, S. Xu, M. Mok, P. C. Lewis, R. Graham, E. Kumacheva. Continuous Microfluidic Reactors for Polymer Particles. *Langmuir*, (2005), **21** (25), 11614-11622.

87. Z. Nie, W. Li, M. Seo, S. Xu, E. Kumacheva. Janus and Ternary Particles Generated by Microfluidic Synthesis: Design, Synthesis, and Self-Assembly. *Journal of the American Chemical Society*, (2006), **128** (29), 9408-9412.

88. D. Dendukuri, K. Tsoi, T. A. Hatton, P. S. Doyle. Controlled synthesis of nonspherical microparticles using microfluidics. *Langmuir*, (2005), **21** (6), 2113-2116.

89. N. J. Carroll, S. B. Rathod, E. Derbins, S. Mendez, D. A. Weitz, D. N. Petsev. Droplet-Based Microfluidics for Emulsion and Solvent Evaporation Synthesis of Monodisperse Mesoporous Silica Microspheres. *Langmuir*, (2008), **24** (3), 658-661.

90. R. Ahmed, D. Hsu, C. Bailey, T. B. Jones. Dispensing picoliter droplets using dielectrophoretic (DEP) microactuation. *Microscale Thermophysical Engineering*, (2004), **8** (3), 271-283.

91. W. Thomas, F. Magalie, A. Manouk, A. S. Howard. Microfluidic flow focusing: Drop size and scaling in pressure versus flow-rate-driven pumping. *Electrophoresis*, (2005), **26** (19), 3716-3724.

92. K. Jin-Woong, S. U. Andrew , F.-N. Alberto, H. Zhibing, A. W. David Fabrication of Monodisperse Gel Shells and Functional Microgels in Microfluidic Devices13. *Angewandte Chemie International Edition*, (2007), **46** (11), 1819-1822.

93. L. Daeyeon, A. W. David. Double Emulsion-Templated Nanoparticle Colloidosomes with Selective Permeability. *Advanced Materials*, (2008), **20** (18), 3498-3503.

94. B. Zheng, J. D. Tice, L. S. Roach, R. F. Ismagilov. A Droplet-Based, Composite PDMS/Glass Capillary Microfluidic System for Evaluating Protein Crystallization Conditions by Microbatch and Vapor-Diffusion Methods with On-Chip X-Ray Diffraction13. *Angewandte Chemie International Edition*, (2004), **43** (19), 2508-2511.

95. T. B. Jones, J. D. Fowler, Y. S. Chang, C. J. Kim. Frequency-based relationship of electrowetting and dielectrophoretic liquid microactuation. *Langmuir*, (2003), **19** (18), 7646-7651.

96. T. B. Jones, M. Gunji, M. Washizu, M. J. Feldman. Dielectrophoretic liquid actuation and nanodroplet formation. *Journal of Applied Physics*, (2001), **89** (2), 1441-1448.

97. K. L. Wang, T. B. Jones. Frequency-dependent bifurcation in electromechanical microfluidic structures. *Journal of Micromechanics and Microengineering*, (2004), **14** (6), 761-768.

98. S. K. Cho, H. J. Moon, C. J. Kim. Creating, transporting, cutting, and merging liquid droplets by electrowetting-based actuation for digital microfluidic circuits. *Journal of Microelectromechanical Systems*, (2003), **12** (1), 70-80.

99. J. Lee, H. Moon, J. Fowler, T. Schoellhammer, C.-J. Kim. Electrowetting and electrowetting-on-dielectric for microscale liquid handling. *Sensors and Actuators A: Physical*, (2002), **95** (2-3), 259-268.

100. J. Berthier, P. Clementz, O. Raccurt, D. Jary, P. Claustre, C. Peponnet, Y. Fouillet. Computer aided design of an EWOD microdevice. *Sensors and Actuators A: Physical*, (2006), **127** (2), 283-294.

101. J.-M. Roux, Y. Fouillet, J.-L. Achard. 3D droplet displacement in microfluidic systems by electrostatic actuation. *Sensors and Actuators A: Physical*, (2007), **134** (2), 486-493.

102. T. B. Jones. On the relationship of dielectrophoresis and electrowetting. *Langmuir*, (2002), **18** (11), 4437-4443.

103. M. G. Pollack, R. B. Fair, A. D. Shenderov. Electrowetting-based actuation of liquid droplets for microfluidic applications. *Applied Physics Letters*, (2000), **77** (11), 1725-1726.

104. M. R. Bringer, C. J. Gerdts, H. Song, J. D. Tice, R. F. Ismagilov. Microfluidic systems for chemical kinetics that rely on chaotic mixing in droplets. *Philosophical Transactions of the Royal Society of London. Series A: Mathematical, Physical and Engineering Sciences*, (2004), **362** (1818), 1087-1104.

105. D. R. Link, S. L. Anna, D. A. Weitz, H. A. Stone. Geometrically Mediated Breakup of Drops in Microfluidic Devices. *Physical Review Letters*, (2004), **92** (5), 054503.

106. L.-H. Hung, K. M. Choi, W.-Y. Tseng, Y.-C. Tan, K. J. Shea, A. P. Lee. Alternating droplet generation and controlled dynamic droplet fusion in microfluidic device for CdS nanoparticle synthesis. *Lab on a chip*, (2006), **6** (2), 174-178.

107. K. Ahn, J. Agresti, H. Chong, M. Marquez, D. A. Weitz. Electrocoalescence of drops synchronized by size-dependent flow in microfluidic channels. *Applied Physics Letters*, (2006), **88** (26), 264105-264103.

108. S. Mohr, Y. H. Zhang, A. Macaskill, P. J. R. Day, R. W. Barber, N. J. Goddard, D. R. Emerson, P. R. Fielden. Numerical and experimental study of a droplet-based PCR chip. *Microfluidics and Nanofluidics*, (2007), **3** (5), 611-621.

109. T. Henkel, T. Bermig, M. Kielpinski, A. Grodrian, J. Metze, J. M. Köhler. Chip modules for generation and manipulation of fluid segments for micro serial flow processes. *Chemical Engineering Journal*, (2004), **101** (1-3), 439-445.

110. V. Srinivasan, V. K. Pamula, R. B. Fair. Droplet-based microfluidic lab-on-a-chip for glucose detection. *Analytica Chimica Acta*, (2004), **507** (1), 145-150.

111. A. A. Garcia, A. Egatz-Gomez, S. A. Lindsay, P. Dominguez-Garcia, S. Melle, M. Marquez, M. A. Rubio, S. T. Picraux, D. Q. Yang, P. Aella, M. A. Hayes, D. Gust, S. Loyprasert, T. Vazquez-Alvarez, J. Wang. Magnetic movement of biological fluid droplets. *Journal of Magnetism and Magnetic Materials*, (2007), **311** (1), 238-243.

112. T. B. Jones, *Electromechanics of particles*. (Cambridge University Press, 1995).

113. H. Morgan, N. G. Green, *AC Electrokinetics: colloids and nanoparticles*. (Research Studies Press Ltd., UK, 2003).

114. O. D. Velev, in *Colloids and Colloid Assemblies,* F. Caruso, Ed. (Wiley-VCH, 2004), pp. 437.

115. K. H. Bhatt, O. D. Velev. Control and modeling of the dielectrophoretic assembly of on-chip nanoparticle wires. *Langmuir*, (2004), **20** (2), 467-476.

116. K. D. Hermanson, S. O. Lumsdon, J. P. Williams, E. W. Kaler, O. D. Velev. Dielectrophoretic assembly of electrically functional microwires from nanoparticle suspensions. *Science*, (2001), **294** (5544), 1082-1086.

117. S. Connolly, D. Fitzmaurice. Programmed assembly of gold nanocrystals in aqueous solution. *Advanced Materials*, (1999), **11** (14), 1202-1205.

118. S. O. Lumsdon, E. W. Kaler, O. D. Velev. Two-Dimensional Crystallization of Microspheres by a Coplanar AC Electric Field. *Langmuir*, (2004), **20** (6), 2108-2116.

119. S. O. Lumsdon, E. W. Kaler, J. P. Williams, O. D. Velev. Dielectrophoretic assembly of oriented and switchable two-dimensional photonic crystals. *Applied Physics Letters*, (2003), **82** (6), 949-951.

120. O. D. Velev, E. W. Kaler. In situ assembly of colloidal particles into miniaturized biosensors. *Langmuir*, (1999), **15** (11), 3693-3698.

121. D. S. Gray, J. L. Tan, J. Voldman, C. S. Chen. Dielectrophoretic registration of living cells to a microelectrode array (vol 19, pg 1765, 2004). *Biosensors & Bioelectronics*, (2004), **19** (12), 1765-1774.

122. H. Morgan, M. P. Hughes, N. G. Green. Separation of submicron bioparticles by dielectrophoresis. *Biophysical Journal*, (1999), **77** (1), 516-525.

123. R. Pethig. Dielectrophoresis: Using inhomogeneous AC electrical fields to separate and manipulate cells. *Critical Reviews in Biotechnology*, (1996), **16** (4), 331-348.

124. L. B. Bangs. New developments in particle-based immunoassays: Introduction. *Pure and Applied Chemistry*, (1996), **68** (10), 1873-1879.

125. C. L. Baylis, in *Detecting pathogens in food*. (T. A. McMeekin, CRC Press LLC, 2004), pp. 217-240.

126. L. B. Bangs, M. T. Kenny. Old, New, Borrowed, Blue. *Industrial Research*, (1976), **18** (8), 46-49.

127. E. T. Gunter, W. Achim. Bio-microarrays based on functional nanoparticles. *Dekker Encyclopedia of Nanoscience and Nanotechnology*, (2004),

128. C. R. Lowe, B. Hin, D. C. Cullen, S. E. Evans, L. D. G. Stephens, P. Maynard. Biosensors. *Journal of Chromatography*, (1990), **510** 347-354.

129. E. P. Meulenberg, W. H. Mulder, P. G. Stoks. Immunoassays for Pesticides. *Environmental Science & Technology*, (1995), **29** (3), 553-561.

130. J. A. Molina-Bolivar, F. Galisteo-Gonzalez. Latex Immunoagglutination Assays. *Polymer Reviews*, (2005), **45** (1), 59 - 98.

131. Z. G. Wang, H. Shang, G. U. Lee. Nanoliter-scale reactor arrays for biochemical sensing. *Langmuir*, (2006), **22** (16), 6723-6726.

132. P. Andreotti, W C. Immunoassay of infectious agents. *Biotechniques*, (2003), **35** (4), 850-859.

133. S.-M. Yang, S.-H. Kim, J.-M. Lim, G.-R. Yi. Synthesis and assembly of structured colloidal particles. *Journal of Materials Chemistry*, (2008), **18** (19), 2177-2190.

134. BangsLabs *Technote #301 Immunological Applications* www.bangslabs.com

135. L. B. Bangs. Latex Immunoassays. *Journal of Clinical Immunoassay*, (1990), **13** (3), 127-131.

136. J. M. Singer, C. M. Plotz. Latex Fixation Test .1. Application to the Serologic Diagnosis of Rheumatoid Arthritis. *American Journal of Medicine*, (1956), **21** (6), 888-892.

137. G. V. F. Seaman, J. W. Goodwin. Physicochemical factors in latex rapid agglutination tests. *American Clinical Products Review*, (1986), 25-31.

138. S. Kabir. Review article: clinic-based testing for Helicobacter pylori infection by enzyme immunoassay of faeces, urine and saliva. *Alimentary Pharmacology & Therapeutics*, (2003), **17** (11), 1345-1354.

139. R.-H. Shyu, H.-F. Shyu, H.-W. Liu, S.-S. Tang. Colloidal gold-based immunochromatographic assay for detection of ricin. *Toxicon*, (2002), **40** (3), 255-258.

140. X. L. Sun, X. L. Zhao, J. Tang, J. Zhou, F. S. Chu. Preparation of gold-labeled antibody probe and its use in immunochromatography assay for detection of aflatoxin B1. *International Journal of Food Microbiology*, (2005), **99** (2), 185-194.

141. BangsLabs *Technote #303 Lateral Flow Tests* www.bangslabs.com

142. K. P. Velikov, O. D. Velev, in *Colloidal particles at liquid interfaces,* B. P. Binks, T. Horozov, Eds. (Cambridge University Press, Cambridge, 2006), pp. 225-297.

143. S. H. Kim, S. Y. Lee, G. R. Yi, D. J. Pine, S. M. Yang. Microwave-assisted self-organization of colloidal particles in confining aqueous droplets. *Journal of the American Chemical Society*, (2006), **128** (33), 10897-10904.

144. S. M. Klein, V. N. Manoharan, D. J. Pine, F. F. Lange. Synthesis of spherical polymer and titania photonic crystallites. *Langmuir*, (2005), **21** (15), 6669-6674.

145. A. D. Dinsmore, M. F. Hsu, M. G. Nikolaides, M. Marquez, A. R. Bausch, D. A. Weitz. Colloidosomes: Selectively permeable capsules composed of colloidal particles. *Science*, (2002), **298** (5595), 1006-1009.

146. R. Aveyard, B. P. Binks, J. H. Clint. Emulsions stabilised solely by colloidal particles. *Advances in Colloid and Interface Science*, (2003), **100-102** 503-546.

147. B. P. Binks. Particles as surfactants--similarities and differences. *Current Opinion in Colloid & Interface Science*, (2002), **7** (1-2), 21-41.

148. S. U. Pickering. Emulsions. *Journal of the Chemical Society*, (1907), **91** 2001-2021.

149. D. Dendukuri, D. C. Pregibon, J. Collins, T. A. Hatton, P. S. Doyle. Continuous-flow lithography for high-throughput microparticle synthesis. *Nature Materials*, (2006), **5** (5), 365-369.

150. O. D. Velev, in *Handbook of Surfaces and Interfaces of Materials,* H. S. Nalwa, Ed. (Academic Press, San Diego, Calif., 2001), vol. 3, pp. 125-169.

151. O. D. Velev, K. Bhatt, B. G. Prevo, S. O. Lumsdon. On-chip dielectrophoretic manipulation and assembly of nanoparticles, microparticles and droplets. *Abstracts of Papers of the American Chemical Society*, (2003), **226** U479-U479.

152. W. Stöber, A. Berner, R. Blaschke. The aerodynamic diameter of aggregates of uniform spheres. *Journal of Colloid and Interface Science*, (1969), **29** (4), 710-719.

153. F. Iskandar, L. Gradon, K. Okuyama. Control of the morphology of nanostructured particles prepared by the spray drying of a nanoparticle sol. *Journal of Colloid and Interface Science*, (2003), **265** (2), 296-303.

154. J. H. Moon, G. R. Yi, S. M. Yang, D. J. Pine, S. B. Park. Electrospray-Assisted Fabrication of Uniform Photonic Balls. *Advanced Materials*, (2004), **16** (7), 605-609.

155. D. M. Kuncicky, K. Bose, K. D. Costa, O. D. Velev. Sessile droplet templating of miniature porous hemispheres from colloid crystals. *Chemistry of Materials*, (2007), **19** (2), 141-143.

156. D. M. Kuncicky, O. D. Velev. Surface-guided templating of particle assemblies inside drying sessile droplets. *Langmuir*, (2008), **24** (4), 1371-1380.

157. J. Genzer, K. Efimenko. Recent developments in superhydrophobic surfaces and their relevance to marine fouling: a review. *Biofouling: The Journal of Bioadhesion and Biofilm Research*, (2006), **22** (5), 339-360.

158. J. Genzer, A. Marmur. Biological and synthetic self-cleaning surfaces. *MRS Bulletin*, (2008), **33** (8), 742-746

.

Chapter 2.

Development and Evaluation of Realistic Microbioassays in Freely Suspended Droplets on a Chip*

* Partially based on Rastogi and Velev, *Biomicrofluidics*, 2007, **1**, 014107-17.

2.1 Introduction

The last five decades have brought forward significant development in the immunological techniques for biomolecular detection and identification.[1,2] Many of the immunoassays for clinical diagnostics and detection of chemical and biological agents are based on particle agglutination principles.[3] They are used in detection of various proteins such as immunoglobulin, toxins, and hormones present in blood serum.[2,4-9] Microscale devices are commonly used in conjunction with immunological methods to process multiple samples in an efficient and rapid manner. Microfluidic operation in small volumes reduces the time needed for analysis of a sample. The volume of analyte solution may be critical in applications such as biodefense and forensic diagnostics where only limited sample amounts are available.

The typical immunoagglutination assays are based on polystyrene latex microspheres with antibody molecules bound to their surface.[3-10] An aqueous suspension of these microspheres is mixed with a sample containing antigen molecules from whole blood, serum, urine, etc. The antigen molecules bind two antibody molecules situated on different microspheres and cause agglutination (aggregation) of latex microspheres. Several techniques such as nephelometry and spectrophotometry could be employed to determine and quantify the aggregation state of the latex particles. The immunoagglutination methods, however, are not readily compatible with conventional microfluidic devices with channels due to problems with mixing, clogging of the channels by particles or aggregates, protein fouling, high pressure heads generated by viscous fluid flow and long result read-out

times.[11,12] Some of these problems can be addressed by "digital microfluidics" - moving droplets on solid surface using electrowetting.[13-15] This technique, however, still may encounter problems with contact angle hysteresis, contact line pinning of droplets and fouling. Complex optical detection methods would be required to read the results of agglutination assays in the sessile droplets.

In this manuscript we explore and characterize a new type of immunoassay based on an alternative droplet microfluidic technique. It is based on a fluidic chip where freely suspended droplets are entrapped and transported by dielectrophoresis without any contact with the solid surfaces.[16-18] The microdroplets are suspended on the surface of perfluorinated hydrocarbon and serve as self-contained microscopic containers and reactors for performing and reading out assays for biological detection. The electric fields that hold and guide the droplets and particles are applied through arrays of electrodes submerged in the oil (Fig.2.1). The droplet technique does not encounter the problems of high pressure head, channel clogging, protein fouling and waste disposal existent in conventional microfluidic devices.

We recently completed a detailed experimental study of the liquid flow and particle distribution, combined with simulation of the heat and mass transfer, inside single floating microdroplets.[19] We established that evaporation from the exposed portion of droplets protruding through the oil leads to internal water circulation, mixing and microseparation of the particles in top part of the droplets. The internal circulation is driven by Marangoni flow. Finite element simulations for hydrodynamic flows inside the droplet were in a good correlation with the experimental observations. Various chemical reactions and materials

synthesis processes can be performed in these microcontainers.[19] We show here how such "droplet engineering" could find applications in novel bioassays.

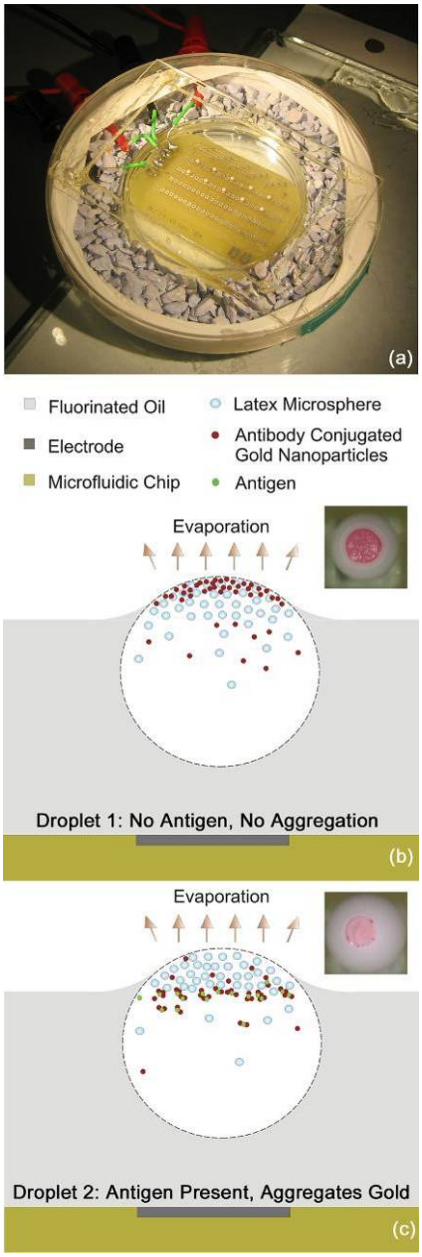

Figure 2.1. (a) Experimental setup with evaporating droplets on a DEP chip. (b) Schematics and optical micrograph from above of evaporating droplet without antigen. (c) Schematics and micrograph of gold nanoparticle aggregation in a droplet containing antigen.

2.1.1. Principles of the immunological bioassays in microdroplets

The evaporation process of the droplets can be used for on-chip detection of antibody-antigen driven agglutination. In the earlier demonstration of the principle we mixed aqueous suspensions of 0.32 μm latex particles and of 40 nm gold nanoparticles coated with goat anti-rabbit IgG.[19] One part of the suspension was kept as is and another part was mixed and incubated with rabbit IgG (the antigen for the IgG bound on the gold nanoparticles). 1.0 μL droplets of each suspension, (Droplet 1 no antigen – "negative control" droplet, Droplet 2 with antigen – "test droplet") were deposited on the F-oil, entrapped by the electric field and observed during drying under the microscope (Fig. 2.1). As the droplets began to dry, a dark gold nanoparticle "eyeball" spot appeared on the top surface of the negative control droplet without rabbit IgG (Fig. 2.1b inset). Deposits of gold nanoparticles in the droplet with rabbit IgG, however, were not visible on the surface (Fig. 2.1c inset).

The differences in the particle collection pattern in the top part of droplets arises because the gold nanoparticles in the test droplet bind to other gold nanoparticles particles via antibody-antigen interaction, forming large clusters as a result of this agglutination process. The gold nanoparticles in the negative control droplet, on the other hand, do not agglutinate in the absence of antigen and remain freely dispersed. The agglutinated gold nanoparticles in the test droplet cannot pass through the interstices between the latex particles collected on the top section of the droplet showing a positive result. The unbound free nanoparticles in the negative control droplet are dragged to the surface and form the

darker spot indicating negative result. Thus microseparation inside the droplets allows direct and easy distinguishing of the aggregation state of the suspended particles affected by biomolecular binding. This process was developed further and investigated in depth in our present study to enable the development of sensitive biological microbioassays.

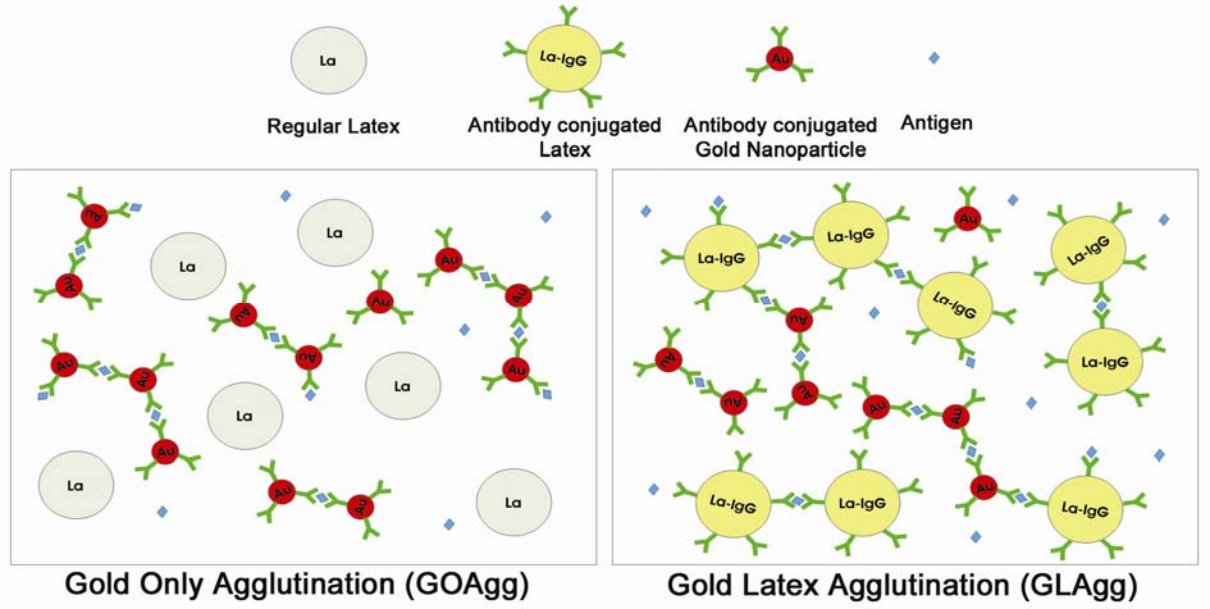

Figure 2.2. Schematics of the immunorecognition and agglutination processes taking place in the two microbioassay formats studied.

2.1.2 Formats of immunoagglutination bioassays studied

We developed two types of assays, schematically shown in Figure 2.2 and performed limit of detection (LOD) experiments. Both assays use gold nanoparticles functionalized with antibodies for the targeted biological or chemical molecule. The difference between the two formats lies in the types of latex particles present in the droplets. The first assay reported here is Gold Only Agglutination (*GOAgg*) which uses non-functionalized latex

microspheres. The functionalized gold nanoparticles agglutinate in the presence of an antigen, forming clusters within the bulk of the droplet. The second assay format, coded here as Gold and Latex Agglutination (*GLAgg*) is based on similar detection principles, but in this case both the gold nanoparticles and the latex spheres are conjugated with immunoglobulin. The antigen leads to agglutination of all particles, including the gold nanoparticles, the latex spheres and cross-agglutination between the gold and latex particles. The detection is carried out by the microseparation procedure and a positive result is detected by the absence of gold nanoparticle ring or spot on the droplet top.

There are important differences between the above mentioned formats of microbioassays. The GOAgg format is less expensive and simpler to implement and read. These assays, however, may be easily oversaturated with antigen, resulting in false negative results. Oversaturation occurs when antigen concentration in the droplets is enough to bind to all antibodies at a ratio of at least 1:1, as a result of which cross-linking of the particles becomes impossible. This ratio was found to be higher in the experiments owing to the slow diffusion and orientation constraints in binding of the particles. The GLAgg format, on the other hand, requires two types of functionalized particles, and thus is a bit more expensive and complex. However, it may be less prone to oversaturation because of the higher number of antigen binding sites available on both latex and gold nanoparticles.

In the following sections we present the experimental data and evaluate the microbioassays (GOAgg and GLAgg) using Goat Anti-Rabbit Immunoglobulin and Rabbit Immunoglobulin pair. The performance of assays was assessed in terms of reliability,

sample volume, limit of detection, incubation time, particle size, and concentration detection range. The microbioassays are also characterized using antibodies and antigens supplied by Critical Reagents Program (CRP, US Department of Defense) for a realistic biological defense application - detection of Ricin. We compare the parameters of the microbioassays developed with the ones of common hand-held assays and laboratory CRP assays using particle agglutination techniques. In the second part of the paper we present results from theoretical model of the kinetics of particle agglutination and correlate them with experimental results.

2.2. Experimental Procedures

2.2.1. Materials

The detection in microbioassay droplets is based on gold nanoparticles penetrating through cavities in the latex particles cap. Calculations for the geometry of the cavity formed between the spheres in a hexagonally close-packed crystal show that the minimal opening size is ~15% of the diameter of microspheres. The diameter of latex particles should be such that the aggregated 40 nm gold nanoparticles cannot pass through the interstices of the latex microspheres. Hence polystyrene latex microspheres of size 0.32 μm were chosen to detect the presence of antigen in the microbioassay droplet. Aqueous surfactant-free sulfate-stabilized 0.32 μm polystyrene latex microspheres were purchased from Interfacial Dynamics Corp. (Portland, OR, USA). Goat Anti-Rabbit IgG (H&L) – Flouresbrite™

Carboxylate YG Beads were purchased from Polysciences Incorporation (Warrington, PA, USA). The microspheres were centrifuged at 1100 g for 10 min with Marathon micro-A centrifuge (Fisher Scientific, USA) and washed with deionized (D.I.) water. The collected microspheres were resuspended in D.I. water and sonicated (Branson Ultrasonics Corp., CT, USA). The DI water used was obtained from Millipore RiOs 16 reverse osmosis water purification systems (Bedford, MA, USA).

An inert, high density perfluorinated oil, FC-70, was purchased from Sigma-Aldrich (St. Louis, MO, USA). 40 nm gold nanoparticles were obtained from British Biocell International (Cardiff, UK). 40 nm goat Anti-Rabbit IgG conjugated gold particles were purchased from EY Labs (San Mateo, CA, USA). Bovine Serum Albumin (BSA) was purchased from Sigma-Aldrich. Rabbit IgG Plasma was purchased from Calbiochem (San Diego, CA, USA). Ricin antigen (Ricin A-Chain) and Ricin antibody (Goat Anti-Ricin Toxin) were supplied by the DOD Critical Reagents Program (CRP). Standard Hand Held Assays (HHA) for the detection of Ricin were also obtained through CRP. These assays operate on immunochromatographic principle.[1]

2.2.2. Experimental Setup

The DEP chip used to capture microdroplets carries arrays of electrodes situated on a circuit board.[20] The square waves of frequency 800 Hz and amplitude of 700 V applied to the electrodes were generated using a FG-7002C Sweep/Function generator (EZ Digital Company Limited, Korea) and a Piezo Driver/Amplifier (Model PZD 700, Trek

Incorporation, USA). The electrode chip was immersed in 4.5 mL high density fluorinated oil (FC-70) contained in a small Petri dish (Millipore Co., MA, USA). The Petri dish was in turn kept inside a bigger chamber containing desiccant to enhance evaporation of droplets (Fig. 2.1).

Microseparation of particles due to evaporation in the droplets was continuously monitored from top using SZ61 0.7-4.5x zoom stereomicroscope (Olympus America Inc., NY, USA). Their images were captured at regular intervals using DSC-V1 Cyber-Shot digital camera (SONY, Japan) coupled with the microscope. Characterization of the droplet geometry was done using Olympus BX-61 optical microscope (Olympus America Inc., NY, USA). Images of the droplets were taken using high resolution DP70 digital CCD microscope camera (Olympus America Inc., NY, USA).

2.2.3. Methodolgy

Water droplets of volume 1.0 μL containing the microspheres, functionalized gold nanoparticles and antigen were dispensed onto the oil surface using ultramicropipette (Eppendorf North America Inc., NY, USA). The droplets for GOAgg microbioassay were prepared by washing the latex particles twice with 0.01 M PBS and centrifuging them at 3000 g for 20 min. The supernatant was decanted, the latex particles were sonicated and then mixed with 0.01 M PBS containing 2 mg/mL BSA and incubated for 30 min. BSA was routinely added to the solutions to prevent any specific adsorption of antigens on the surface of latex microspheres during the microbioassays.[21] In the next step the microspheres were

again washed with PBS and then centrifuged to remove unadsorbed immunoglobulin in the solution. Subsequently a solution containing 0.2 mg/mL BSA and 0.1 wt% Tween-20 in 0.01 M PBS (referred to further as "PBSA") was added with sonication to adjust final latex concentration to 15 wt%.

The latex solution was then mixed in 1:1 volume ratio with goat anti-rabbit IgG conjugated suspension containing 0.04 wt% of 40 nm gold particles. 10.0 μL aliquots of this latex/gold mix were taken and increasing concentrations of antigen (Negative control – no antigen, 1.0 μg/mL, 10.0 μg/mL, and 100.0 μg/mL) were added to each. To study the effect of incubation time, several sets of 10.0 μL aliquots of latex and antibody coated gold were prepared. Aliquots of each set were then mixed with antigen concentration varying from 0 to 10.0 μg/mL. These assays were incubated for times ranging from 5 min to 45 min.

Latex solutions for the GLAgg assay were prepared using goat anti-rabbit IgG coated Flouresbrite™ Carboxylate YG Beads of 1.03 μm diameter. These antibody-coated particles were pretreated by the same procedures as described above for latex in GOAgg assay to adjust latex concentration to 2.6 wt%. The latex suspension was then mixed in 1:1 volume ratio with 0.04 wt% suspension of antibody-conjugated 40 nm gold nanoparticles. The latex/gold particle suspension was divided into 10.0 μL aliquots and increasing concentrations of antigen were added before incubation and deposition of 1.0 μL droplets on the chip.

We examined the effect of gold nanoparticles and Tween-20 on the evaporation rate of droplets in order to characterize the drying process leading to detection. This was done

with sets of droplets, which had similar contents except for the presence of gold nanoparticles and Tween-20. The preparation procedure was the same as for droplets in GOAgg microbioassays. Two sets of 1.0 μL droplets were compared. The droplets in the first set contained 15 wt% latex and a mixture of latex and 0.04 wt% gold nanoparticles in PBSA. The droplets in the second set had the same particles, but 0.05 wt% Tween-20 was added to all samples. The droplets were entrapped on the DEP chip and their diameter was measured with time using high magnification optical microscopy to compare the rate of evaporation.

2.3. Results and Discussion

2.3.1. Gold Only Agglutination Microbioassay (GOAgg)

In the initial set of experiments we verified that the assay functions as expected. We then performed a detailed study of the effects of the major experimental parameters. The results can be summarized as follows.

Effect of antigen concentration: The suspension containing latex and gold nanoparticles and varying concentration of antigen was pre-incubated for 30 min. Images of droplets evaporating on F-oil surface were then taken at regular intervals. After 12 min of drying time, the droplets showed clear difference in the collection pattern of colloidal gold on top (Fig. 2.3). The gold nanoparticles in negative control droplets were able to pass through the interstices between latex microspheres and collect on top. No nanoparticle

aggregation had taken place owing to the absence of antigen. The droplet with 1.0 µg/mL antigen concentration showed the least amount of gold nanoparticle collection on top. This points out that the gold nanoparticles had agglutinated strongly and formed aggregates large enough to get entrapped in the cavities between the latex particles.

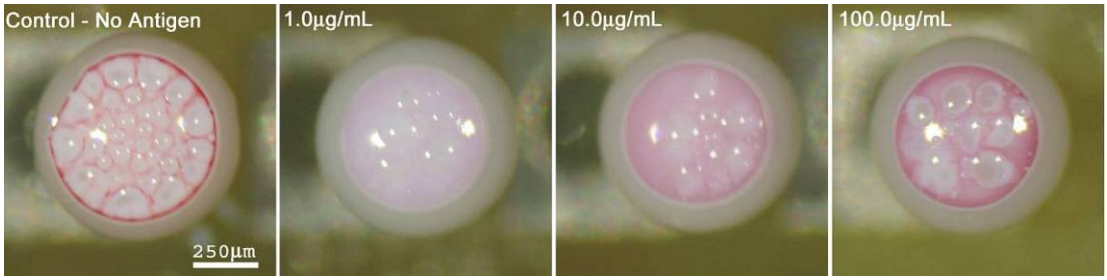

Figure 2.3. Optical micrographs of droplets in a Gold Only Agglutination (GOAgg) assay. 1.0 µg/mL antigen concentration shows the least amount of gold nanoparticles collection on top for 30 min incubation time. The white areas in the top of the droplets are the dense latex particle phases. The gold nanoparticles reaching the top are easily observed because of their intensively red color.

The assay droplets containing 10.0 µg/mL antigen displayed more gold nanoparticles collected in its top portion than the 1.0 µg/mL antigen droplets. This can be explained with effective over-saturation of the antigen-binding antibody sites on the gold nanoparticles. The binding process occurs when free antibody on one particle gets in contact with an antigen bound to an antibody on another particle. The binding does not take place when both antibodies on the two particles are saturated with antigen. The collision of heavily antigen-covered gold particle with another antigen-saturated nanoparticle site does not lead to

aggregation. A larger number of gold nanoparticles remained unaggregated, passing through the interstices of collected latex particles cap and migrating to droplet top.

The droplet with 100.0 μg/mL antigen showed maximal amount of gold nanoparticle collection. The concentration of antigen in this droplet was high enough to saturate all or nearly all antigen binding sites on the surface of the colloidal gold. Thus, the gold particles did not aggregate and collected in the top portion of the droplet. Notably, the color of the gold nanoparticles collected here differs from the one of the negative control, displaying a more bluish tint. This can be explained by the partial aggregation of the nanoparticles before full surface saturation takes place. The plasmon absorption band of colloidal gold depends on the effective size of the nanoparticles and as the nanoparticles aggregate they show a red shift in the absorption spectra.[22] In practice, the difference in the color could not be a parameter reliable enough to distinguish the negative control droplets from the oversaturated ones. Thus, oversaturation (in this case occurring at an antigen concentration ~100 times higher than the optimal one) could lead to error in the readout of these assays.

Scanning electron microscopy observations of a dried microbioassay droplet confirm the assumption of hexagonal closed packing of latex particles in the top portion of droplets. Micrographs of the bottom side of the particle aggregate were taken after flipping it over an SEM grid, illustrating how the agglutinated gold nanoparticle clusters get captured in between the interstices of the latex particles (Fig. 2.4).

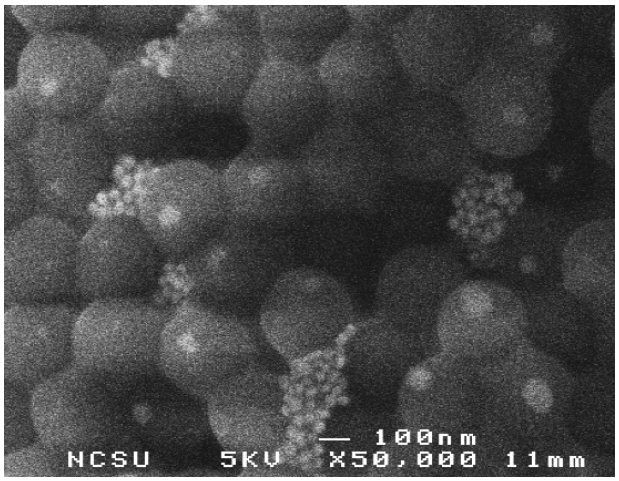

Figure 2.4. Scanning electron micrograph showing cluster of aggregated gold nanoparticles trapped in the interstices between latex particles in the bottom portion of droplet cap.

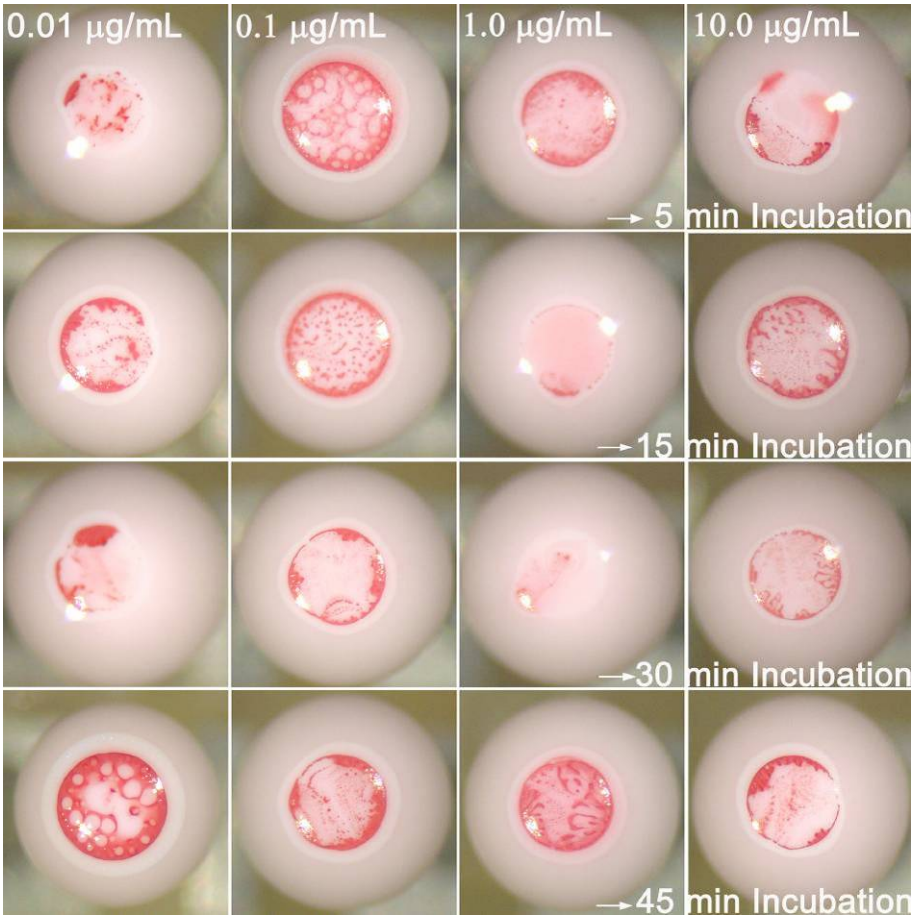

Figure 2.5. Optical micrographs of GOAgg microbioassay for varying incubation times (vertical direction) and varying concentration (horizontal direction).

Effect of incubation time: The influence of incubation time (before depositing and drying the droplets) on the performance of microbioassays was evaluated using the GOAgg system (Fig. 2.5) Short incubation times (< 5 min) did not result in visible pattern that can be interpreted for successful antigen detection. The gold nanoparticles and antigen molecules do not undergo enough effective collisions at such short times. The gold nanoparticles get pushed to the droplet top by the evaporation flux before they had formed big enough clusters to be caught in the latex particles pores. The microbioassays show differentiable pattern for 15 min of incubation time. The smallest amount of gold nanoparticles coming to the top is registered after 30 minutes incubation, indicating that this is about the optimal incubation time, during which the major fraction of the Au nanoparticles have been included into aggregates large enough to prevent them from reaching the top surface during the evaporation.

Surprisingly, we consistently observed larger fraction of gold nanoparticle collection for the assays after 45 min incubation in comparison to the ones performed at smaller incubation times (see bottom row in Fig. 2.5). The difference between the positive and negative control assays becomes hard to visualize. Thus the assays seemed to deteriorate and free particles were released from the aggregates formed. We hypothesize that the detachment is caused by the thermal motion of the gold nanoparticles and the presence of a large pool of free surfactant (Tween-20) in the medium. The antibodies are physically adsorbed on the gold surface and can be pulled off partially during the thermal fluctuations on the large agglutinated gold particles. Once an antibody gets pulled off partially from the

nanoparticle surface, the surfactant molecules present in the droplet compete to adsorb at their place and prevent immunoglobulin re-adsorption. The danger of "over-incubating" the assays is significant for practical applications and will be investigated in the future due to its complex origins.

2.3.2. Gold and Latex Agglutination Microbioassay (GLAgg)

The GLAgg agglutination process involves more complex interactions in comparison to the GOAgg microbioassay. This assay includes agglutination of both the antibody conjugated latex microspheres and the antibody conjugated gold particles (Fig. 2.2). Aliquots of 10.0 μL latex and gold nanoparticle suspension were incubated for 15 min and 55 min to allow for completion of the agglutination processes. The droplets were then dispensed on the DEP liquid-liquid chip to follow the microseparation due to evaporation. We observed similar gold nanoparticles collection pattern on top for a wider range of antigen concentrations (0.1 μg/mL ~ 10.0 μg/mL), regardless of the time during which droplets are incubated (Fig. 2.6). This was in contrast to GOAgg microassays, which only performed optimally for 30 min incubation at a concentration of 1.0 μg/mL. In addition to the lack of dark red spot, the latex particles do not collect effectively on the surface due to the formation of loose latex aggregates.

In contrast to the GOAgg microbioassays, the Gold and Latex Agglutination systems were not sensitive to the size of the latex particles. GOAgg assays with spheres 0.78 μm and larger were not successful because the large size interstices in the latex cap allowed even

aggregated gold nanoparticles to pass through. The GLAgg assays worked successfully with particles of 1.03 μm in size, because the gold nanoparticles are prevented from reaching the surface by binding rather than filtering in the cavities. A gold particle with antibody sites covered with antigen rising to the droplet surface can become attached to the latex particles collected in the top portion of the droplets via their antigen free antibody sites.

The comparison between the two assay formats leads us to the conclusion that the GLAgg microbioassays are less affected by incubation time and less responsive to analyte concentration. There are more antigen binding sites that can adsorb more antibodies before saturating. In addition, the gold particles in GLAgg microbioassays have low probability of making it to the top surface of latex particles cap even if the cavities between the particles are larger than that in the GOAgg assays.

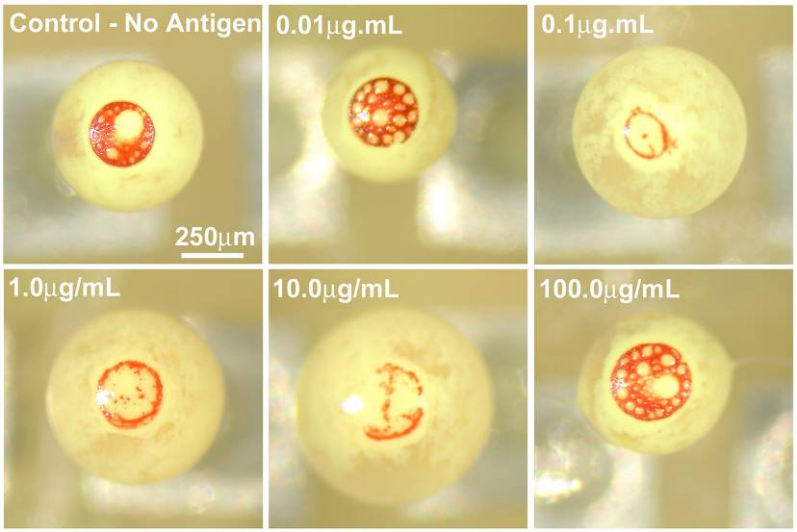

Figure 2.6. Optical micrographs of droplets with GLAgg assays at increasing antigen concentrations.

In summary, the results point out that the rapid and reliable detection in these assays depends on the balance between incubation time and analyte concentration. GOAgg assays are simpler and are, in principle, more sensitive. The GLAgg microbioassays can give faster results and appear less prone to oversaturation in comparison to GOAgg format due to the presence of larger amount of antigen binding sites available on both types of particles.

2.3.3. Gold Only Agglutination Microbioassay (GOAgg) with Ricin Antibody

Assays based on goat anti-rabbit antibodies are a research standard, but they might not be a realistic enough simulation for practical toxin antigens. For this purpose we experimented with GOAgg bioassays based on gold nanoparticles coated with ricin antibody. The antibody was conjugated to the colloidal gold using the protocol given by Beesley.[23-26] The experiment was then conducted by the same protocol as for GOAgg microbioassays. This experiment also allowed us to evaluate the performance of the droplet assays to the one of the standard DOD hand held assays (HHA) operating on immunochromatographic principles.[1,27,28] The Ricin droplet microbioassays showed minimum gold nanoparticles collection for 1.0 μg/mL concentration at 30 min incubation time (Fig. 2.7). This correlates well with the results of GOAgg microbioassays made with goat anti-rabbit IgG conjugated gold. The hand held assays needed at least 10 μg/mL to yield positive results.

A summary of the evaluation of the Ricin droplet microbioassays and the conventional Hand Held Assays (HHA) is presented in Table 2.1. The droplet based assays take three times as much time as HHA to produce detection results. However, they have 10 times lower limit of detection (LOD) and are also 100 times more efficient in utilizing sample volume. These advantages make them suitable for analysis of biotoxin agents and forensic samples of microscopic volumes and low concentrations. Assays based on other antibodies for Ricin with higher sensitivity have been reported previously.[27,29,30] However, these assays use larger sample volumes in comparison to the droplet based microbioassay.

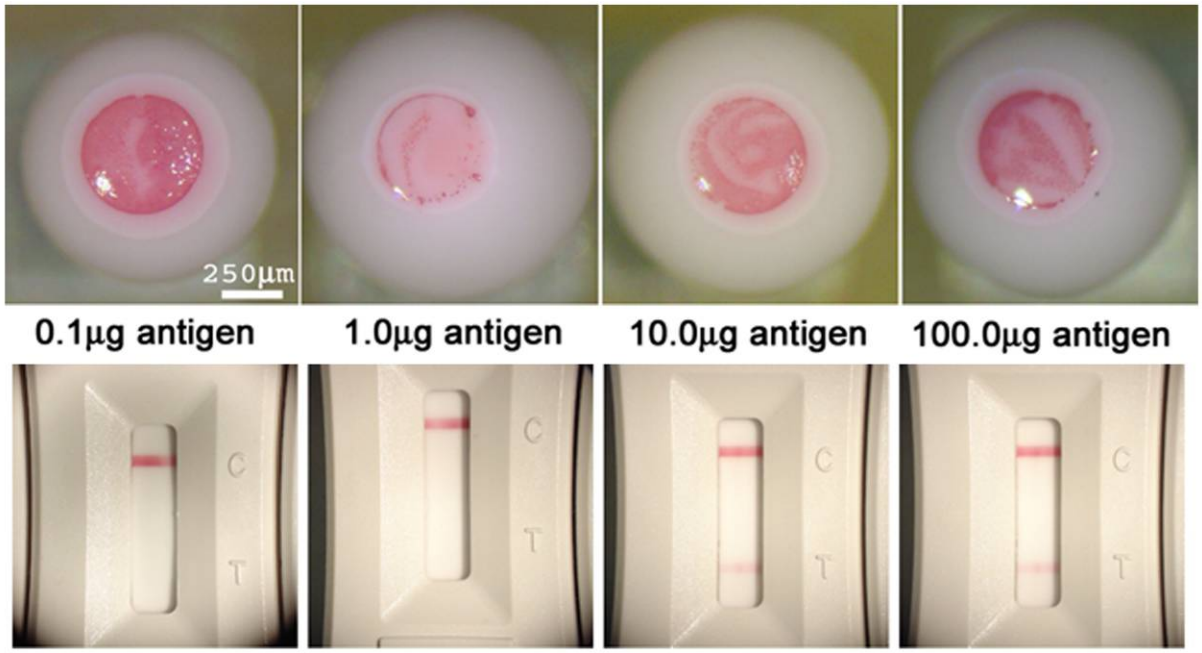

Figure 2.7. Comparison between optical micrographs of droplet GOAgg assay with Ricin as an antigen (top) and conventional Hand Held Assay for Ricin. 30 min incubation.

Table 2.1. Summary comparison between HHAs and droplet based microbioassays.

Parameter	Hand Held Assay	Droplet Based Assay
Incubation time	~15 min	~45 min
Volume of sample	> 100 μL	< 1.0 μL
Lower limit of detection	10.0 μg/mL	1.0 μg/mL

2.3.4. Factors affecting evaporation rate of droplets.

The speed of microseparation of particles in the top section of the droplets is controlled by evaporation. The microbioassays can provide faster results if the evaporation rate of droplets is increased. In order to facilitate the future improvement and optimization of the droplet assays, we investigated the effect of gold nanoparticle concentration, presence of Tween-20, background protein (BSA) concentration, and electric field intensity to the evaporation rate. Four sets of drying droplets were compared to examine the effect of Tween-20 and Au nanoparticles on evaporation rate (Fig. 2.8). The protocol for these experiments is detailed in the Methods section. The data indicate that the presence of surfactant assures a slower but more uniform drying of the droplets (compare Fig 2.8(a) with Fig 2.8(c), Fig 2.8(b) with Fig 2.8(d)). On the other hand, the gold nanoparticles strongly increased the evaporation rate in comparison to the surfactant (compare Fig 2.8(a) with Fig 2.8(b), Fig 2.8(c) with Fig 2.8(d)).

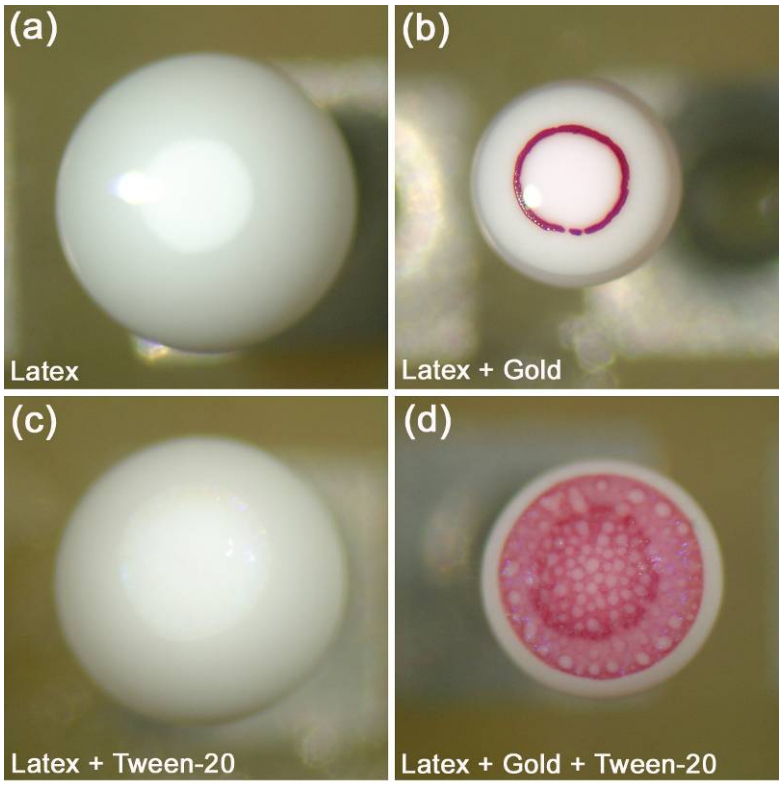

Figure 2.8. Micrographs of typical droplets, illustrating the effect of presence of gold nanoparticles and Tween-20 on the drying rate of droplets. (a) Latex only, (b) Latex and gold nanoparticles, (c) Latex and Tween-20, (d) Latex, gold nanoparticles and Tween-20. All droplets were allowed to evaporate for 65 minutes.

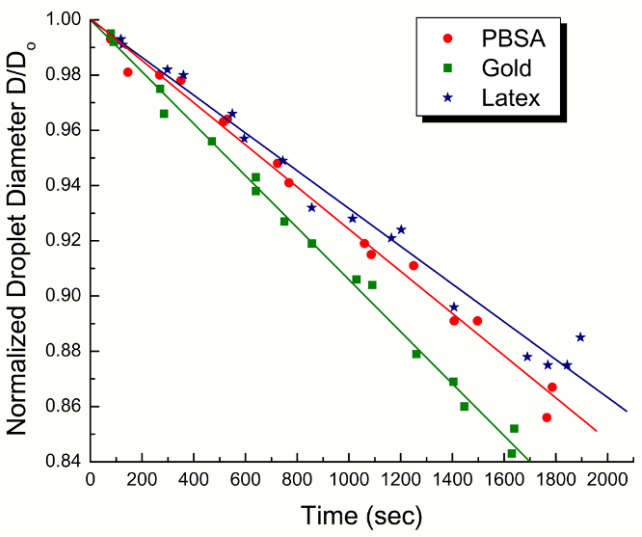

Figure 2.9. Droplet diameter variation with evaporation time for droplets containing different ingredients.

The gold nanoparticle effect on evaporation was examined quantitatively by measuring the diameter with time for three types of droplets (Fig. 2.9). The concentration of gold nanoparticles was kept the same as in GOAgg droplet bioassays. The normalized droplet diameter in all cases decreased approximately linearly with time. The difference in slope points out that droplets containing nanoparticles were evaporating faster in comparison to the PBSA and latex droplets. This supports the conclusion drawn from Figure 2.8 that the presence of gold nanoparticles increases the evaporation rate of droplets. The higher evaporation rate in the presence of nanoparticles is possibly a consequence of the deformation and corrugation of the surface by the layer of particles collected and pressed against it from the water side and the resulting higher area of evaporation. The results in

general point out that the concentration of nonionic surfactant and nanoparticles should be sustained constant in order to compare the results of the various assays.

Since the droplets are attracted to the underlying electrodes where the electric field intensity is high, it was also speculated that higher field intensities can pull down them down towards the electrodes and thus control the degree to which they protrude from the surfaces. This could change the size of the meniscus and the top open area where evaporation takes place. Droplets containing PBS were observed while varying the magnitude of electric field intensity in the operating range of 50,000 V/cm ~ 80,000 V/cm. Contrary to our hypothesis, however, we found that changing electric field intensity does not affect the droplet meniscus size in our system. The major factor in assay performance recognized so far is the dynamics of particle agglutination. The next section evaluates the particle aggregation dynamics for GOAgg microbioassay on the basis of modified agglutination theory and kinetic models available in the literature.

2.4. Model of Particle Agglutination Dynamics

The optimization of droplet microbioassays requires fast aggregation of antibody-coated particles to produce rapid detection results. We develop here a particle agglutination model to explain the binding dynamics of the biologically functionalized particles in the microbioassays. Several assumptions and modifications were made to existing theories to make this model simple yet versatile enough. The particles are

approximately spherical, so we can assume that the process is similar to reaction between spheres for which the rate constant can be expressed as

$$K = \frac{k_D \, k_R}{(k_D + k_R)} \tag{2.1}$$

where $k_D = 4\pi D R$ is the diffusion rate constant (R is the sum of the radii of reacting spheres, D is the relative diffusion constant) and k_R is the reaction constant, which characterizes the binding of the biomolecules on the particle surfaces.[31] Antigen-antibody binding reactions are specific and their rate is known to be rapid in comparison to the rate of diffusion.[32] However, for certain system geometries the binding process may be reaction limited. The ratio of the reaction control to the diffusion control in the binding process can be estimated by Damkohler number. It is defined as

$$D_a = \frac{R \, k_f \, \Gamma_o}{D_B} \tag{2.2}$$

where R is the radius of the gold nanoparticles in cm, k_f is the maximum forward reaction rate in ml/(mol-s) considering orientation and other rate limiting factors, Γ_o is the surface concentration of antibody sites on the gold nanoparticles in mol/cm^2 and D_B is the diffusion constant for antigen molecules in cm^2/s. For our system D_a = 0.6, which suggests that it is reaction limited. This reaction control, however, switches to diffusion control after a certain time interval (δ) which is defined as[33]

$$\delta = \frac{D_B}{(k_f \, \Gamma_o)^2} \tag{2.3}$$

For our system, δ is on the order of few milliseconds, which signifies that the aggregation (agglutination) process in our system is effectively diffusion controlled. Equation 1 for the aggregation kinetics then simplifies to

$$K = k_D = 4\,\pi\,(D_A + D_B)\,(r_A + r_B) \tag{2.4}$$

where k_D is given by Smoluchowski theory[33,34], r_A and r_B are the radius of reacting spheres. The diffusion constants of the spheres can be related to their radii by the Stokes-Einstein equation

$$D_A = \frac{k_B\,T}{6\,\pi\,\eta\,r_A} \text{ and } D_B = \frac{k_B\,T}{6\,\pi\,\eta\,r_B} \tag{2.5}$$

where η is the fluid viscosity, T is absolute temperature and k_B is the Boltzmann constant. Equation (4) can be rewritten as

$$k_D = k_{oe}\,f_r \tag{2.6}$$

where $k_{oe} = 8\,k_B\,T\,/\,3\,\eta$ is the universal rate constant for particles of equal radius and $f_r = (r_A + r_B)^2\,/\,4\,r_A\,r_B$ is the geometrical factor.

The aggregation process in the GOAgg microbioassay system takes place in two steps. The first step includes binding between antigen molecules and antibodies conjugated to gold particles. In the second step the antigen bound to an antibody site on one gold

particle binds with another free antibody site on another gold particle and binds the two gold particles together (Fig. 2.10).

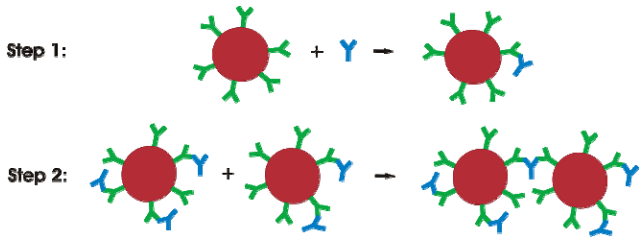

Figure 2.10. Schematics of two step model for aggregation of gold nanoparticles in the presence of antigen.

The diffusion rate constant mentioned in equation (6) takes into account only the translational diffusion of reacting spheres. It is accurate only when the surface of the sphere is completely covered with reactive sites and all collisions are fully effective. However, in our case the gold nanoparticles have an average of 10-12 antigen binding sites per particle available for biomolecular reaction. Even if the reactive sites of the particles come into contact during collision, they might not aggregate because of unfavorable orientation. Apart from rotational diffusion, steric factors and reactive site area need to be considered for the calculation of rate constant. For the first step of aggregation after steric factors are taken into account, the reaction rate constant is given as

$$k_{D1} = 4\,\pi\,D\,R\,r_B / 2\,r_A = k_{oe}\,\frac{1}{8}\left(\frac{r_B}{r_A}+1\right)^2 \qquad (2.7)$$

where $D = D_A + D_B$, $R = r_A + r_B$, r_B is the radius of the smaller reactant and r_A the radius of the larger particle.[33] For the second step we consider two spheres A and B, having reactive

sites described by parameters θ_A and θ_B respectively. θ is the ratio of the radius of reactive site on the particle and the particle radius itself. The diffusion rate constant in this case is given by[35]

$$k_{D2} = 4\,\pi\,D\,R\,\theta_A\,\theta_B\,(\theta_A + \theta_B)/8 \tag{2.8}$$

In our system $r_A = r_B$, hence $\theta_A = \theta_B = r_S / r_A$, where r_s is the radius of the reactive site, which corresponds to the radius of the area occupied by the IgG onto the surface of gold. The rate constant for the second step of aggregation can then be expressed as

$$k_{D2} = k_{oe} f_r \text{, where } f_r = \frac{1}{4}\left(\frac{r_s}{r_A}\right)^3 \tag{2.9}$$

Agglutination of two antibody-coated gold nanoparticles requires that an antibody site with bound antigen on one gold particle collides with an antigen-free antibody site on another gold nanoparticle. The rate of agglutination depends on the concentration of antigen, which in turn controls the number of antigen-bound and antigen-free antibody sites on the gold nanoparticles. The concentration of single gold nanoparticles not only changes via collision with other single gold nanoparticles but also via collision with bigger aggregates (doublets, triplets, etc.). For spherical particles of the same size, the concentration of any aggregate can be calculated using the theory of Smoluchowski as

$$[C_j] = [C]_o^{tot}\left(\frac{t}{\tau}\right)^{j-1}\left(1+\frac{t}{\tau}\right)^{-j-1} \tag{2.10}$$

$$\tau = \frac{2}{k_D [C]_o^{tot}} \tag{2.11}$$

$[C]_o^{tot}$ is the initial concentration of antibody conjugated gold nanoparticles (monomers), τ is the characteristic half-time of aggregation and k_D is the diffusion rate constant. The value of j varies as 1, 2, 3… corresponding respectively to monomers, dimers, trimers etc.[34-36] The theory assumes that the diffusion rate constant is the same for dimers, trimers and higher order aggregates. This is in contrast to what equation 9 suggests. However, this simplification does not affect our evaluations, as we are interested only in the formation of aggregates of second order (dimers).

To account for the probability of a successful binding collision leading to agglutination, the diffusion rate constant should include a collision frequency factor.[37,38] The collision frequency factor *P* can be estimated as follows

$$P = 2(\phi)(1-\phi) \tag{2.12}$$

where ϕ is the number of antibody sites with bound antigen molecules and $(1-\phi)$ is the number of antibody sites not bound to antigen molecules. After taking the collision frequency into account, we can calculate the corrected half time for aggregation as

$$\tau = \frac{2}{P\, k_D [C]_o^{tot}} \tag{2.13}$$

For a given value of the diffusion rate constant and initial concentration, the half time is minimal at maximal probability. The collision frequency factor has a maximum at the value of ϕ = 0.5 for 50% coverage of antibody sites by antigen on each particle.

Immunoglobulins are Y-shaped bi-functional structures, so each antibody site can bind two antigen molecules.[39] As mentioned before, on average there are 6 antibody sites on every gold nanoparticle, leading to a total of 12 antigen binding sites available on each gold nanoparticle. For maximum collision efficiency factor, the number of antigen binding sites covered is 6.

The values of the parameters used in the estimates are listed in the Appendix. The diffusion rate constant for the second process (particle collision) is two orders of magnitude lower than for the first one, suggesting that it is the rate limiting step for binding kinetics. After $3\,\tau_2$= 44.6 min, 94% of the gold nanoparticles in the solution form at least a dimer. The time of 44.6 min is close to the one observed in the experiments (30 min incubation followed by 20 min of drying). For 3.09×10^{17} particle/m^3 of gold nanoparticles, the concentration of antigen must be 1.854×10^{18} particle/m^3, which corresponds to an optimal antigen concentration of 0.5 μg/mL. This is close to the value of 1.0 μg/mL that we established in the experimental results.

The concentration of each type of gold nanoparticle aggregate (relative to initial antibody-coated gold nanoparticles concentration) is plotted with respect to time in Figure 2.11. As predicted by the aggregation half-time τ, the concentration of unaggregated antibody-coated gold nanoparticles (black curve) goes down to 6% of its initial value in about 45 min. For comparison we also plot the time evolution of the concentration of aggregates like dimers (red curve), trimers (green curve), tetramers (blue curve) and other higher order aggregates.

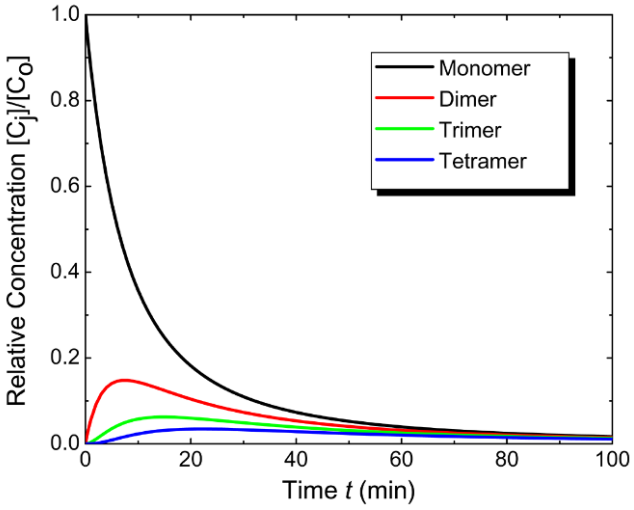

Figure 2.11. Concentration profiles of different types of aggregates relative to initial gold nanoparticle concentration (equations 2.10 and 2.13).

A comparison between the experimental results and the theoretically calculated values is given in Table 2.2. The agreement between experiments and theory suggests that the model can be used to predict the behavior of the microbioassays for any change in system parameters. This can be used for calculating the optimal particle concentration and minimal incubation times in designing future microbioassays, both in droplet on a chip or other formats. The applicability of the model to the case of Ricin was verified on the basis of the similarity in size and correspondingly in diffusion rates.[40,41]

Table 2.2. Comparison between experimental results and theoretical values for droplet microbioassays.

Parameter	Experimental value	Evaluated by theory
Incubation time	~ 50 min (30 min incubation, 20 min drying)	45 min
Optimum antigen concentration	1.0 μg/mL	0.5 μg/mL

Table 2.3. List of constants and variables used in the theoretical calculations

Concentration of gold nanoparticles $C_A = 3.09\times10^{17}$ particle/m^3
Molecular weight of immunoglobulin M_{IgG} = 160 kDa[30]
Antigen concentration $C_B = (C N_A)/(M_{IgG})$ where C is antigen concentration in μg/mL
$C_B = 3.764\times10^{18}$ particle/m^3 for C = 1.0 μg/mL
Radius of gold nanoparticles $r_A = 2.0\times10^{-8}$ m
Average radius of IgG[42] $r_B = 3.5\times10^{-9}$ m
Diffusion rate constant for first step $k_{D1} = 1.87\times10^{-18}$ m^3/s (Equation 1.7)
Diffusion rate constant for second step $k_{D2} = 1.45\times10^{-20}$ m^3/s (Equation 1.9)
Half time constant for first step of aggregation τ_1 = 0.564 sec
Half time constant for second step of aggregation τ_2 = 891.2 sec = 14.86 min

2.5. Concluding remarks

We show that microliter droplets captured by DEP can be used as containers for microscopic bioassays. The detection is based on agglutination of antibody functionalized

particles in the presence of antigen. We demonstrate two microbioassay formats based on the type of functionalized particles, Gold Only Agglutination (GOAgg) and Gold Latex Agglutination (GLAgg). The experiments prove that both assay formats can be used to detect antibodies as expected. GOAgg assay has lower limit of detection since only gold nanoparticles have binding sites available to consume antigen molecules but it requires longer time for detection and is oversaturated more easily. However, the antigen concentration threshold for oversaturation is higher than expected for both microbioassays, probably because of the slow mass transfer processes.

We describe the performance of the microbioassays as a function of several parameters including sample size, particle size, analyte concentration, limit of detection, incubation time and rate of evaporation. The results from the droplet microbioassays were compared with the ones from Hand Held Assays (HHA) obtained from Critical Reagents Program, DOD in terms of incubation time, sample volume and lower limit of detection (Table 2.1). The HHA needed three times less time for result read-out. On the other hand the lower limit of detection for GOAgg assays was also found to be 10 times better, 1.0 μg/mL as opposed to 10.0 μg/mL needed for HHA. The microbioassays consumed 100 times less sample volume than HHAs. Efficient usage of sample makes it a viable immuno-detection method for biological defense applications, with a tradeoff in terms of testing time.

We matched the results against a model of particle aggregation kinetics developed on the basis of the kinetic theory of agglutination by Smoluchowski using rate constants provided in the literature. The calculations for the aggregation time of particles using this

model were in good correlation with the experimental values (Table 2.2). The calculated antigen concentration was of the same order as the ones observed in experiments. The quantification of the agglutination and detection process can in the future be improved by measurement of the amount of nanoparticles on the droplet surfaces by image processing. By identifying the experimental conditions conducive to efficient detection in the assays and developing a model that could predict the kinetic response we make possible the further development of efficient microbioassays on a chip.

2.6. Acknowledgements

This research was supported by the US Army Research Office. We are thankful to Stephen Lee and the DOD CRP program for providing realistic antibodies and antigens. We thank Suk Tai Chang for valuable discussions and Brian Prevo for assistance with SEM imaging.

2.7. References

1. C. L. Baylis, in *Detecting pathogens in food*. (T. A. McMeekin, CRC Press LLC, 2004), pp. 217-240.

2. L. B. Bangs. New developments in particle-based immunoassays: Introduction. *Pure and Applied Chemistry*, (1996), **68** (10), 1873-1879.

3. P. Andreotti, W C. Immunoassay of infectious agents. *Biotechniques*, (2003), **35** (4), 850-859.

4. Z. G. Wang, H. Shang, G. U. Lee. Nanoliter-scale reactor arrays for biochemical sensing. *Langmuir*, (2006), **22** (16), 6723-6726.

5. J. A. Molina-Bolivar, F. Galisteo-Gonzalez. Latex Immunoagglutination Assays. *Polymer Reviews*, (2005), **45** (1), 59 - 98.

6. L. B. Bangs, M. T. Kenny. Old, New, Borrowed, Blue. *Industrial Research*, (1976), **18** (8), 46-49.

7. G. E. M. Tovar, A. Weber, in *Dekker Encyclopedia of Nanoscience and Nanotechnology* J. A. Schwarz, C. I. Contescu, K. Putyera, Eds. (Marcel Dekker, 2004), vol. 1, pp. 277-286.

8. C. R. Lowe, B. Hin, D. C. Cullen, S. E. Evans, L. D. G. Stephens, P. Maynard. Biosensors. *Journal of Chromatography*, (1990), **510** 347-354.

9. E. P. Meulenberg, W. H. Mulder, P. G. Stoks. Immunoassays for Pesticides. *Environmental Science & Technology*, (1995), **29** (3), 553-561.

10. L. B. Bangs. Latex Immunoassays. *Journal of Clinical Immunoassay*, (1990), **13** (3), 127-131.

11. H. A. Stone, S. Kim. Microfluidics: Basic issues, applications, and challenges. *Aiche Journal*, (2001), **47** (6), 1250-1254.

12. H. A. Stone, A. D. Stroock, A. Ajdari. Engineering flows in small devices: Microfluidics toward a lab-on-a-chip. *Annual Review of Fluid Mechanics*, (2004), **36** 381-411.

13. S. K. Cho, H. J. Moon, C. J. Kim. Creating, transporting, cutting, and merging liquid droplets by electrowetting-based actuation for digital microfluidic circuits. *Journal of Microelectromechanical Systems*, (2003), **12** (1), 70-80.

14. V. Srinivasan, V. K. Pamula, R. B. Fair. An integrated digital microfluidic lab-on-a-chip for clinical diagnostics on human physiological fluids. *Lab on a chip*, (2004), **4** (4), 310-315.

15. F. Su, K. Chakrabarty, R. B. Fair. Microfluidics-based biochips: Technology issues, implementation platforms, and design-automation challenges. *IEEE Transactions on Computer-Aided Design of Integrated Circuits and Systems*, (2006), **25** (2), 211-223.

16. O. D. Velev, K. Bhatt, B. G. Prevo, S. O. Lumsdon. On-chip dielectrophoretic manipulation and assembly of nanoparticles, microparticles and droplets. *Abstracts of Papers of the American Chemical Society*, (2003), **226** U479-U479.

17. O. D. Velev, K. H. Bhatt. On-chip micromanipulation and assembly of colloidal particles by electric fields. *Soft Matter*, (2006), **2** (9), 738-750.

18. O. D. Velev, B. G. Prevo, K. H. Bhatt. On-chip manipulation of free droplets. *Nature*, (2003), **426** (6966), 515-516.

19. S. T. Chang, O. D. Velev. Evaporation-induced particle microseparations inside droplets floating on a chip. *Langmuir*, (2006), **22** (4), 1459-1468.

20. J. R. Millman, K. H. Bhatt, B. G. Prevo, O. D. Velev. Anisotropic particle synthesis in dielectrophoretically controlled microdroplet reactors. *Nature Materials*, (2005), **4** (1), 98-102.

21. L. B. Bangs. Particle-based tests and assays - Pitfalls and problems in preparation. *American Clinical Laboratory*, (1990), **9** (4), 16-17.

22. J. Turkevich. Collidal Gold. Part II. *Gold Bulletin*, (1985), **18** (4), 125-131.

23. J. E. Beesley, *Colloidal gold: a new perspective for cytochemical marking*. Microscopy Handbooks (Royal Microscopical Society, Oxford, England, 1989), vol. 17.

24. D. Malamud, J. W. Drysdale. Isoelectric Points of Proteins - Table. *Analytical Biochemistry*, (1978), **86** (2), 620-647.

25. P. G. Righetti, T. Caravaggio. Isoelectric points and molecular weights of proteins : A table. *Journal of Chromatography A*, (1976), **127** (1), 1-28.

26. J. Roth, *The protein A-Gold (pAg) Technique - A qualitative and quantitative approach for antigen localization on thin sections*. G. R. Bullock, P. Petrusz, Eds., Techniques in immunocytochemistry (Academic Press, London, 1982), vol. 1, pp. 107-134.

27. R.-H. Shyu, H.-F. Shyu, H.-W. Liu, S.-S. Tang. Colloidal gold-based immunochromatographic assay for detection of ricin. *Toxicon*, (2002), **40** (3), 255-258.

28. X. L. Sun, X. L. Zhao, J. Tang, J. Zhou, F. S. Chu. Preparation of gold-labeled antibody probe and its use in immunochromatography assay for detection of aflatoxin B1. *International Journal of Food Microbiology*, (2005), **99** (2), 185-194.

29. C. Lubelli, A. Chatgilialoglu, A. Bolognesi, P. Strocchi, M. Colombatti, F. Stirpe. Detection of ricin and other ribosome-inactivating proteins by an immuno-polymerase chain reaction assay. *Analytical Biochemistry*, (2006), **355** (1), 102-109.

30. H.-F. Shyu, D.-J. Chiao, H.-W. Liu, S.-S. Tang. Monoclonal Antibody-Based Enzyme Immunoassay for Detection of Ricin. *Hybridoma and Hybridomics*, (2002), **21** (1), 69-73.

31. K. Solc, W. H. Stockmayer. Kinetics of Diffusion-Controlled Reaction between Chemically Asymmetric Molecules. I. General Theory. *The Journal of Chemical Physics*, (1971), **54** (7), 2981-2988.

32. D. A. Dmitriev, Y. S. Massino, O. L. Segal. Kinetic analysis of interactions between bispecific monoclonal antibodies and immobilized antigens using a resonant mirror biosensor. *Journal of immunological methods*, (2003), **280** (1-2), 183-1202.

33. M. Stenberg, H. Nygren. Kinetics of antigen-antibody reactions at solid-liquid interfaces. *Journal of immunological methods*, (1988), **113** (1), 3-15.

34. D. F. Evans, H. Wennerstrom, *The Colloidal Domain : where Physics, Chemistry, Biology, and Technology meet*. Advances in interfacial engineering series (Wiley-VCH, New York, ed. 2, 1999), pp. 417-428.

35. O. G. Berg, P. H. Vonhippel. Diffusion-Controlled Macromolecular Interactions. *Annual Review of Biophysics and Biophysical Chemistry*, (1985), **14** 131-160.

36. J. M. Schurr, K. S. Schmitz. Orientation constraints and rotational diffusion in bimolecular solution kinetics. A simplification. *The Journal of Physical Chemistry*, (1976), **80** (17), 1934-1936.

37. R. Hogg. Collision efficiency factors for polymer flocculation. *Journal of Colloid and Interface Science*, (1984), **102** (1), 232-236.

38. V. K. Lamer. Filtration of Colloidal Dispersions Flocculated by Anionic and Cationic Polyelectrolytes. *Discussions of the Faraday Society*, (1966), (42), 248-&.

39. M. Quesada, J. Puig, J. M. Delgado, J. M. Peula, J. A. Molina, R. Hidalgo-Álvarez. A simple kinetic model of antigen-antibody reactions in particle-enhanced light scattering immunoassays. *Colloids and Surfaces B: Biointerfaces*, (1997), **8** (6), 303-309.

40. Radius of Ricin is c.a. 2.5 nm as compared to 3.5 nm for IgG. The diffusion rate for the first step is roughly 118 times larger than the rate of diffusion for second step. The antibody used to detect Ricin is also an immunoglobulin attached onto the gold nanoparticle surface. Hence our assumption of second step to be the rate limiting step is still valid and the model explains the dynamics of Ricin GOAgg assays.,

41. E. Rutenber, B. J. Katzin, S. Ernst, E. J. Collins, D. Mlsna, M. P. Ready, J. D. Robertus. Crystallographic Refinement of Ricin to 2.5-A. *Proteins-Structure Function and Genetics*, (1991), **10** (3), 240-250.

42. D. A. Handley, *Colloidal Gold: Principles, Methods and Applications*. M. A. Hayat, Ed., (Academic Press, San Diego, CA, 1989), vol. 1, pp. 1.

Chapter 3.

Synthesis of Light-Diffracting Assemblies from Microspheres and Nanoparticles in Droplets on a Superhydrophobic Surface*

* Partially based on Rastogi, Melle, Calderón, García, Marquez and Velev, *Advanced Materials*, 2008, 20, 4263-4268.

3.1 Introduction

Self-assembly of colloidal particles into crystalline arrays can be an effective tool for fabricating novel materials with advanced functionality. The colloidal periodicity at the micron and submicron length scales imparts light manipulation capability to these artificial structures in a manner similar to the one in natural opals. Properties such as long range ordering, maximal packing density, well defined pore size, and high surface to volume ratio make these assemblies usable in areas such as photonics,[1-13] optical diffraction[1,14,15], anti-reflective coatings,[3,16,17] sensing,[18,19] separation processes, catalysis[20,21] and anisotropic particle fabrication.[22]

Several methods have been devised to arrange organic or inorganic particles into well ordered arrays.[23] Some techniques assemble the colloidal particles into macroscopic spherical structures that can encapsulate proteins, cells, food flavours, drugs, and other functional components. Such structures have been named colloidosomes, supraparticles or supraballs.[24-26] The techniques for preparing supraparticles from monodisperse particle suspensions can be classified into two broad categories: Wet Self-Assembly (WSA) and Dry Self-Assembly (DSA). The WSA forms supraparticles by assembly inside or around droplet templates suspended in liquid media.[24,26-31] Examples of WSA include adsorption of particles on two-phase interfaces of emulsion droplets,[24,26,28-30,32,33] evaporation of floating colloidal suspension droplets[26] or organization of particles with the assistance of microwaves.[34] The WSA is problematic in regards to the subsequent use of assembled structures because of the need to extract them out of the liquid media, water or oil. The

drying of the oil trapped inside the supraparticle pores slows down the process and may pose environmental problems. WSA does not allow robust control over the final shape of supraparticles.

DSA encompasses methods for fabricating supraparticles using droplet templates dispensed on solid substrates. The oil removal step is avoided and the assembled structures can be easily collected without further processing. The drying of the droplet leads to colloidal crystal formation by slowly restricting the thermal motion of particles through reduction of free volume.[35-37] The shape of the dried colloidal crystal depends on the wettability of the substrate. Park *et al.* have developed a DSA technique to create an array of hemispherical colloidal crystals using an inkjet printing method.[37] Kuncicky *et al.* have shown that both the contact angle of the surface and the initial particle concentrations play an important role in determining the shape of colloidal assemblies.[35,36]

3.2. Experimental Section

Surfactant-free sulfate-stabilized polystyrene latex microspheres were purchased from Interfacial Dynamics Corp. (Portland, OR, USA). Deionized (DI) water was obtained from Millipore RiOs 16 reverse osmosis water purification systems (Bedford, MA, USA). 20 vol% latex particle suspensions in water were prepared by washing the latex particles twice with DI water and centrifuging them at 3000 g for 20 min. After decanting the supernatant, the latex particles were sonicated and mixed with DI water to obtain the desired volume fraction. The gold nanoparticles used for doping of the latex opal balls were

synthesized by reduction of $HAuCl_4$ with sodium citrate and tannic acid, which yielded suspensions of ~22 nm gold nanoparticles.[38] All chemicals were used as purchased from Fisher (Pittsburgh, PA) or Aldrich (Milwaukee, WI). The nanoparticle suspensions were concentrated 100-fold via centrifugation (1500 g for 10 min) in Millipore Biomax 5 centrifuge filters. Residual salts were washed by centrifuging DI water through the filters (1500 g for 10 min). The gold nanoparticles were further concentrated another 10-fold using the Marathon micro A microcentrifuge at 8500 g for 15 min. The final concentration of gold nanoparticles in the water suspensions studied was approx. 0.21 wt%. The precise nanoparticle concentrations were measured by UV/vis spectrophotometry at the gold nanoparticle surface plasmon resonance (SPR) peak. The position of the SPR peak for all samples remained constant at 522±1 nm, which is consistent with stable, unaggregated suspensions of 20-22 nm size particles.[39] The latex suspension was mixed in 1:1 volume ratio with 0.21 wt% gold nanoparticle suspension.

5.0 μL droplets containing the suspension of microspheres and gold nanoparticles were dispensed onto the super- hydrophobic substrate using an ultramicropipette (Eppendorf North America Inc., NY, USA). The droplets were allowed to dry at ambient temperature (22±1 °C) in a dry environment created using desiccant. Microseparation of particles due to evaporation in the droplets was monitored from the top using SZ61 (0.7-4.5× zoom) stereomicroscope (Olympus America Inc., NY, USA). Their images were captured at regular intervals using DSC-V1 Cyber-Shot digital camera (SONY, Japan) coupled with the microscope.

3.3. Results and Discussion

We report here a technique for colloidal assembly in droplets residing on superhydrophobic substrates, which yields better control over the final shape and creates supraparticles that are easily detached and ready-to-use. The results of this process are near-spherical and spheroidal supraballs in dry environment. Droplets of 5.0 μL from a concentrated suspension of latex particles are dispensed on a superhydrophobic substrate coated with low density polyethylene (LDPE).[40] LDPE was chosen because it is flexible, naturally hydrophobic and inexpensive. The surfaces were generated by coating LDPE sheets with a solution of LDPE pellets in a mixture of xylene and methyl ethyl ketone (correspondingly solvent and non-solvent). The purpose of the non-solvent is to increase the roughness and contact angle of the substrates. The LDPE substrate contact angles were in the range of 140°-150°. This enabled aqueous suspension droplets to assume near spherical shape, which led to the macroscopic casting of colloidal crystals (Fig. 3.1). We also used silicon nanowire (Si-NW) coated superhydrophobic substrates,[40] which had contact angle higher than 170° and virtually no contact angle hysteresis.

The droplet templates easily roll off such substrates due to their extremely high hydrophobicity and low contact angle hysteresis. Hence, artificial local pinning spots were created by scratching with a sharp needle on Si-NW substrates to anchor the droplets templates. We did not encounter this problem while working with LDPE substrates because of the measurable difference in their advancing and receding contact angle.[40] The cracks between the LDPE crystals on the substrate act as small pinning areas. These areas were

used to hold the droplets in place while letting them dry. The free volume available for the latex particles in the water droplets keeps decreasing due to solvent evaporation, hence the particles are forced to organize into close-packed microsphere crystals (inset of Fig. 3.1(a)). The droplets were continuously monitored during the drying process while illuminated with near-collimated beam of light. The surface of the drying droplets begins to display colored ring-like diffraction patterns within 15 minutes of dispensing the droplets. The colored rings appear because of the formation of colloidal crystals from latex spheres adjacent to the surface by concentration of the particles left behind by the evaporating water. A typical timeline of appearance of colored ring patterns in suspended droplets with latex spheres is presented in Figure 3.2 (a). We refer to these structures as “opal balls” due to their colorful appearance. After ca. 60 min almost all of the solvent has evaporated and a supraball with hexagonal close-packed crystal arrangement of polystyrene spheres is formed (inset in Fig. 3.1(a)). We dispensed multiple droplets on the same substrate and studied the shape of the final dried supraballs by imaging their top and side profiles. Their structure and resulting diffraction pattern are analyzed and discussed in the later part of this paper.

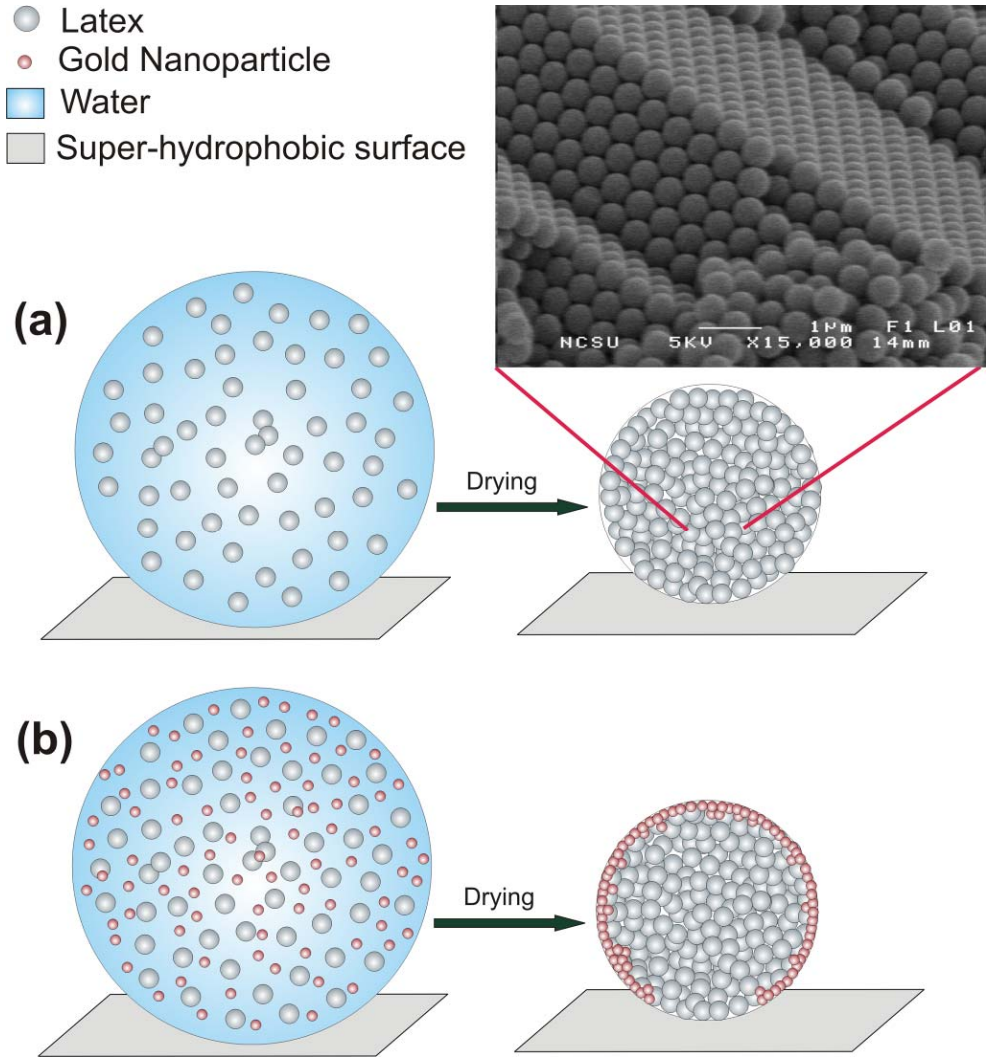

Figure 3.1. Schematics of the process for making spherical colloidal assemblies on superhydrophobic surface, (a) latex opal ball and (b) latex and gold opal ball. The inset is a SEM image displaying hexagonal close-packed structure of latex spheres inside an opal ball from 540 nm latex.

In the next step of the experiments, we made supraparticles from a mixed suspension of latex microspheres and gold nanoparticles. Since the gold nanoparticles are small enough to pass through the interstices of the latex particles, most of them are transported to the surface during to the solvent evaporation. Thus, the concentration of gold nanoparticles near the supraparticle surface increases over time. During the final stages of drying, the gold nanoparticle suspension dewets the latex microsphere network and forms clusters within some of the crystal domains on the supraparticle surface. Continuous monitoring with high magnification optical microscopy and SEM analysis of dried supraparticle surfaces (Fig. 3.3) provide evidence for the dewetting phenomena. The results point out that during the co-assembly process the gold nanoparticle aggregates are deposited in and around the voids in latex crystal network without altering the packing density of the latex spheres in the supraballs. The gold nanoparticle network does not change the structure or cover completely the latex crystal domains on the supraball surface, which retain similar coloured ring appearance as in the latex-only supraballs. The microsphere arrangement was analyzed by comparing scanning electron micrographs of latex opal balls (inset Fig. 3.1(a)) with latex and gold opal balls (Fig. 3.3). The presence of gold nanoparticles aids in observing high contrast colors on the surface of the assemblies (Fig. 3.2 (b) and (c)).

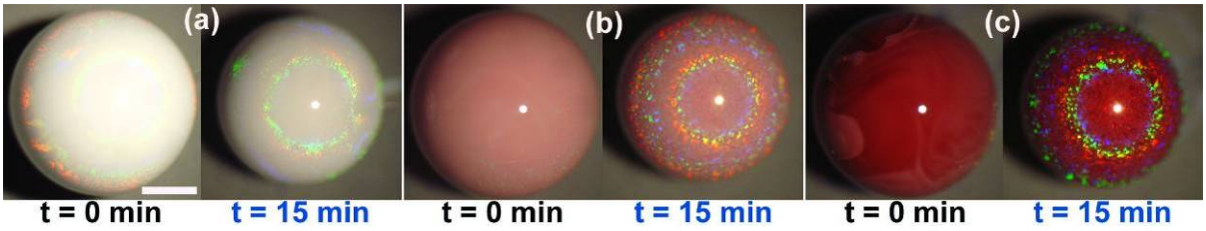

Figure 3.2. Timeline of formation of spherical opal assemblies on superhydrophobic Si-NW substrate. (a) latex, (b) latex and 0.1 wt% Au nanoparticles, and (c) latex and 1.0 wt% Au nanoparticles. The latex microsphere diameter is 540 nm in each droplet. The Au nanoparticle diameter is 22 nm. Scale bar is 500 μm.

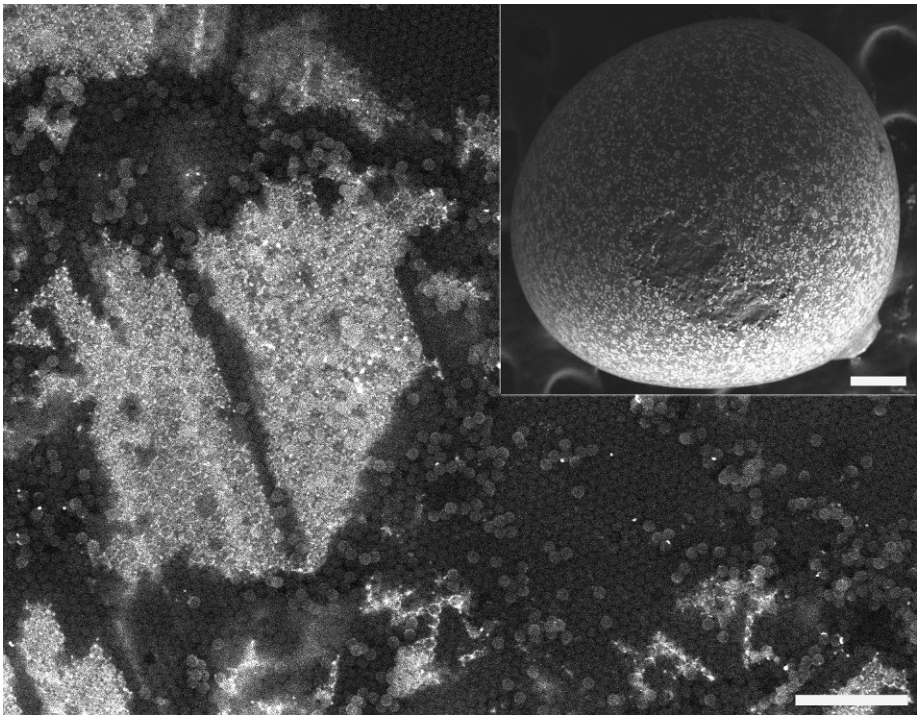

Figure 3.3. Scanning electron micrograph of the surface of a supraparticle made from a mixture of 540 nm latex and 22 nm gold nanoparticles. Dark spheres are latex and bright regions are clusters of gold nanoparticles. Scale bar is 5 μm. The inset is a SEM of the whole supraparticle with patches of gold scattered all over the surface. The scale bar in the inset is 200 μm.

A notable feature of these assemblies is that they sparkle in a multitude of colors. The colored domains are organized in series of concentric rings. The surface of the opal balls is made of localized crystal domains, which diffract light in different directions depending on the relative orientation of their crystal plane with respect to a fixed position light source and the opal ball. That is why the rings appear fragmented in domains of slightly different colors. We used different size latex particles to determine how their diameter affects both size and color of the diffraction rings on the surface of the supraballs. The diameters of the latex particles were 320 nm, 420 nm, 540 nm, 720 nm, 810 nm and 1000 nm (Fig. 3.4). These latex suspensions were also mixed with 0.21 wt% colloidal gold suspension in 1:1 volumetric ratio to make latex and gold opal balls (Fig. 3.5). The gold suspension dilutes the latex particles suspension by 50%, so the supraballs in Figure 5 are smaller than the ones in Figure 3.4. We observe reductions in the sizes of the colored rings on the supraball surface as the diameter of latex microspheres is increased from 420 nm to 1000 nm. The number of rings also increases with increasing latex diameter. The supraballs from 320 nm latex particles exhibit only one blue ring (Figs. 3.4 and 3.5), while supraballs with higher latex diameters produce blue, green, yellow and red rings.

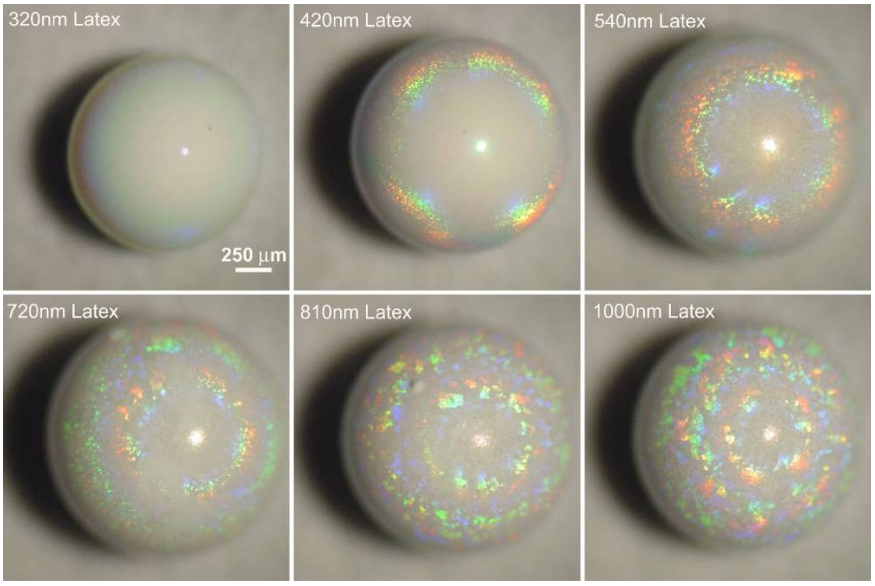

Figure 3.4. Optical micrographs of latex opal balls made of microspheres with varying sizes taken under identical illumination conditions.

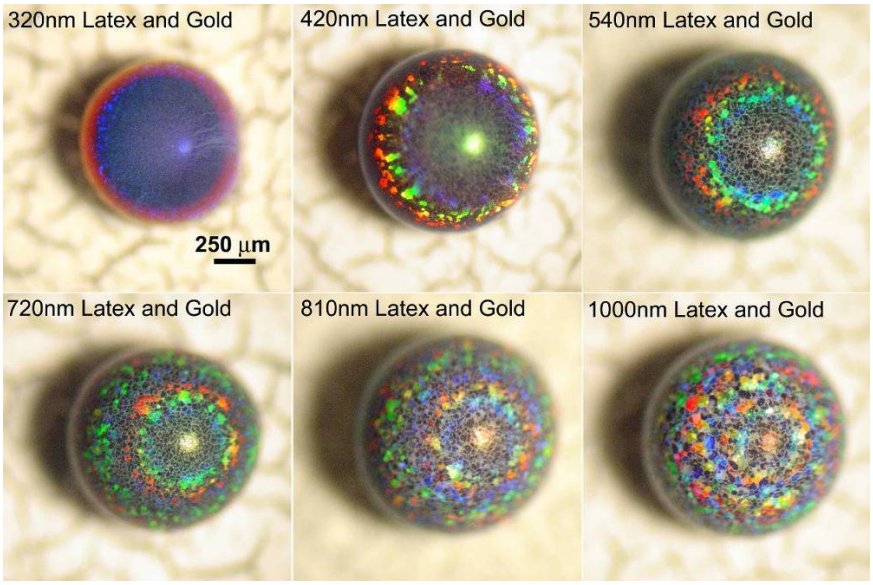

Figure 3.5. Optical micrographs of latex and gold nanoparticle opal balls containing microspheres of varying sizes as in Fig. 3.4.

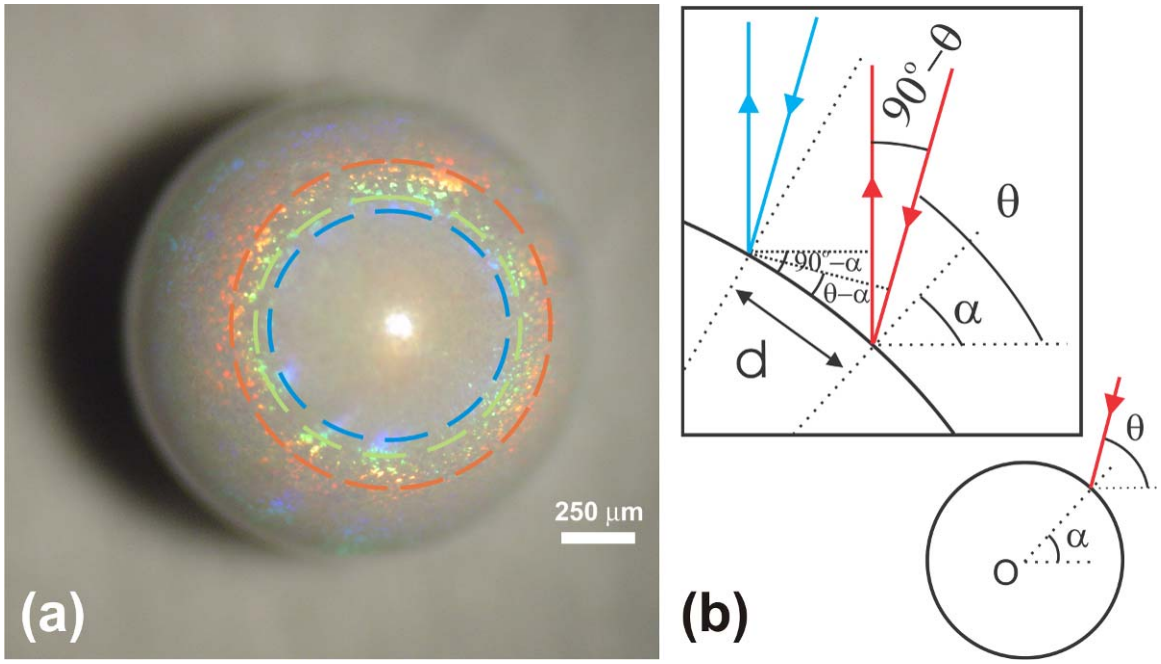

Figure 3.6. (a) Colored rings in the top view of a 540 nm latex opal ball; (b) Side view schematics of the angles used in the theoretical calculation of wavelength for a particular color ring.

We investigated the physical origin of the colored rings and their correlation with microsphere diameter and size of the supraballs. The commonly reported Bragg diffraction from in-depth parallel layers of colloidal crystals does not explain our experimental results. Instead, we considered how the rows of particles on the surface of the supraballs interact with the incident light to render Bragg type diffraction pattern. Interparticle spacing on the surface is varied by changing the size of the latex particles, which is analogous to changing groove density in a diffraction grating. Light waves reflected from two adjacent "grooves" (particle lines) on the supraparticle surface undergo constructive or destructive interference, depending on the path difference. The diffraction-reflection phenomenon occurs solely on the surface so the effective refractive index of the media is the same as air. The following formula for the path difference was derived from the geometry of the curved supraparticle surface (Fig. 3.6)

$$m\lambda = d \times [sin(90 - \alpha) + sin(\theta - \alpha)] \quad (3.1)$$

where m = 1, 2, 3 … for first, second, and third sets of rings, respectively. The wavelength, λ, of the specific spot on a colored ring and is estimated by comparing circular spots of 10 pixel diameter from the colored rings in the optical micrograph of the opal ball to the standard CIE 1931 chromaticity diagram.[41] d is the interplanar spacing for the colloidal crystal. The latex particles in the opal balls are arranged in the form of a FCC lattice with the (111) plane parallel to the outer interface.[42] The interplanar spacing for (111) planes is $d = \sqrt{2/3}D$ [43] (D is the diameter of latex particles). θ is the angle between the incident beam

direction and the horizontal plane (Fig. 3.6). The calculations for θ were done using two different geometrical methods. The first method takes into account the position of the shadow edge relative to the geometrical center of the supraparticle in the optical micrograph. Height and distance trigonometry formulae were applied using measurements from side and top profile images of the opal balls for determining θ. We also estimated θ from the relative position of the illuminator spot with respect to the geometric centre of the supraparticle. The values of θ obtained from both methods agree well with each other. For the images analyzed here θ takes a value close to 66º. The angle α (between the radial direction and the horizontal plane) is calculated using the position of the colored spot under consideration relative to the center of the supraball.

A qualitative inspection of Eq. (3.1) allows us to arrive to the following conclusions in agreement with the experimental observations (see Fig. 3.4). First, as we move further away from the position of the illuminator spot (which corresponds to m = 0, that is $\alpha - \theta = 90° - \alpha$) along the supraball surface, the path difference increases and thus shorter wavelength rings will appear closer to the illuminator spot. Second, an increase of latex particle size will lead to smaller diameter rings since the path difference should decrease proportionally to particle size. Note that the angular position of the rings (determined by α) will not be affected by the overall size of the opal balls. Opal balls with different sizes formed by latex particles of equal diameters will show the same pattern of diffraction rings. Indeed, identical coloured ring patterns formed in the experiment in supraballs of varying sizes synthesized from same diameter latex. The number of rings and their angular positions

(determined by α) in each supraball was similar regardless of their overall size, satisfying the conditions for same α values in Equation 3.1.

The numerical measurements of the reflected wavelengths allowed us to compare our experimental results with Eq. (3.1) in a more quantitative way. In Fig. 3.7 we plot the variation of the normalized path length $[sin(90-\alpha)+sin(\theta-\alpha)]$ with respect to the normalized wavelength $m\lambda/d$ for latex opal balls without Au nanoparticles. The experimental data follow a linear trend as predicted by Eq. (3.1) *without the use of any fitting parameter* (Fig. 3.7). All data points are scattered close to the $y = x$ line, which corresponds well with our theoretical estimates. This seems to indicate that the colors of the rings of the supraparticles arise from surface light diffraction and are independent of the internal structure.

The same type of optical analysis was done for the diffraction properties of latex and gold nanoparticle supraballs. The data for latex and gold nanoparticle balls match very well the diffraction grating theory in the same fashion as the latex opal balls (Fig. 3.7). The colored rings in latex and gold opal balls have exactly the same functional dependence on microsphere diameter and supraparticle size as the latex opal balls. This points out that the plasmon resonance of the gold nanoparticles on the surface does not affect the formation of the colored rings and corroborates our previous conclusion that the interparticle spacing in the latex crystal does not change in the presence of the Au nanoparticles. The presence of gold nanoparticles in the pores between the latex, however, attenuates the backscattering of light from the bulk leading to the blackish appearance of latex and gold opal balls. This unexpected result also proves in another way our assumption that there is no contribution

from bulk scattering inside the supraparticles in the development of colored rings. The nanoparticles simply enhance the visual attractiveness of the supraparticles by providing a dark background to create a better contrast for sharper visibility of the colored rings.

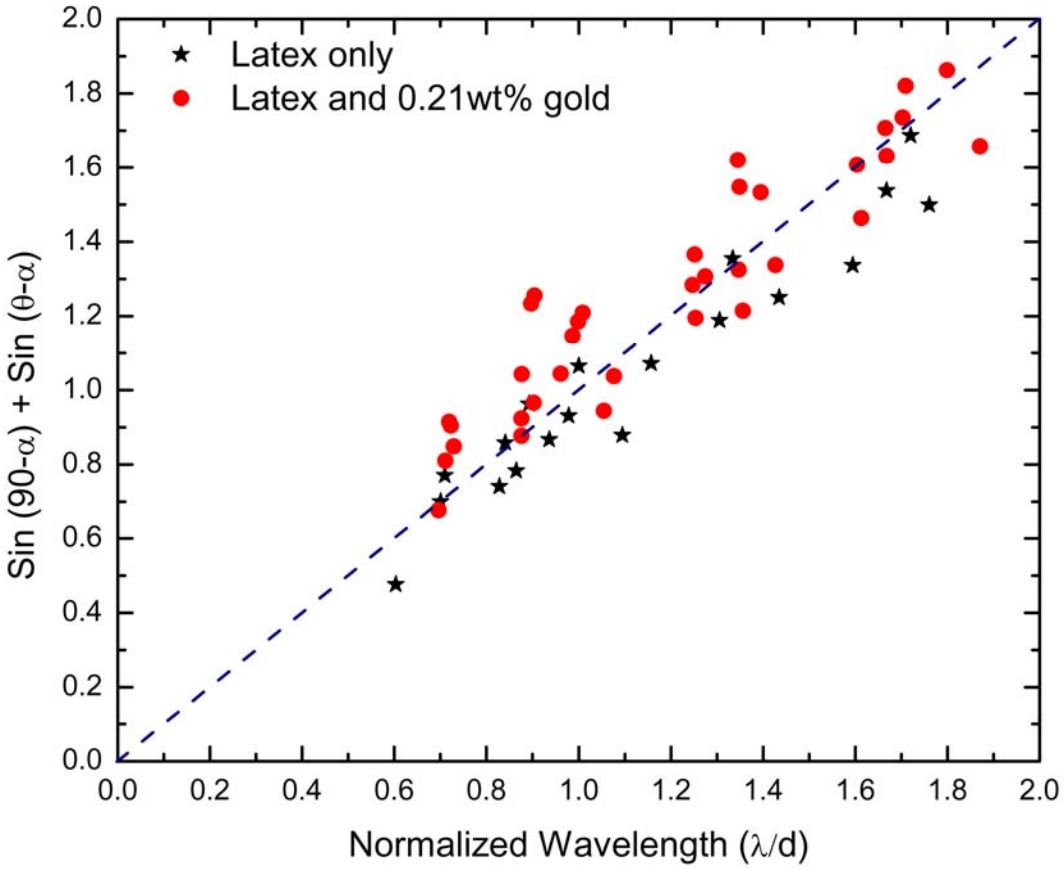

Figure 3.7. Normalized path difference versus the normalized wavelength for colored rings patterns in latex opal balls and latex/gold opal balls.

The method reported here is extremely easy to implement and avoids the oil removal step,[26] thus making the colloidal assemblies ready to collect and use. They can be easily detached from the substrate by gently tapping on the bottom of the superhydrophobic substrate. The dried spherical particle assemblies sometimes have a small flat area on the bottom due to the initial pinning of droplet templates. A detailed analysis of the evolution of the droplet shape is beyond the scope of this paper. A substrate with a higher degree of hydrophobicity and lower difference between advancing and receding contact angles can reduce the pinning area, thus minimizing deviation from spherical shape in colloidal particles assemblies. However, this poses the problem of holding the droplets in place during manual dispensing. One solution could be to use inkjet printing to dispense the droplets on a substrate with predefined pinning spots of minimal dimensions. The production of supraballs can be easily automated by continuous dispensing of droplets on one side of a LDPE crystal coated "conveyor belt" and collecting dried assemblies on the other side.

3.4. Conclusions

The opal balls do not disintegrate when exposed to water. The near spherical shape allows creation of discrete color bands upon exposure to collimated white light. Such particles can be used in decorative coatings. The well defined and uniform pore size of supraparticles can be used in applications such as drug delivery to provide slow controlled rate release of infused drug. The conjugation of the microsphere surface with enzymes before forming supraparticles or including live cells within the structure can be utilized in

the preparation of biocatalytic supports.[26] Magnetic functionality can be introduced in latex opal balls by adding magnetic nanoparticles to the initial latex suspension. We showed that nonuniform magnetic fields can pull the magnetic microparticles into the top hemisphere. Such anisotropic magnetic particles can be easily rotated and used, e.g., for mixing in microfluidic devices. The methods and the types of supraballs formed can be diversified much in future research. The supraballs that we assembled to date are of mm-scale diameter. Depending on the precision in metering of initial droplet volume and local substrate properties, supraballs produced in the same batch had a variation of 10% in shape and size. Further refinements are required for control of the final size of the supraparticles. Due to their close-packed structure, the latex spheres have maximum contact with their neighboring particles. However, the supraparticles still manifest brittleness due to low strength of van der Waals attraction at small contact areas between microspheres. This creates the need for further reinforcement procedures to increase mechanical stability of the structures.

In summary we demonstrate here a simple yet powerful technique that can be used in massively parallel manufacturing of diffracting particle assemblies in droplets suspended on superhydrophobic substrates. The reflection bands in the "opal balls" originate from diffraction by the parallel crystal rows on the surface, instead of bulk Bragg scattering. The presence of metallic nanoparticles in the structure does not lead to shift of the reflection band by plasmon resonance, but enhances the diffraction color by increased reflectance and suppressed backscattering. The uniform supraballs can find application in photonics, drug delivery, special coatings, sensors and microfluidics.

3.5. Acknowledgements

This research was supported by Interdisciplinary Network of Emerging Science and Technology (INEST). We gratefully acknowledge John Schneider (ASU) for preparing superhydrophobic substrates and Dr. Chuck Mooney (AIF, NCSU) for SEM imaging.

3.6. References

1. A. van Blaaderen. Opals in a New Light. *Science*, (1998), **282** (5390), 887-888.

2. P. V. Braun, S. A. Rinne, F. García-Santamaría. Introducing Defects in 3D Photonic Crystals: State of the Art. *Advanced Materials*, (2006), **18** (20), 2665-2678.

3. V. L. Colvin. From opals to optics: Colloidal photonic crystals. *Mrs Bulletin*, (2001), **26** (8), 637-641.

4. A.-P. Hynninen, J. H. J. Thijssen, E. C. M. Vermolen, M. Dijkstra, A. van Blaaderen. Self-assembly route for photonic crystals with a bandgap in the visible region. *Nat Mater*, (2007), **6** (3), 202-205.

5. J. D. Joannopoulos, P. R. Villeneuve, S. H. Fan. Photonic crystals: Putting a new twist on light. *Nature*, (1997), **386** (6621), 143-149.

6. C. Lopez. Three-dimensional photonic bandgap materials: semiconductors for light. *Journal of Optics a-Pure and Applied Optics*, (2006), **8** (5), R1-R14.

7. Y. Lu, Y. Yin, Y. Xia. Three-Dimensional Photonic Crystals with Non-spherical Colloids as Building Blocks. *Advanced Materials*, (2001), **13** (6), 415-420.

8. F. Meseguer. Colloidal crystals as photonic crystals. *Colloids and Surfaces A: Physicochemical and Engineering Aspects*, (2005), **270-271** 1-7.

9. D. J. Norris. Photonic Crystals: A view of the future. *Nat Mater*, (2007), **6** (3), 177-178.

10. R. Rengarajan, P. Jiang, D. C. Larrabee, V. L. Colvin, D. M. Mittleman. Colloidal photonic superlattices. *Physical Review B*, (2001), **64** (20), 205103.

11. G. Subramania, K. Constant, R. Biswas, M. M. Sigalas, K. M. Ho. Optical photonic crystals fabricated from colloidal systems. *Applied Physics Letters*, (1999), **74** (26), 3933-3935.

12. Y. A. Vlasov, V. N. Astratov, O. Z. Karimov, A. A. Kaplyanskii, V. N. Bogomolov, A. V. Prokofiev. Existence of a photonic pseudogap for visible light in synthetic opals. *Physical Review B*, (1997), **55** (20), R13357.

13. Y. Xia, B. Gates, Z. Y. Li. Self-Assembly Approaches to Three-Dimensional Photonic Crystals. *Advanced Materials*, (2001), **13** (6), 409-413.

14. H. Fudouzi, Y. Xia. Colloidal Crystals with Tunable Colors and Their Use as Photonic Papers. *Langmuir*, (2003), **19** (23), 9653-9660.

15. F. García-Santamaría, J. F. Galisteo-López, P. V. Braun, C. López. Optical diffraction and high-energy features in three-dimensional photonic crystals. *Physical Review B*, (2005), **71** (19), 195112.

16. B. Gates, Y. Lu, Z. Y. Li, Y. Xia. Fabrication and characterization of photonic crystals with well-controlled thickness and stop-band attenuation. *Applied Physics A-Materials Science & Processing*, (2003), **76** (4), 509-513.

17. S. I. Matsushita, Y. Yagi, T. Miwa, D. A. Tryk, T. Koda, A. Fujishima. Light propagation in composite two-dimensional arrays of polystyrene spherical particles. *Langmuir*, (2000), **16** (2), 636-642.

18. K. Burkert, T. Neumann, J. J. Wang, U. Jonas, W. Knoll, H. Ottleben. Automated preparation method for colloidal crystal arrays of monodisperse and binary colloid mixtures by contact printing with a pintool plotter. *Langmuir*, (2007), **23** (6), 3478-3484.

19. V. Rastogi, O. D. Velev. Development and evaluation of realistic microbioassays in freely suspended droplets on a chip. *Biomicrofluidics*, (2007), **1** (1), 014107-014117.

20. A. Cho. Connecting the Dots to Custom Catalysts. *Science*, (2003), **299** (5613), 1684-1685.

21. D. R. Rolison. Catalytic nanoarchitectures - The importance of nothing and the unimportance of periodicity. *Science*, (2003), **299** (5613), 1698-1701.

22. J. R. Millman, K. H. Bhatt, B. G. Prevo, O. D. Velev. Anisotropic particle synthesis in dielectrophoretically controlled microdroplet reactors. *Nature Materials*, (2005), **4** (1), 98-102.

23. O. D. Velev, A. M. Lenhoff. Colloidal crystals as templates for porous materials. *Current Opinion in Colloid & Interface Science*, (2000), **5** (1), 56-63.

24. A. D. Dinsmore, M. F. Hsu, M. G. Nikolaides, M. Marquez, A. R. Bausch, D. A. Weitz. Colloidosomes: Selectively permeable capsules composed of colloidal particles. *Science*, (2002), **298** (5595), 1006-1009.

25. V. Â N. Paunov, O. J. Cayre. Supraparticles and "Janus" Particles Fabricated by Replication of Particle Monolayers at Liquid Surfaces Using a Gel Trapping Technique. *Advanced Materials*, (2004), **16** (9), 788-791.

26. O. D. Velev, A. M. Lenhoff, E. W. Kaler. A class of microstructured particles through colloidal crystallization. *Science*, (2000), **287** (5461), 2240-2243.

27. V. N. Manoharan, A. Imhof, J. D. Thorne, D. J. Pine. Photonic Crystals from Emulsion Templates. *Advanced Materials*, (2001), **13** (6), 447-450.

28. O. D. Velev, K. Furusawa, K. Nagayama. Assembly of latex particles by using emulsion droplets as templates .1. Microstructured hollow spheres. *Langmuir*, (1996), **12** (10), 2374-2384.

29. O. D. Velev, K. Furusawa, K. Nagayama. Assembly of latex particles by using emulsion droplets as templates .2. Ball-like and composite aggregates. *Langmuir*, (1996), **12** (10), 2385-2391.

30. O. D. Velev, K. Nagayama. Assembly of latex particles by using emulsion droplets .3. Reverse (water in oil) system. *Langmuir*, (1997), **13** (6), 1856-1859.

31. K. P. Velikov, O. D. Velev, in *Colloidal particles at liquid interfaces,* B. P. Binks, T. Horozov, Eds. (Cambridge University Press, Cambridge, 2006), pp. 225-297.

32. S. M. Klein, V. N. Manoharan, D. J. Pine, F. F. Lange. Synthesis of spherical polymer and titania photonic crystallites. *Langmuir*, (2005), **21** (15), 6669-6674.

33. S. Melle, M. Lask, G. G. Fuller. Pickering emulsions with controllable stability. *Langmuir*, (2005), **21** (6), 2158-2162.

34. S. H. Kim, S. Y. Lee, G. R. Yi, D. J. Pine, S. M. Yang. Microwave-assisted self-organization of colloidal particles in confining aqueous droplets. *Journal of the American Chemical Society*, (2006), **128** (33), 10897-10904.

35. D. M. Kuncicky, K. Bose, K. D. Costa, O. D. Velev. Sessile droplet templating of miniature porous hemispheres from colloid crystals. *Chemistry of Materials*, (2007), **19** (2), 141-143.

36. D. M. Kuncicky, O. D. Velev. Surface-guided templating of particle assemblies inside drying sessile droplets. *Langmuir*, (2008), **24** (4), 1371-1380.

37. J. Park, J. Moon, H. Shin, D. Wang, M. Park. Direct-write fabrication of colloidal photonic crystal microarrays by ink-jet printing. *Journal of Colloid and Interface Science*, (2006), **298** (2), 713-719.

38. J. W. Slot, H. J. Geuze. A New Method of Preparing Gold Probes for Multiple-Labeling Cyto-Chemistry. *European journal of cell biology*, (1985), **38** (1), 87-93.

39. S. Link, M. A. El-Sayed. Size and temperature dependence of the plasmon absorption of colloidal gold nanoparticles. *Journal of Physical Chemistry B*, (1999), **103** (21), 4212-4217.

40. A. Egatz-Gómez, J. Schneider, P. Aella, D. Yang, P. Domínguez-García, S. Lindsay, S. T. Picraux, M. A. Rubio, S. Melle, M. Marquez, A. A. García. Silicon nanowire and polyethylene superhydrophobic surfaces for discrete magnetic microfluidics. *Applied Surface Science*, (2007), **254** (1), 330-334.

41. J. Orava, T. Jääskeläinen, J. Parkkinen, V. P. Leppanen. Diffractive CIE 1931 chromaticity diagram. *Color Research & Application*, (2007), **32** (5), 409-413.

42. S. C. Mau, D. A. Huse. Stacking entropy of hard-sphere crystals. *Physical Review E*, (1999), **59** (4), 4396 LP.

43. A. Richel, N. P. Johnson, D. W. McComb. Observation of Bragg reflection in photonic crystals synthesized from air spheres in a titania matrix. *Applied Physics Letters*, (2000), **76** (14), 1816-1818.

Chapter 4.

Anisotropic Particle Synthesis inside Droplet Templates on Superhydrophobic Surface*

* Partially based on Rastogi, García, Marquez and Velev, *Macromolecular Rapid Communications*, 2009 doi: 10.1002/marc.200900587

4.1 Introduction

Recent advances in the field of self-assembly have led to the development of multiple techniques for the fabrication of micro and nano sized particle aggregates. Droplet templated colloidal assembly is one of the most widely investigated techniques for large scale fabrication of hierarchical structures and special particles.[1-13] The implementations of this process can be categorized as either Wet Self Assembly (WSA) or Dry Self Assembly (DSA).[8] WSA is typified by the fabrication of highly ordered structures within droplets suspended in a second liquid phase immiscible with the liquid used to suspend the particles. The liquid entrained within the pores of particle assemblies has to be extracted to make them ready for further applications. Control over shape and size of the final assemblies is not easy to accomplish. The templating droplets in the second method, DSA, are deposited on solid substrates and dried in air.[4,7,14,15] The originally suspended colloidal particles assemble into close packed structures, whose final shape is dictated by the shape and transitions of the droplet during drying. An extensive research effort has been focused on understanding shape transitions of drying sessile droplets from colloidal suspensions on solid surfaces.[4,16-20] However, to our knowledge there has not been any development in fabricating anisotropic structures via droplet templates dispensed on superhydrophobic substrates. Hence, little is known of the underlying principles for the development of shape and composition anisotropy during such a process.

Recently we reported a method for the fabrication of light-diffracting assemblies using droplet templates on superhydrophobic substrates.[7] We now demonstrate how this

method can be modified to manufacture both shape-anisotropic and composition-anisotropic supraparticle structures. Shape anisotropy is demonstrated by fabricating "doughnut" assemblies using droplets containing both pure silica microspheres and silica suspensions mixed with gold nanoparticles, while composition anisotropy is achieved by redistribution of the magnetic nanoparticles inside template droplets containing mixtures of latex and magnetic particles. The nanoparticle redistribution and patterning is dictated by the pattern of the magnetic field that is applied while the droplet templates are drying. We also investigate and discuss the significance of the operational parameters, which lead to the development of shape and composition anisotropies in the resultant supraparticles.

4.2. Experimental Section

Monodisperse hydroxyl-stabilized silica microsphere suspensions were purchased from Bangs Laboratories Inc. (Fishers, IN, USA). The microsphere diameters were 330 nm, 540 nm and 1000 nm. Deionized (DI) water was obtained from Millipore RiOs 16 reverse osmosis water purification systems (Bedford, MA, USA). The 20 vol.-% silica microsphere suspensions in water were prepared by first washing the silica suspensions twice with DI water and centrifuging at 1100 g for 20 min. After decanting the supernatant, the silica microspheres were sonicated for 10 min and mixed with DI water to obtain the final volume fraction. The gold nanoparticles used for doping of the silica doughnut supraparticles were synthesized by reduction of $HAuCl_4$ with sodium citrate and tannic acid,[21] which yielded

suspensions of ~22 nm gold nanoparticles. All chemicals were used as purchased from Fisher (Pittsburgh, PA) or Aldrich (Milwaukee, WI).

The gold nanoparticle suspensions were concentrated 100-fold via centrifugation (1500 g for 10 min) using Millipore Biomax 5 centrifuge filters. Residual salts were washed by centrifuging DI water through the filters (1500 g for 10 min). The gold nanoparticles were further concentrated another 10-fold using a Marathon micro A microcentrifuge at 8500 g for 15 min. The concentration of synthesized gold nanoparticle suspensions was determined using UV/VIS spectrophotometry by observing the gold nanoparticle surface plasmon resonance (SPR) peak. The position of the SPR peak for all samples remained constant at 522±1 nm, which corresponds to unaggregated and stable suspensions of 20-22 nm size particles.[22] The final concentration of gold nanoparticles in the water suspensions studied was c.a. 0.21 wt.-%. The silica microspheres and gold nanoparticle suspension were then mixed at a 1:1 volumetric ratio.

Surfactant-free, sulfate-stabilized polystyrene latex microspheres (diameter = 1.0 μm) were purchased from Interfacial Dynamics Corp. (Portland, OR, USA). The 20 vol.-% latex microsphere suspensions were prepared using the same protocol as for silica microspheres. The centrifugation was done at 3000 g for 20 min. The magnetic Iron-Nickel alloy (Fe 55%, Ni 45%) nanoparticles were further coated with polysiloxane. To perform the coating process, 4 g of Fe/Ni powder was dispersed in a mixture of 40 mL ethanol and 10 mL tetraorthosilicate. An aliquot of 2.5 mL of 25% ammonium hydroxide was added dropwise to this suspension and stirred at regular intervals of 2 hours for 48 hours.

Suspended particles were centrifuged and washed three times with ethanol and three times with DI water. The final concentration was adjusted to 2 wt.-% by suspending the nanoparticles in DI water. The size of the magnetic particles was determined as 180 ± 20 nm using scanning electron microscopy. The latex and magnetic particle suspensions were mixed at a 1:1 volumetric ratio for the fabrication of so-called "patchy" magnetic supraparticles.

The rod magnets used to fabricate patchy magnetic supraparticles were obtained from Magcraft (National Imports LLC, Vienna, VA, USA). The magnets used for single patch and bi-patch magnetic supraparticles had the following specifications: diameter = 6.4 mm, length = 12.7 mm, and field strength = 0.5 Tesla. The tri-patch magnetic particles were fabricated using rod magnets with the following specifications: diameter = 3.2 mm, length = 12.7 mm, and strength = 0.5 Tesla. Multiple single patch magnetic supraparticles were manipulated on solid and liquid surfaces using a spherical magnet with a diameter of 12.7 mm and a strength of 0.5 Tesla. The magnetic field simulations were done using VIZIMAG software (http://www.vizimag.com).

Unless otherwise stated, 5.0 μL droplets containing the suspension of micro- and nanoparticles were dispensed onto a superhydrophobic substrate using an ultra micropipette (Eppendorf North America Inc., NY, USA). The substrates were prepared by coating low density polyethylene (LDPE) sheets with a solution of LDPE pellets dissolved in a mixture of xylene (solvent) and methyl ethyl ketone (anti-solvent).[23] All droplets were allowed to dry at ambient temperature (22±1 °C) under routine laboratory conditions. The assembly

process of particles due to evaporation in the droplets was monitored from the top, side, and at various angles using a SZ61 (0.7 - 4.5× zoom) stereomicroscope (Olympus America Inc., NY, USA). Optical micrographs were recorded at regular intervals using a DSC-V1 Cyber-Shot SONY digital camera attached to the microscope.

4.3. Results and Discussion

The shape of droplets suspended on surfaces is determined by the Bond number which is the ratio of gravitational to surfaces forces acting on the droplets,[24] $B_o = \left(\Delta\rho g r^2/\gamma\right)$. Here $\Delta\rho$ is the difference in the densities of droplet and the surrounding fluid, g is the acceleration due to gravity, r is the characteristic dimension (in our case droplet radius), and γ is the interfacial tension. All aqueous suspension droplets (5.0 μL volume) dispensed on superhydrophobic substrate assumed a near-spherical shape because of the unique combination of high contact angle with the superhydrophobic surface and low Bond number $(B_o = 0.61)$. Droplets containing silica and gold nanoparticles retain their shape during the initial stages of drying. However, in the later stages of drying, the top part of the droplet folded inward, which resulted in the templating of doughnut-like supraparticles (Fig. 4.1). Interestingly, this final stage shape transition was found to be dependent on initial particle volume fraction, microsphere diameter and substrate properties (e.g., advancing contact angle, contact angle hysteresis[4]). It appears that gold nanoparticles do not play a significant role in the formation of doughnuts since we were able to fabricate

silica-only doughnut particles with droplets at similar initial conditions. We performed a systematic study of the effect of process parameters on the formation of anisotropic structures in droplets containing colloidal silica spheres in order to learn more about the shape evolution of the doughnuts. The initial particle volume fraction was varied between 20% and 1.25% (e.g. 20%, 10.0%, 5.0%, 2.5%, and 1.25%), and silica nano/microsphere diameters of 330 nm and 1000 nm were selected.

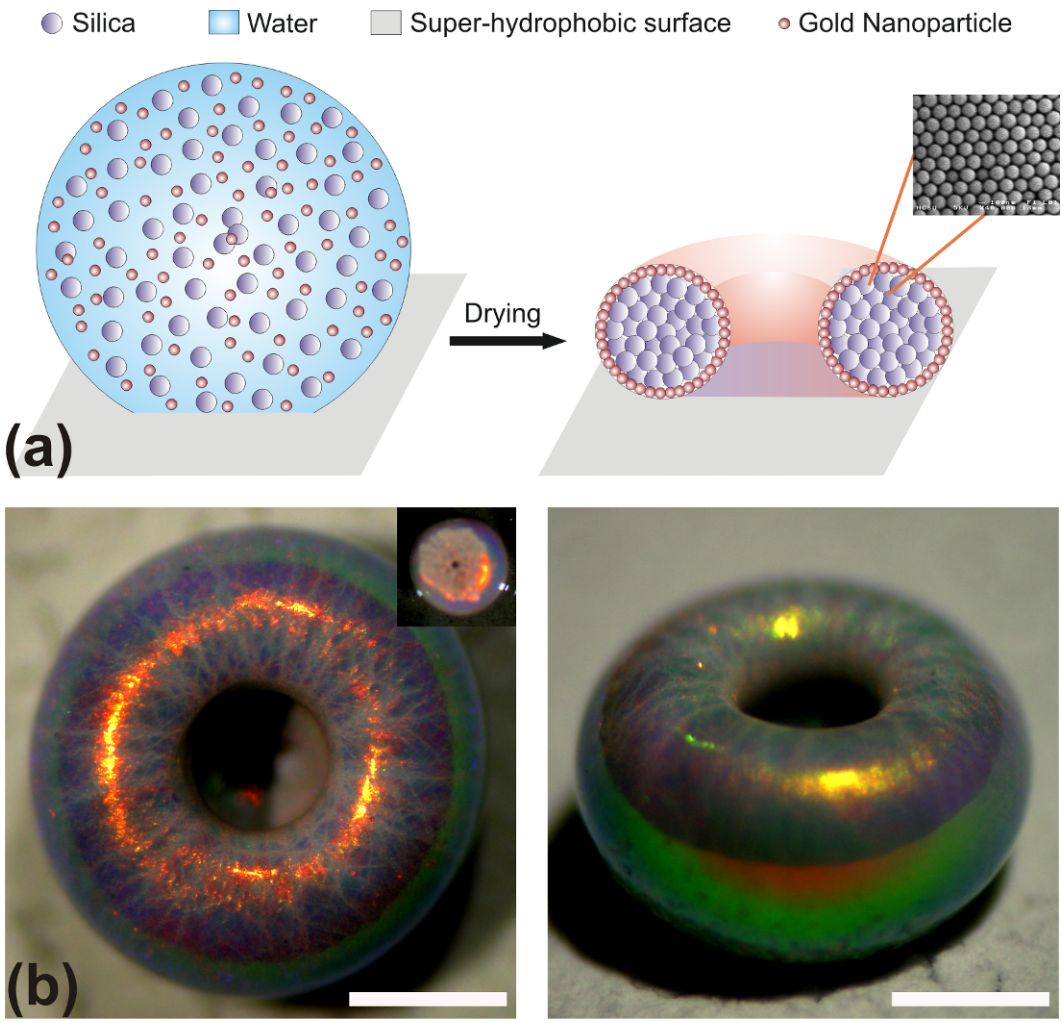

Figure 4.1. (a) Schematic of supraparticle formation by evaporating a droplet containing suspension of silica and gold nanoparticles. (b) Top and angled view of "golden doughnut" supraparticles fabricated from a droplet containing 330 nm diameter silica and 22 nm gold particles. The scale bars in both images correspond to 500 μm.

Colloidal particle redistribution drives the formation of the special shapes during the drying process. Evaporation leads to the formation of a spheroidal envelope of nano/microparticles at the exposed surface of the droplet.[25,26] The appearance of a colored diffraction pattern indicates that a close packed crystalline surface layer of microspheres is formed much before most of the solvent has evaporated.[7] The accumulation of particles leads to the formation of a boundary layer within the liquid envelope through which the concentration of nano/microspheres varies from ϕ_s (surface volume fraction) to ϕ_o (volume fraction in the bulk). The thickness of the boundary layer L_d is diffusion limited and grows with time as $L_d = (Dt)^{0.5}$, where D is the nano/microparticle diffusion coefficient and t is time. The rigidity of the shell increases drastically as ϕ_s reaches maximum packing concentration. Consequently, the droplet stops shrinking transversally, and the meridian radius R plateaus to a critical value R_c (Fig. 4.2).

The thickness and, in turn, rigidity of the shell depends on the initial volume fraction of the silica particles. Thus, the initial volume fraction directly controls the supraparticle shape. For very high initial volume fractions (> 15%) the shell is rigid enough to retain the droplet shape and there is no deformation. However, intermediate initial volume fractions (5% - 15%) lead to the formation of a relatively thin and elastic shell, which pins both at the periphery and at the three phase contact line, and the top portion undergoes introversion. The deformation, influenced significantly by the pressure gradient across the spheroidal shell, takes place in two steps similar to earlier reports for sessile droplets.[27] First the shell

flattens at the top and reverses in curvature at the center due to stretching. This happens because of pinning at the periphery and the inhomogeneous nature of the shell since it is thin and less rigid at the top as compared to the sides. The rate of evaporation from the infolded or concave portion is suppressed, which decreases the stiffness of the shell, allowing further deformation.

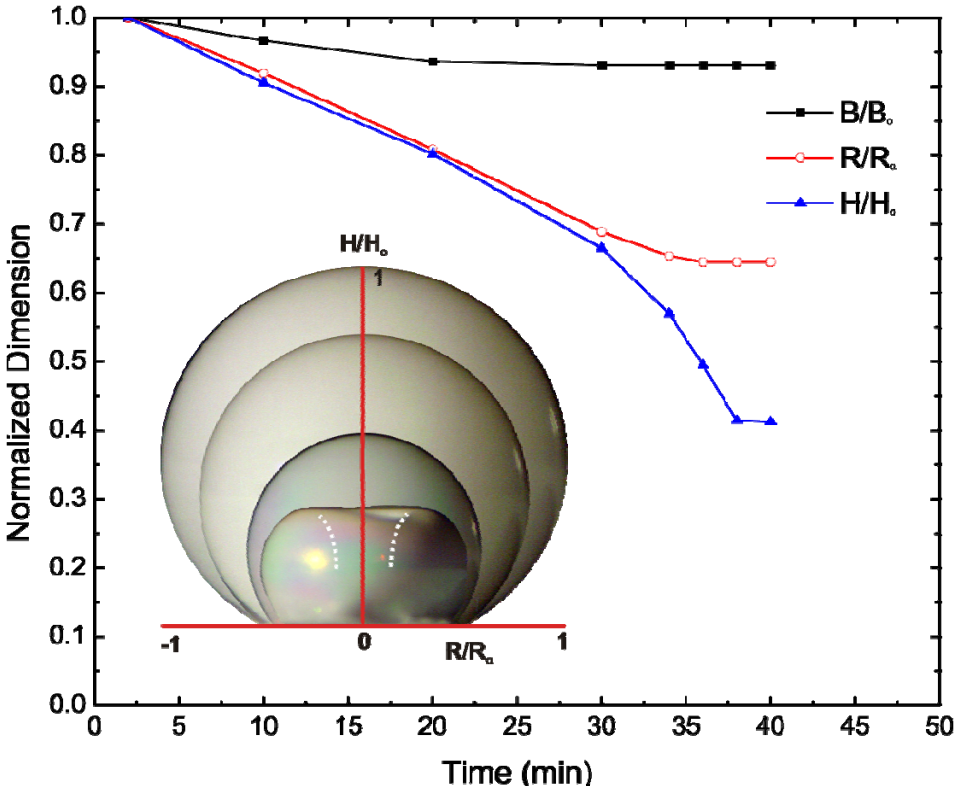

Figure 4.2. Evolution of dimensions recorded for a drying a droplet with 10% initial volume fraction of 330 nm diameter silica particles. Normalized diameter was calculated using the original dimension values at the time of dispensing the droplet. The parameters shown are as follows: *B* is the droplet base, *R* is meridian radius and *H* is the height. The inset shows an overlay of experimental images for the side-view profile of a drying droplet with silica particles over time.

A sharp decline in droplet height as compared to the meridian radius during the final stages of drying demonstrates the introversion leading to doughnut formation (Fig. 4.2). The internal pinning is a necessary condition for the formation of a doughnut-shaped assembly. For very low initial particle volume fractions, the drying process is akin to the process that results in the so-called "coffee ring effect".[16] The droplet pins only at the three phase contact line while the meridian is shrinking until it joins the base and dewets, thus producing ring-like structures. These structures were fragile and break when transferring them into a storage container (see Fig. 4.3a).

The effect of nano/microsphere diameter was investigated by fabricating supraparticles with suspensions of 330 nm and 1000 nm silica microsphere of varying initial particle volume fractions. Sedimentation effects dominated in the droplets containing 1000 nm particles as expected since they have a high Peclet number. The Peclet number is defined here as $Pe = (4\pi r_p^4 \Delta\rho g)/3kT$, and is used as a relative measure of sedimentation versus Brownian or thermal motion where r_p is the microsphere radius, $\Delta\rho$ is the difference in densities of microspheres and surrounding fluid, k is Boltzman constant and T is the temperature.[28] For the silica particles used $Pe \approx 10$, and the majority of the microspheres settled inside the droplet leading to dimpled supraparticles, unlike the well-developed doughnut structures formed using 330 nm microsphere suspensions (Fig. 4.3c and 4.3d). For both particle sizes, very high initial particle volume fractions (> 15%) do not lead to shape introversion because of the rigid nature of the shell (Figure 4.3e and 4.3j). The silica microsphere packing in the bulk of the final doughnut or spherical assemblies was found to

be uniform upon observations by scanning electron microscopy of broken particles. The inside of the particles at any point was typically made of multiple crystal domains with stacked layers of hexagonal microsphere organization.

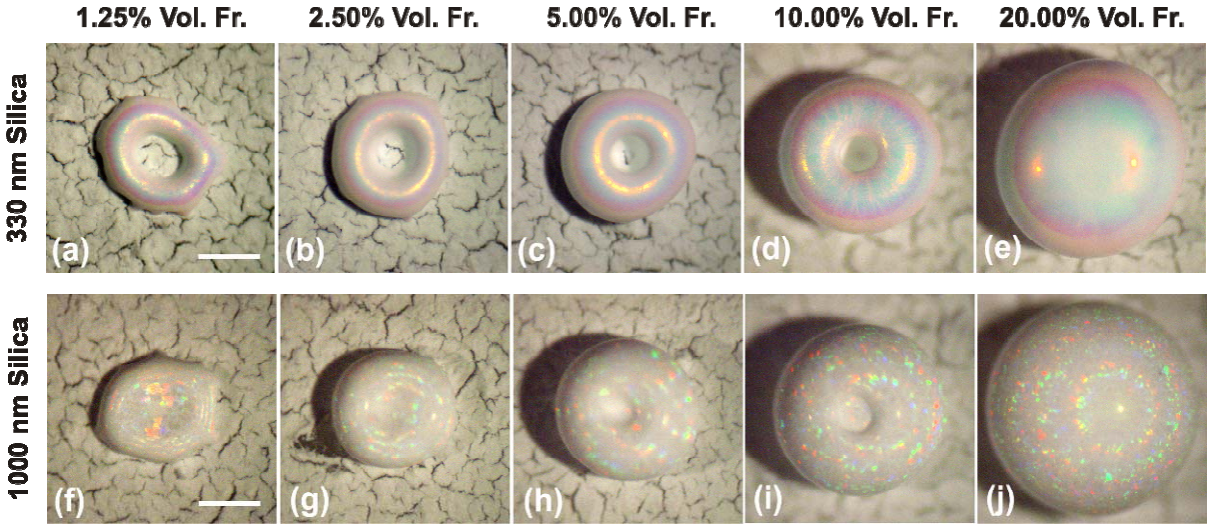

Figure 4.3. Top view optical micrographs of silica supraparticles fabricated from droplets with varying initial particle volume fractions. The scale bars in all images are 500 μm.

In summary, the formation of "doughnut" assemblies is facilitated by intermediate volume fractions of particles of larger size or higher density that do settle rapidly. An important difference between droplet drying on these superhydrophobic substrates, compared to normal surfaces where coffee ring formation or deformation of sessile droplets is observed[4,16-20] is that the pinning in our system is only a result of the internal formation of a dense particle structure in the lower side of the droplets. This pinning occurs in the absence of friction and anchoring to the underlying substrate. The lack of physical contact

and adhesion to the substrate allows easy detachment of the final assemblies from the substrate, which in turn makes possible the large-scale production of supraparticles.

Compositionally anisotropic particles were fabricated using a mixed suspension of 1000 nm diameter latex microparticles and magnetic (Fe55/Ni45) nanoparticles. We did not observe "doughnut formation" when these latex suspensions are dried on superhydrophobic surfaces. The reason is that their main component was latex microspheres (whose sedimentation rate is much smaller than silica); in addition, as we started at high initial latex volume fraction the assemblies did not deform during the relatively rapid formation process. However, by incorporating magnetic nanoparticles and subjecting the drying droplets to non uniform magnetic fields, the Fe/Ni nanoparticles can be clustered in specific regions of the resultant spherical supraparticles. The non-uniform magnetic fields were generated by a predefined planar pattern of rod like magnets (Fig. 4.4). The magnetic particles in such a field experience a magnetophoretic force $\vec{F}$ given by the following equation[29]

$$\vec{F} = \frac{V \cdot \Delta\chi}{\mu_o}\left(\vec{B} \cdot \nabla\right)\vec{B}$$

where V is the nanoparticle volume, $\Delta\chi = \chi_p - \chi_m$ is the difference in magnetic susceptibility between the magnetic nanoparticle (χ_p) and the surrounding medium (χ_m), and B is the magnitude of the external field. The particles only respond to inhomogeneous fields and are collected in the highest intensity areas defined by the field gradient.

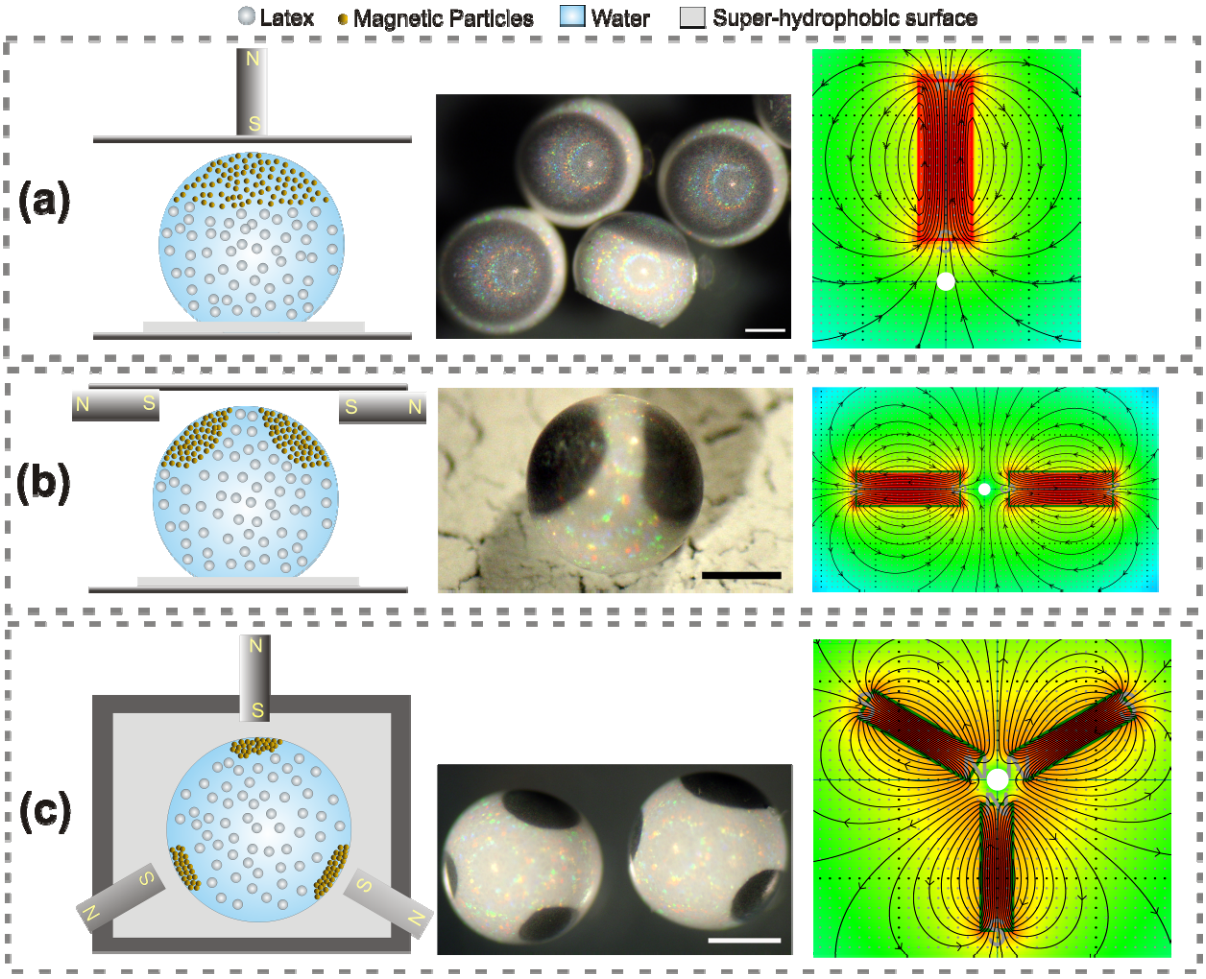

Figure 4.4. Schematics of the assembly configuration, optical micrographs and simulation patterns of applied external magnetic fields for (a) Single patch magnetic supraparticles, (b) bi-patch magnetic supraparticles, and (c) tri-patch or so-called "Mickey Mouse" magnetic supraparticles. The scale bars are 500 μm in length. The magnetic simulation pattern is drawn to scale; one square on the grid represents an area of 1 mm^2.

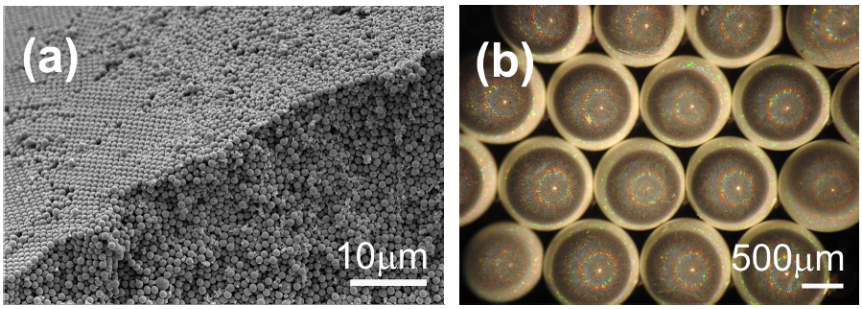

Figure 4.5. (a) Scanning electron micrograph on the surface of a supraparticle illustrating the junction of magnetic nanoparticle rich patch (right) with the bulk constituting of close packed latex microsphere arrays (left). (b) Close-packed array of multiple single-patch supraparticles on solid surface assembled by using remote magnetic manipulation.

Single patch magnetic supraparticles were fabricated using one magnet positioned at the top while the droplets were drying (Fig. 4.4a). Due to the magnetic force, the iron/nickel alloy nanoparticles collected at the top of the droplet. Once all of the solvent has evaporated, the redistributed particles within the droplets are trapped in place and result in the composite structures shown in Figure 4.4. The magnetic nanoparticles within the latex array can be observed by scanning electron microscopy (Fig. 4.5a). The resultant magnetic supraparticles allow their easy manipulation and assembly thanks to their anisotropy. For example, by placing multiple single-patch magnetic supraparticles in a Petri dish and subjecting them to non-uniform magnetic field of a rod magnet, we could organize the supraparticles into hexagonal close-packed structures (Fig. 4.5b). The magnetophoretic force generated by the non-uniform externally applied magnetic field reversibly compresses the near-spherical single-patch supraparticles into an array. The single-patch supraparticles suspended in DI

water could also be manipulated using a spherical magnet. The assemblies can be easily translated, arranged into close packed structures, and rotated.

Bi-patch magnetic supraparticles were fabricated by symmetrically placing the drying droplet in between two rod like magnets in the horizontal plane with like poles facing each other (Figure 4.4b). Tri-patch "Mickey Mouse" magnetic supraparticles were fabricated by symmetrically placing the drying droplet in the center of three rod like magnets with their axes at an angle of 120° and in the same plane (Fig. 4.4c). The number of patches on such particles is only limited by the number of magnets that can be easily incorporated into various patterns around the drying template droplets.

Two-dimensional magnetostatic numerical simulations were performed to compare the results to the actual pattern of magnetic field lines in the drying droplets for each anisotropic supraparticle structure formed. The solution space was divided into three sub-domains: magnet, droplet and air. The geometry of the system is defined in a 2-D cross section side view when a single magnet is used (Figure 4.4a). A top view is used for the two and three magnet arrangements (Figure 4.4b and 4.4c). Relative dimensions in the simulation were drawn to scale and the color and field lines are based on the calculations performed using parameter estimates for our system. The number and orientation of the high magnetic field regions in the simulation results match very well the position and distribution of magnetic patches on the resulting supraparticles (Figure 4.4). More complex patchy particles can also be designed using this computer-aided, magnetostatic simulation.

4.4. Conclusions

We present a facile, droplet-based technique for the fabrication of anisotropic hierarchical colloidal assemblies. The method can be used to create assemblies with either shape or composition anisotropies. For the first time, the fabrication of doughnut assemblies and patchy magnetic supraparticles by using superhydrophobic surfaces is demonstrated. For the doughnut assemblies, the shape and the size of the final structures are shown to be dependent on the initial particle volume fraction, microsphere diameter and substrate properties. By using magnetic fields generated solely by permanent magnets and thus not requiring additional energy, magnetic nanoparticles can be sequestered within specific regions leading to well oriented and easily manipulated supraparticles.

The novel method is simple and efficient and can be scaled up by using relatively simple devices for continuous droplet generation and particle harvesting. For example, inkjet printing onto superhydrophobic substrates can be used to scale the process for industrial manufacturing through automation.[30] The superhydrophobic surfaces can be reused and no additional solvents are needed, thus minimizing environmental impact. The doughnut particles can be utilized as catalyst support due to their high surface area and hierarchical porosity. Single-patch magnetic particles have the potential to be utilized as remotely manipulated drug delivery vehicles with therapeutics infused in the well-defined pores of the latex matrices. Bi-patch and tri-patch magnetic supraparticles could potentially find application in microfluidic mixing[31] and as model systems to study the complex assembly of patchy anisotropic particles.[32]

4.5. Acknowledgements

This research was supported by the Interdisciplinary Network of Emerging Science and Technology (INEST) and Camille Dreyfus Teacher-Scholar Award. We gratefully acknowledge John Schneider (ASU) for preparing superhydrophobic substrates and Dr. Chuck Mooney (AIF, NCSU) for SEM imaging.

4.6. References

1. A. D. Dinsmore, M. F. Hsu, M. G. Nikolaides, M. Marquez, A. R. Bausch, D. A. Weitz. Colloidosomes: Selectively permeable capsules composed of colloidal particles. *Science*, (2002), **298** (5595), 1006-1009.

2. A. Imhof, D. J. Pine. Ordered macroporous materials by emulsion templating. *Nature*, (1997), **389** (6654), 948-951.

3. S. M. Klein, V. N. Manoharan, D. J. Pine, F. F. Lange. Synthesis of spherical polymer and titania photonic crystallites. *Langmuir*, (2005), **21** (15), 6669-6674.

4. D. M. Kuncicky, O. D. Velev. Surface-guided templating of particle assemblies inside drying sessile droplets. *Langmuir*, (2008), **24** (4), 1371-1380.

5. J. R. Millman, K. H. Bhatt, B. G. Prevo, O. D. Velev. Anisotropic particle synthesis in dielectrophoretically controlled microdroplet reactors. *Nature Materials*, (2005), **4** (1), 98-102.

6. R. Mukhopadhyay. Diving into droplets. *Analytical Chemistry*, (2006), **78** (5), 1401-1404.

7. V. Rastogi, S. Melle, O. G. Calderón, A. A. García, M. Marquez, O. D. Velev. Synthesis of Light-Diffracting Assemblies from Microspheres and Nanoparticles in Droplets on a Superhydrophobic Surface. *Advanced Materials*, (2008), **20** (22), 4263-4268.

8. K.-H. Roh, D. C. Martin, J. Lahann. Biphasic Janus particles with nanoscale anisotropy. *Nat Mater*, (2005), **4** (10), 759-763.

9. O. D. Velev, K. Furusawa, K. Nagayama. Assembly of latex particles by using emulsion droplets as templates .1. Microstructured hollow spheres. *Langmuir*, (1996), **12** (10), 2374-2384.

10. O. D. Velev, K. Furusawa, K. Nagayama. Assembly of latex particles by using emulsion droplets as templates .2. Ball-like and composite aggregates. *Langmuir*, (1996), **12** (10), 2385-2391.

11. O. D. Velev, A. M. Lenhoff, E. W. Kaler. A class of microstructured particles through colloidal crystallization. *Science*, (2000), **287** (5461), 2240-2243.

12. O. D. Velev, K. Nagayama. Assembly of latex particles by using emulsion droplets .3. Reverse (water in oil) system. *Langmuir*, (1997), **13** (6), 1856-1859.

13. K. P. Velikov, O. D. Velev, in *Colloidal particles at liquid interfaces,* B. P. Binks, T. Horozov, Eds. (Cambridge University Press, Cambridge, 2006), pp. 225-297.

14. D. M. Kuncicky, K. Bose, K. D. Costa, O. D. Velev. Sessile droplet templating of miniature porous hemispheres from colloid crystals. *Chemistry of Materials*, (2007), **19** (2), 141-143.

15. J. Park, J. Moon, H. Shin, D. Wang, M. Park. Direct-write fabrication of colloidal photonic crystal microarrays by ink-jet printing. *Journal of Colloid and Interface Science*, (2006), **298** (2), 713-719.

16. R. D. Deegan, O. Bakajin, T. F. Dupont, G. Huber, S. R. Nagel, T. A. Witten. Capillary flow as the cause of ring stains from dried liquid drops. *Nature*, (1997), **389** (6653), 827-829.

17. G. McHale, S. Aqil, N. J. Shirtcliffe, M. I. Newton, H. Y. Erbil. Analysis of droplet evaporation on a superhydrophobic surface. *Langmuir*, (2005), **21** (24), 11053-11060.

18. F. Parisse, C. Allain. Drying of colloidal suspension droplets: Experimental study and profile renormalization. *Langmuir*, (1997), **13** (14), 3598-3602.

19. R. G. Picknett, R. Bexon. Evaporation of Sessile or Pendant Drops in Still Air. *Journal of Colloid and Interface Science*, (1977), **61** (2), 336-350.

20. Y. Zhang, S. Yang, L. Chen, J. R. G. Evans. Shape changes during the drying of droplets of suspensions. *Langmuir*, (2008), **24** (8), 3752-3758.

21. J. W. Slot, H. J. Geuze. A New Method of Preparing Gold Probes for Multiple-Labeling Cyto-Chemistry. *European journal of cell biology*, (1985), **38** (1), 87-93.

22. S. Link, M. A. El-Sayed. Size and temperature dependence of the plasmon absorption of colloidal gold nanoparticles. *Journal of Physical Chemistry B*, (1999), **103** (21), 4212-4217.

23. A. Egatz-Gómez, J. Schneider, P. Aella, D. Yang, P. Domínguez-García, S. Lindsay, S. T. Picraux, M. A. Rubio, S. Melle, M. Marquez, A. A. García. Silicon nanowire

and polyethylene superhydrophobic surfaces for discrete magnetic microfluidics. *Applied Surface Science*, (2007), **254** (1), 330-334.

24. H. M. Princen, in *Surface and Colloid Science,* E. Matijevic, Ed. (Wiley, New York, 1969), vol. 2, pp. 1-84.

25. S. T. Chang, O. D. Velev. Evaporation-induced particle microseparations inside droplets floating on a chip. *Langmuir*, (2006), **22** (4), 1459-1468.

26. D. A. Head. Modeling the elastic deformation of polymer crusts formed by sessile droplet evaporation. *Physical Review E (Statistical, Nonlinear, and Soft Matter Physics)*, (2006), **74** (2), 021601-021608.

27. L. Pauchard, Y. Couder. Invagination during the collapse of an inhomogeneous spheroidal shell. *Europhysics Letters*, (2004), **66** (5), 667-673.

28. W. B. Russel, D. A. Saville, W. R. Schowalter, *Colloidal Dispersions*. (Cambridge University Press, New York, 1989).

29. N. Pamme. Magnetism and microfluidics. *Lab on a chip*, (2006), **6** (1), 24-38.

30. H. Y. Ko, J. Park, H. Shin, J. Moon. Rapid self-assembly of monodisperse colloidal spheres in an ink-jet printed droplet. *Chemistry of Materials*, (2004), **16** (22), 4212-4215.

31. P. Tierno, T. H. Johansen, T. M. Fischer. Magnetically driven colloidal microstirrer. *Journal of Physical Chemistry B*, (2007), **111** (12), 3077-3080.

32. S. C. Glotzer, M. J. Solomon. Anisotropy of building blocks and their assembly into complex structures. *Nat Mater*, (2007), **6** (7), 557-562.

Chapter 5.

Microfluidic Characterization of Sustained Release from Porous Supraparticles*

* Partially based on Rastogi, Velikov, and Velev, *Physical Chemistry and Chemical Physics*, **to be submitted**

5.1 Introduction

Researchers have explored avenues of novel drug delivery based on liposomes[1-4], microbubbles[5-7], and solid and liquid nanoparticles.[8] Particulate drug delivery systems have received special attention since they offer a number of advantages as compared to the methods based on liposomes and micelles.[9,10] These systems present a range of parameters like well defined porosity, narrow size distributions, and size which can be easily controlled and in turn provide a handle over the release rate of administered drug from the system.[11] Particle based delivery techniques offer encapsulation of both hydrophilic and hydrophobic substances, small and large molecules, proteins and nucleic acids. Additionally they provide enhanced stability, high carrier capacity and the possibility of variable routes of administration, including oral application and inhalation.[12,13] Nanoparticles can be designed or assembled in hierarchical porous structures to allow controlled (sustained) drug release from the matrix.[1,9,12] The introduction of magnetic patches in the drug loaded porous particle carriers can transform them into remotely addressed vehicles, which can be transported in-vivo to the target site thus improving drug bioavailability and reduction of the dosing frequency.[11,14]

Researchers have reported various routes for fabricating porous supraparticles by self assembly of micro and nanoparticle, which can be classified into the categories of wet self assembly (WSA)[15-22] and dry self assembly (DSA)[23-25]. We recently reported a scalable DSA technique for the fabrication of three dimensional hierarchical porous assemblies of micro and nanoparticles inside droplet templates.[26] The control in the system parameters and

droplet composition allow production of assemblies with unique photonic, anisotropic and magnetic properties.[14,26] The infusion of well defined pore structure with a drug and introduction of magnetic patches in our supraparticles can transform them into remotely driven drug delivery vehicles.

Estimation and characterization of drug release rate from nanoparticle and micro particulate clusters in a live environment is an essential part of the drug design.[27] The rate of release of drug from particulate systems is dependent on a range of parameters which include porosity, particle size distribution, nature of the surrounding environment, affinity between drug and particle material, crystallinity of the system, volume of liquid surrounding the particle and loading concentration of drug. The conventional method used to monitor the release profile of drug from polymer matrices comprises of dispersing the drug-loaded particles in aqueous environment and then withdrawing samples at equal time intervals.[28] The concentration of the sample is measured using spectrophotometry and plotted against time to determine drug release profiles. However, the conventional method has a limitation on the number of parametric combinations that can be screened in a given amount of time. Such setup calls for constant manual effort or expensive robotic tools to carry out time-consuming intermediate steps.[29]

We report here a new microfluidic channel device based in-vitro method for the characterization of sustained release of dye (drug simulant) from polymeric supraparticles. Our technique overcomes the need for complex laboratory setup for regular sampling and measurements done in conventional evaluation of release profiles of drug from polymer

matrices. The operation of our microfluidic chip is demonstrated by exposing the dye-infused hierarchical porous assemblies to the solvent flow environment and performing colorimetric measurements on the dye release patterns. We also interpret the pattern of dye leaching in microfluidic channel based on two separate theoretical models available in literature.[30,31] Mass transfer modeling allows us to extend our understanding and analyze the release of drug from supraparticle carriers of varying porosity, size and chemistry.

5.2. Experimental Section

Surfactant-free, sulfate-stabilized polystyrene latex microspheres of 320 nm diameter were purchased from Interfacial Dynamics Corp. (Portland, OR, USA). Deionized (DI) water was obtained from a Millipore RiOs 16 RO water purification system (Bedford, MA, USA). The original latex suspension was washed twice with DI water followed by centrifugation at 3000 g for 20 min. After decanting the supernatant, the microspheres were sonicated for 10 min and diluted with DI water to adjust the final volume fraction (20% v/v). The Allura Red (AR) dye (Aldrich) was dissolved in DI water to prepare 5% w/v solution. A coating of polysiloxane was deposited around the magnetic Iron-Nickel alloy (Fe 55%, Ni 45%) nanoparticles. To perform the coating process, 4.0 g of Fe/Ni powder was dispersed in a mixture of 40 mL ethanol and 10 mL tetraorthosilicate. An aliquot of 2.5 mL of 25% ammonium hydroxide was added dropwise to this suspension and stirred for 48 hours. The suspended particles were centrifuged and washed three times with ethanol and three times

with DI water. Their final concentration in DI water was adjusted to 2% w/v. The size of the magnetic particles was determined as 180 ± 20 nm using SEM.

5.2.1. Fabrication of 'Dye Pellet' and 'Dye Infused Latex Supraparticle'

Suspension Mixture A for Dye Pellet (D-Pellet): The dye and magnetic particle suspensions were mixed at 9:1 volumetric ratio for the fabrication of dye pellet. Ultra micropipette (Eppendorf North America Inc., NY, USA) was used to dispense 2.5 µL droplets of the suspension mixture onto a silicon nanowire (Si-NW) coated superhydrophobic substrate.[32] A rod like magnet (National Imports LLC, Vienna, VA, USA) with a field strength = 0.5 Tesla was used to hold the drying dye droplets in place.

Suspension Mixture B for Dye Infused Latex Supraparticle (DIL-Supraparticle): The latex microsphere suspension, dye suspension and magnetic particle suspension were mixed in 9:9:2 volumetric proportions and 5.0 µL droplets of the mixture were dispensed onto a LDPE coated superhydrophobic substrate using an ultra micropipette.[32]

All droplets were allowed to dry at ambient temperature (22±1 °C) under routine laboratory conditions to fabricate supraparticles.

5.2.2. Fabrication of microfluidic channel network for release monitoring

The masters for the microfluidic channel devices were created by coating SU-8 2050 photoresist (MicroChem, Inc.) on a silicon wafer to a thickness of 600 µm using a spin-coater (Model P6700, Specialty Coating Systems, Inc.). The transparency photomasks

containing 500 μm wide channel designs were brought into contact with the SU-8 photoresist followed by UV exposure (Model B-100A, Black-Ray). After post-baking, the UV-exposed wafers were treated in SU-8 developer solution (MicroChem, Inc.) and hard-baked. The PDMS precursor (Sylgard 184, Dow Corning) was cast on the channel masters and cured at 70 °C. After peeling off the PDMS layers the channels were closed by a glass slide. The holes to connect the fluid inlet and outlet tubes were punched at each end of the channel using a blunt 16-gauge needle. The resulting microfluidic chips had a length of 36 mm, a width of 0.5 mm, and a height of 0.6 mm. The 3 mL syringe (Becton, Dickinson and Co.) used for pumping the DI water is attached to an 8-syringe pump (Model NE-1800, www.syringepump.com) and the syringe needle is connected to the inlet of microchannel using microbore tubing (TYGON S-54-HL, Saint-Gobain PPL. Corp.). The outlet of the microchannel is connected through microbore tubing to an open liquid collecting reservoir.

5.2.3. Dye intensity measurements

The color intensity change of dye in the observation chamber of the microfluidic characterization devices was recorded from the top using a SZ61 (0.7 - 4.5× zoom) Olympus stereomicroscope. Optical micrographs of the observation chamber were recorded at regular intervals under constant illumination conditions using a digital camera attached to the microscope and later analyzed using Adobe Photoshop to develop dye intensity profiles. Dye concentration standards were developed by pumping aqueous dye solutions of known concentration through the microfluidic characterization chip at 5 μL/min. The standards

were used to translate the dye intensity recorded in the observation chamber into release rate of dye.

5.3. Results and Discussion

The process begins with the fabrication of dye infused supraparticles using droplet templated dispensed on solid substrates (Fig. 5.1). Aqueous suspension droplets when dispensed on superhydrophobic substrates[26,32] assume near spherical shape due to the combined effect of high contact angle values and low Bond Number[33] ($B_o = \Delta\rho g r^2 / \gamma$) where $\Delta\rho$ is the density difference between droplet and surrounding fluid, g acceleration due to gravity, r droplet radius and γ is the interfacial tension. The initial particle volume fraction in the dye and latex suspension droplets is higher than 10% which dictates the final shape of the porous latex dried assemblies to be near spherical (inset Fig 5.1).[14] The free volume available for random thermal motion of the microparticle inside the droplets keeps reducing due to evaporation of the solvent, thus forcing the microspheres to self assemble into close packed structure. During the fabrication of dye infused latex supraparticle (DIL-Supraparticle), dye migrates towards the exposed part of the droplets with the evaporating solvent flux thus producing an enclosure layer (Fig. 5.1).

The droplet templates for the dye pellets (D-Pellet) were not easy to dispense due to low contact angle hysteresis of the silicon nanowire substrates. The problem of holding the droplets in place during drying was overcome by mixing magnetic nanoparticles in the suspensions and immobilizing the droplets using a rod-like magnet held under the

superhydrophobic substrates (Fig. 5.1). However, during the final stages of drying the droplet meniscus invaginates and final assembly acquires a dimple due to internal pinning.[14] The minimum size of the droplet that could be easily dispensed (> 2.0 μL) was the determining factor for the initial mass of dye present in the dye pellets. The initial concentration of dye also needed to be maintained above 5 wt% to avoid the formation of coffee ring[34] and fabricate near spherical pellets.[14] The amount of dye (drug simulant) present in the porous latex matrix and the dye pellet was kept constant (9×10^{-5} g) for comparative study of sustained release.

The fabricated particle assemblies (D-Pellet or DIL-Supraparticle) are introduced into the loading chamber of the microfluidic chip (Figure 5.2) for sustained release characterization. DI water is pumped from left to right to expose the supraparticle to a steady flow of liquid and observe the dye leaching phenomena. Two pillar stoppers in the loading chamber prevent the particle from reaching the channel neck and clogging it. The inlet fluid flow rate was maintained at 5 μL/min. The low flow rates allow enough time for the diffusive mixing in the channel network before the leached dye reaches the observation chamber thus preventing significant variations in dye intensity due to non-uniform velocity profile across the cross section of rectangular channel.

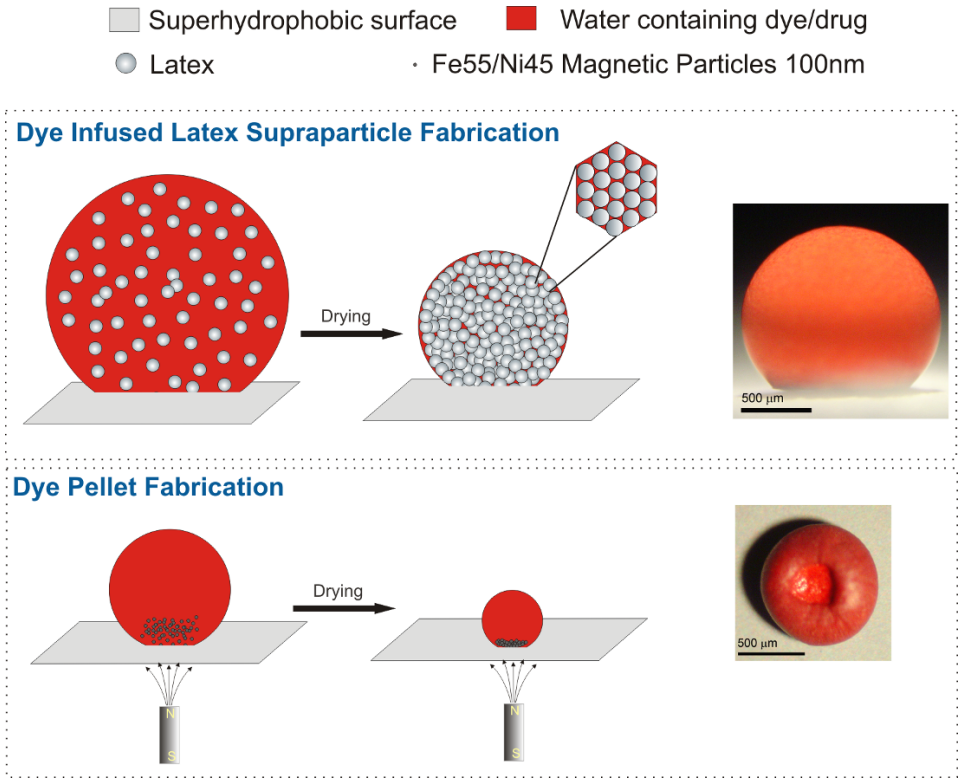

Figure 5.1. Schematics (not drawn to scale) of the formation process of DIL-Supraparticle and D-Pellet. The optical micrographs on the right show the side profile of D-Supraparticle and top profile of D-Pellet. All scale bars are 500 µm.

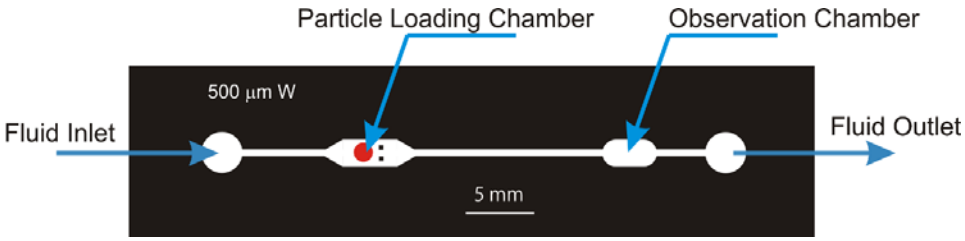

Figure 5.2. Schematic representation of soft lithography based microfluidic channel network employed to characterize the release rate of dye from porous microsphere network matrices.

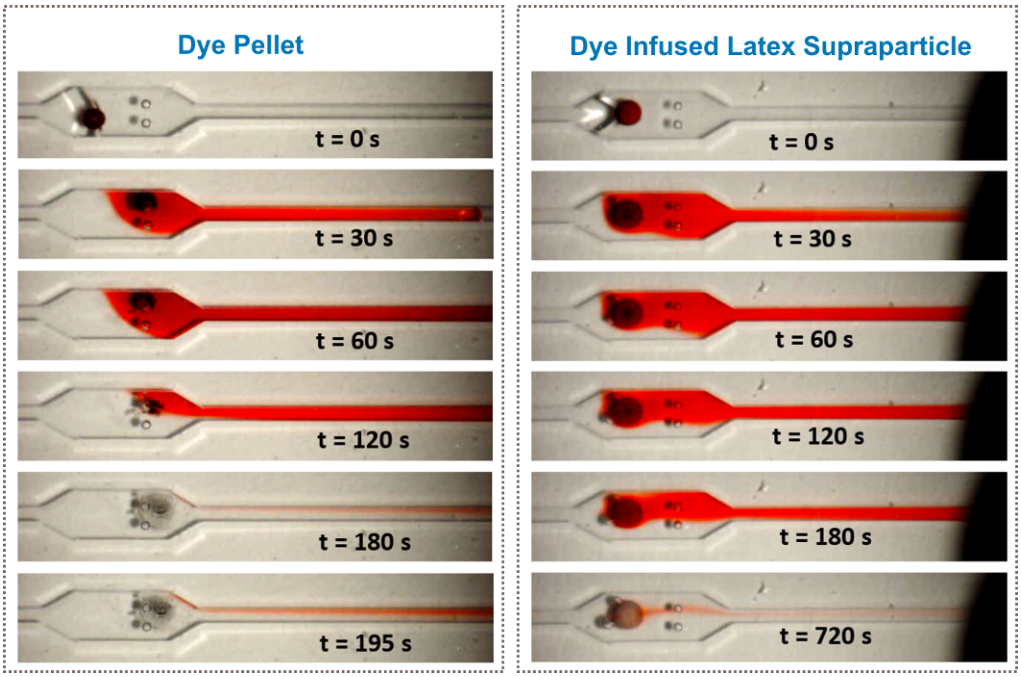

Figure 5.3. Snapshots of microfluidic network taken during the dye release characterization experiments. The first and second series shows the comparison of dye dissolution from the D-Pellet and DIL-Supraparticle respectively.

The comparison of movie snapshots of dye release inside the loading chamber, from D-Pellet and DIL-Supraparticle highlight the sustained release performance of porous microsphere support (Fig 5.3). The dye pellet starts dissolving quickly and reaches its peak intensity (60 s) and then decays until the magnetic nanoparticles core is exposed (120 s). The magnetic nanoparticles core then acts like a porous matrix and release the dye at a slower rate until all dye is dissolved (~180 s). In contrast the porous latex matrices take four times longer to release the same amount of dye under the same flow conditions. The release rate of dye from the supraparticle reaches its peak by ~60 s but decays at a sustained rate for

a longer time (~720 s). The resistance for slow release arises due to the need for the solvent to enter the pores of the latex microsphere matrix and then dissolve the dye.

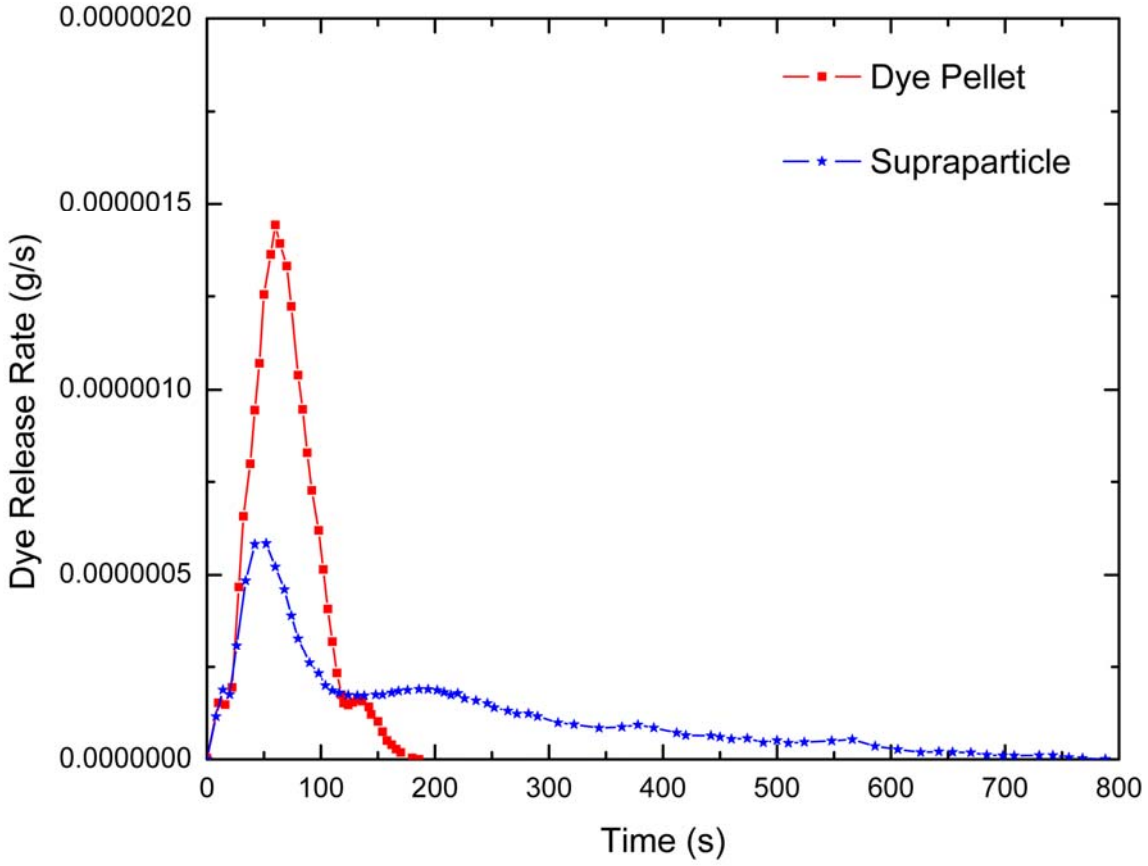

Figure 5.4. Release rate of dye measured for D-Pellet and DIL-Supraparticle in the novel microfluidic characterization system.

The dye intensity data for the D-Pellet and the DIL-Supraparticle at the observation chamber were recorded and compared with dye-concentration standards to quantify the amount of dye released (Fig. 5.4). The dye intensity for the D-Pellet rapidly reaches a peak

value and then decays at approximately the same speed. The initial rapid release before reaching the peak value can be explained as an artifact of lag time required for the hydration and subsequent dissolution of dye. The dye intensity profile for DIL-Supraparticle exhibits similar behavior, which explains the dissolution of dye covering layer formed during the fabrication. However the peak intensity value for the DIL-Supraparticle is three times lower. The porous supraparticle sustains the dye and releases it over an extended time interval as is evident from a long decay tail of the dye release curve (Fig. 5.4). The area under the curves for dye release rate of both D-Pellet and the DIL-Supraparticle match well within practical experimental limits, which verifies the complete leaching of dye mass, initially present in equal amounts. The experimental data were normalized so that the area under curves is equal to the initial amount of dye present in the D-Pellet and DIL-Supraparticle.

We investigated the pattern of dye release from porous latex matrices and the dye pellet based on diffusion and dissolution models available in literature.[30,31] Our assumptions for the model are that the particles are spherical, concentration of dye is uniform throughout the particle and diffusion coefficient of dye is concentration independent. We also assume that the system acts in a perfect sink condition wherein all the dye that is leached is instantly removed by the incoming flow of solvent. The calculations are done only for the concentration decay part of dye release profiles due to unavailability of complete information for the initial section of experimental curves.

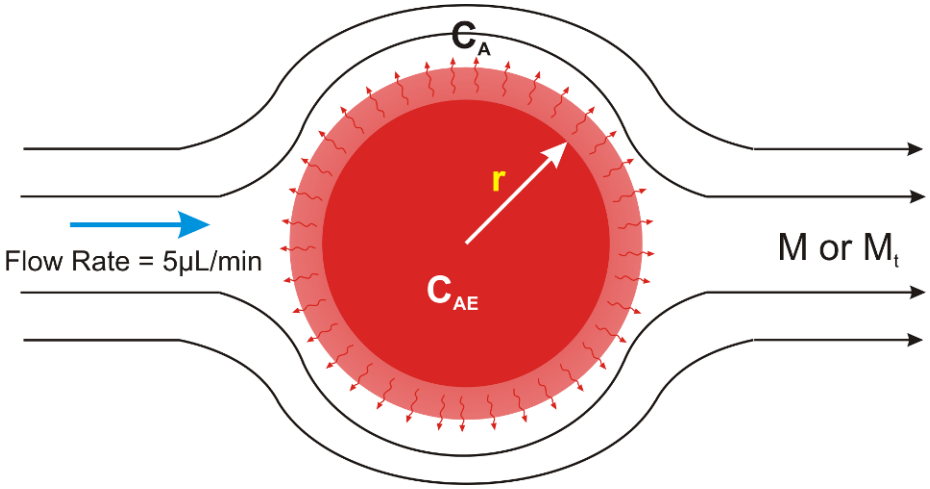

Figure 5.5. Schematics of the system parameters and streamline flow around the spherical particle inside the loading chamber.

Release Model for D-Pellet: The release of dye from the pellet in an aqueous environment can be modeled as unsteady-state convective mass transfer from the surface of a solid sphere in a laminar flow (Figure 5.5).[30] The diameter of the D-Pellet particle decreases with time. The mass balance on the D-Pellet follows a classical Noyes-Whitney equation[35]

$$\frac{dM}{dt} = 4\pi r^2 M_w k_{ls} (C_A - C_{A_E}) \qquad (5.1)$$

where M is the mass of 'dye pellet' at any time t, r is the radius at any time t, M_w is the molecular weight of dye (496.2 g/mol)[36], k_{ls} is the mass transfer coefficient, C_A is the concentration of dye at any time t and C_{A_E} = 22 wt% is the saturation concentration[36] of

dye. To estimate the mass transfer coefficient for liquids and a Reynolds number range of 2 – 2000 the following expressions can be used[30]

$$N_{Sh} = 2 + 0.95 N_{\mathrm{Re}}^{0.5} N_{Sc}^{1/3} \tag{5.2}$$

Sherwood Number $$N_{Sh} = \frac{k_{ls} D_p}{D_{AB}} \tag{5.3}$$

Schmidt Number $$N_{Sc} = \frac{\mu}{\rho_l D_{AB}} \tag{5.4}$$

Reynolds Number $$N_{\mathrm{Re}} = \frac{D_p v \rho_l}{\mu} \tag{5.5}$$

where D_p = initial particle diameter (0.02616 cm), D_{AB} is the binary diffusion coefficient of dye in water, μ is viscosity of the media surrounding the sphere, assumed to be the same as water (0.001 Pa-s), ρ_l is density of the water = 1000 kg/m^3, v is flow velocity of water. C_A can be assumed to be zero since all dye that is released from the pellet is swept away by liquid flow. Hence, the dye release rate can be expressed as

$$\dot{M} = \frac{dM}{dt} = -4\pi r^2 M_w k_{ls} C_{A_E} \tag{5.6}$$

The values of dye release rate estimated from the model correlate well with our experimental results except for the final stages where the dye pellet seems to behave as sustained release carrier (Fig. 5.6). We expect such behavior is due to the presence of magnetic nanoparticles core which acts as porous support and slows the release of dye in

controlled fashion much alike porous latex supraparticle. The value of diffusion coefficient of dye which fits the experimental data is 1.44×10^{-5} cm^2/s.

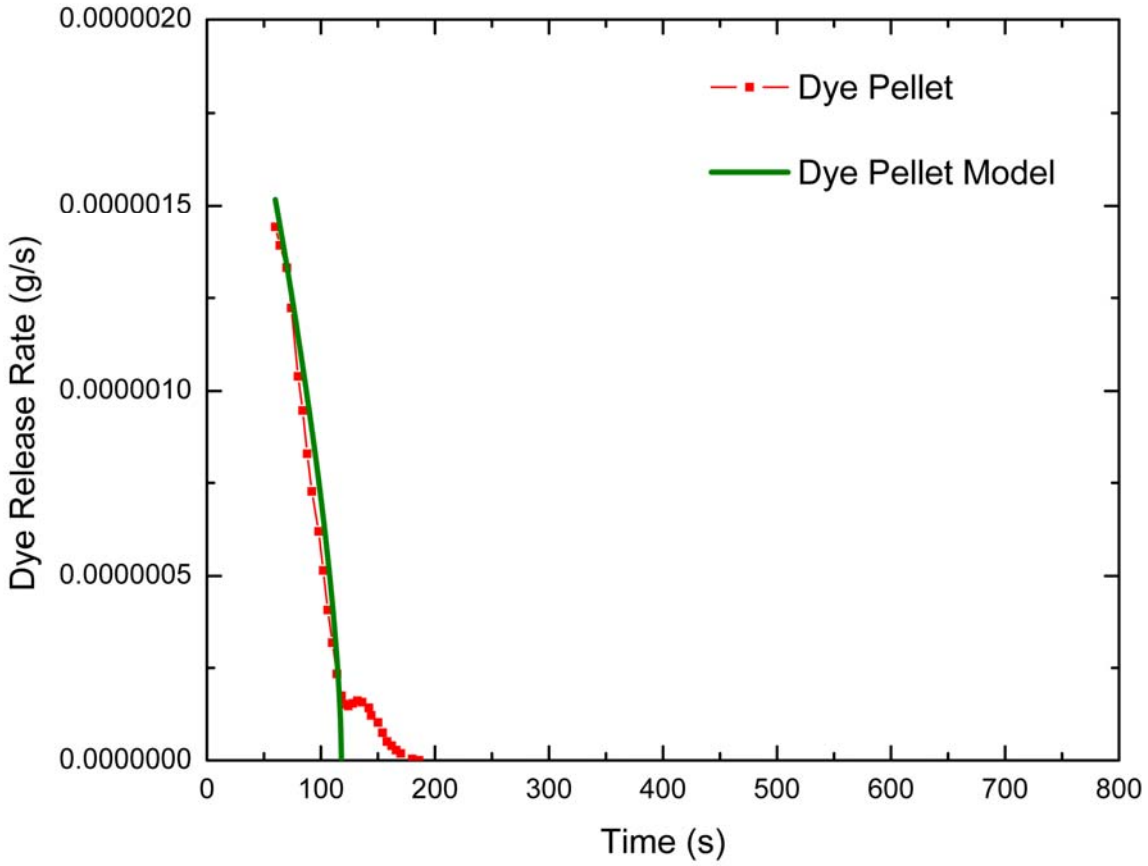

Figure 5.6. Comparison between dye release rates from dye pellet and the predictions of theoretical model.

Release Model for DIL-Supraparticle: The release of dye from the latex supraparticle matrix can be estimated using the theoretical model proposed by Peppas et al.[31] The model takes into account the role of both diffusion and the dissolution process of dye in the kinetics of release from porous non-swellable polymeric microsphere system. Transient Fickian diffusion equation is combined with a linear first order dissolution term. The solution of the equation provides the following expression for the estimation of total amount of dye released from the porous supraparticle at any time t

$$M_t = 8\pi R^3 \varepsilon C_{A_E} \sum_{n=1}^{\infty} \frac{(D_i + n^2\pi^2) D_i \tau + n^2\pi^2 \{1 - \exp[-(D_i + n^2\pi^2)\tau]\}}{(D_i + n^2\pi^2)^2} \tag{5.7}$$

$$\tau = D'_{AB} t / R^2 \tag{5.8}$$

$$D_i = KR^2 / D'_{AB} \tag{5.9}$$

where M_t is the total mass of dye release by time t, R is the radius of supraparticle, ε is the porosity (0.252 for hexagonal closed packing of microspheres), τ is the dimensionless time, K is the first order dissolution constant, D_i is a dimensionless number analogous to Damköhler Number representing the ratio of dissolution/diffusion contribution. D'_{AB} is the effective diffusion coefficient which is related to the dye diffusion coefficient and the tortuosity δ of the pores of latex microsphere matrix as

$$D'_{AB} = D_{AB} / \delta \tag{5.10}$$

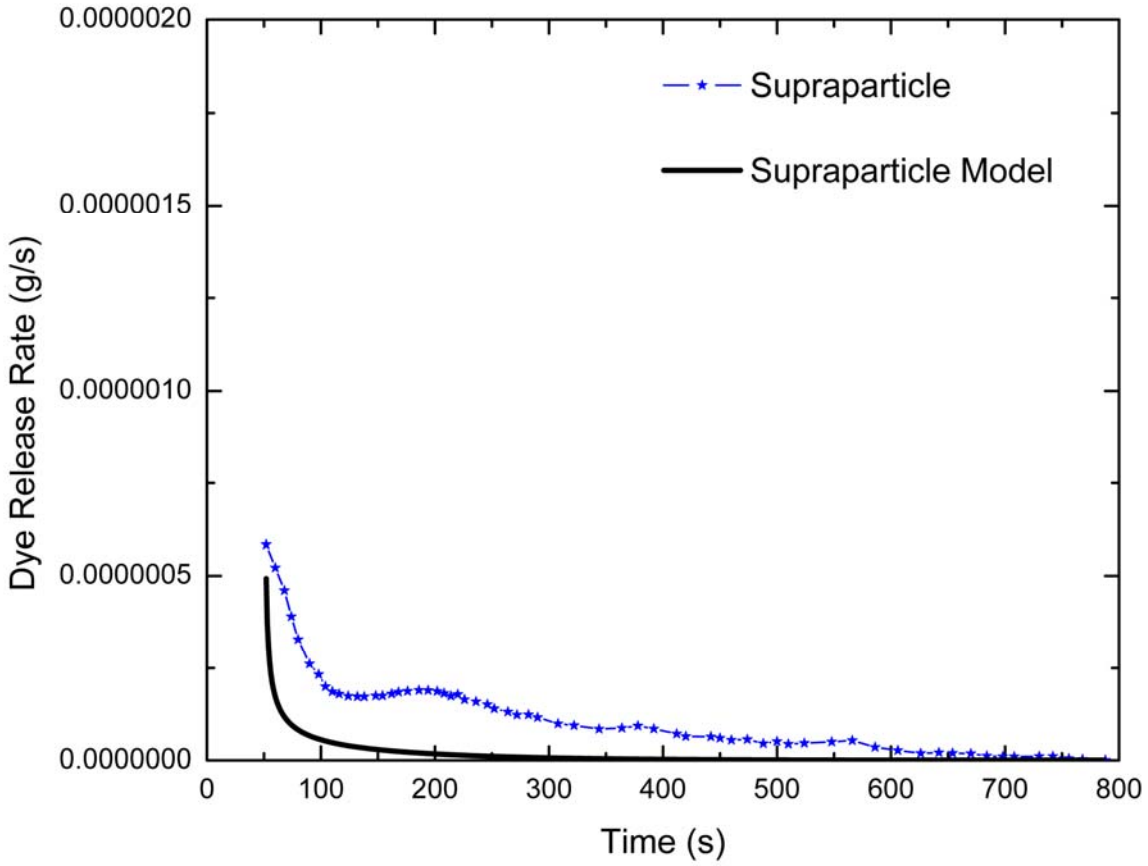

Figure 5.7. Comparison between dye release rates from DIL-Supraparticle and the predictions of the model.

For all practical purposes the tortuosity (δ) can be approximated as 3. The peak value of the dye release rate calculated from the mass transfer model matches well with the experimental data (Fig. 5.7). However, the diffusion model for supraparticle underevaluates the rate of release of dye as is evident from significant difference in the area under the experimental and theoretical curves. The limitation of the model with regards to our microfluidic chip system is that it treats the release from the particle in a static solvent environment. However, our system exposes the supraparticle to laminar flow where the solvent is entering the pores of the matrix and dissolving the dye at higher rate than predicted by theory. Our hypothesis is that there is a need to account for the effect of hydrodynamic flow on the particles, which might explain the rapid dissolution of dye. We aim to develop a generalized mass transfer model to explain and quantify the effect of fluid dynamics on the release of material from porous support.

5.4. Conclusions

We present a novel microfluidic based method for the characterization of sustained release of soluble material from porous supraparticle assemblies. The method overcomes the need for bulk laboratory setup and at the same time minimizes the amount of reagents used in the drug development process. The experimental results demonstrate the utility of porous microsphere matrices as drug delivery carriers. Our technique has potential for inexpensive simultaneous characterization of multiple drug loaded particles under well defined

experimental conditions. The design of our microfluidic chip can be easily modified to incorporate more than one particle and scrutinize their release performance.

We have characterized the release pattern of dye based on diffusion and dissolution models available in the literature. The dye pellet dissolution data correlate well with model calculations with the exception of sustained release behavior of magnetic nanoparticles core. However, the model for dye release from polymer matrices is not capable of completely describing the release rates of the latex supraparticles. Our next step will be to study the fluid dynamics around the supraparticle and incorporate the effect of hydrodynamic flow into the existing theoretical model which potentially is able to account for faster release of dye.

5.5. Acknowledgements

This research was supported by Unilever Research & Development, Netherlands. We gratefully acknowledge Prof. Antonio A. Garcia (ASU) for providing us with the superhydrophobic substrates, Ahmet Burak Uçar for assistance in the design and fabrication of microfluidic channel masters. We also thank Nathaniel A. Cain for the fruitful discussion on theoretical modeling of dye release.

5.6. References

1. B. Coldren, C. Boyer, E. T. Kisak, C. A. Evans, J. A. Zasadzinski. The Vesosome - A Multicompartment Drug Delivery Vehicle. *Current Medicinal Chemistry*, (2004), **11** (2), 199-219.

2. A. Jahn, J. Reiner, W. Vreeland, D. DeVoe, L. Locascio, M. Gaitan. Preparation of nanoparticles by continuous-flow microfluidics. *Journal of Nanoparticle Research*, (2008), **10** (6), 925-934.

3. A. Jahn, W. N. Vreeland, D. L. DeVoe, L. E. Locascio, M. Gaitan. Microfluidic Directed Formation of Liposomes of Controlled Size. *Langmuir*, (2007), **23** (11), 6289-6293.

4. J. A. Zasadzinski. Novel approaches to lipid based drug delivery. *Current Opinion in Solid State and Materials Science*, (1997), **2** (3), 345-349.

5. E. C. Unger, T. Porter, W. Culp, R. Labell, T. Matsunaga, R. Zutshi. Therapeutic applications of lipid-coated microbubbles. *Advanced Drug Delivery Reviews*, (2004), **56** (9), 1291-1314.

6. E. Talu, M. M. Lozano, R. L. Powell, P. A. Dayton, M. L. Longo. Long-Term Stability by Lipid Coating Monodisperse Microbubbles Formed by a Flow-Focusing Device. *Langmuir*, (2006), **22** (23), 9487-9490.

7. K. Pancholi, E. Stride, M. Edirisinghe. Dynamics of bubble formation in highly viscous liquids. *Langmuir*, (2008), **24** (8), 4388-4393.

8. J. Williams, R. Lansdown, R. Sweitzer, M. Romanowski, R. LaBell, R. Ramaswami, E. Unger. Nanoparticle drug delivery system for intravenous delivery of topoisomerase inhibitors. *Journal of Controlled Release*, (2003), **91** (1-2), 167-172.

9. S. Gelperina, K. Kisich, M. D. Iseman, L. Heifets. The Potential Advantages of Nanoparticle Drug Delivery Systems in Chemotherapy of Tuberculosis. *Am. J. Respir. Crit. Care Med.*, (2005), **172** (12), 1487-1490.

10. N. Tsapis, D. Bennett, B. Jackson, D. A. Weitz, D. A. Edwards. Trojan particles: Large porous carriers of nanoparticles for drug delivery. *Proceedings of the National Academy of Sciences of the United States of America*, (2002), **99** (19), 12001-12005.

11. P. Shah. Use of nanotechnologies for drug delivery. *MRS Bulletin*, (2006), **31** (11), 894-899.

12. M. E. Davis, Z. Chen, D. M. Shin. Nanoparticle therapeutics: an emerging treatment modality for cancer. *Nature Reviews Drug Discovery*, (2008), **7** (9), 771-782.

13. D. A. Edwards, J. Hanes, G. Caponetti, J. Hrkach, A. Ben-Jebria, M. L. Eskew, J. Mintzes, D. Deaver, N. Lotan, R. Langer. Large Porous Particles for Pulmonary Drug Delivery. *Science*, (1997), **276** (5320), 1868-1872.

14. V. Rastogi, A. García, A., M. Marquez, O. Velev, D. Anisotropic Particle Synthesis Inside Droplet Templates on Superhydrophobic Surfaces. *Macromolecular Rapid Communications*, (2009), DOI: 10.1002/marc.200900587.

15. A. D. Dinsmore, M. F. Hsu, M. G. Nikolaides, M. Marquez, A. R. Bausch, D. A. Weitz. Colloidosomes: Selectively permeable capsules composed of colloidal particles. *Science*, (2002), **298** (5595), 1006-1009.

16. S. M. Klein, V. N. Manoharan, D. J. Pine, F. F. Lange. Synthesis of spherical polymer and titania photonic crystallites. *Langmuir*, (2005), **21** (15), 6669-6674.

17. S. Melle, M. Lask, G. G. Fuller. Pickering emulsions with controllable stability. *Langmuir*, (2005), **21** (6), 2158-2162.

18. O. D. Velev, K. Furusawa, K. Nagayama. Assembly of latex particles by using emulsion droplets as templates .1. Microstructured hollow spheres. *Langmuir*, (1996), **12** (10), 2374-2384.

19. O. D. Velev, K. Furusawa, K. Nagayama. Assembly of latex particles by using emulsion droplets as templates .2. Ball-like and composite aggregates. *Langmuir*, (1996), **12** (10), 2385-2391.

20. O. D. Velev, A. M. Lenhoff, E. W. Kaler. A class of microstructured particles through colloidal crystallization. *Science*, (2000), **287** (5461), 2240-2243.

21. O. D. Velev, K. Nagayama. Assembly of latex particles by using emulsion droplets .3. Reverse (water in oil) system. *Langmuir*, (1997), **13** (6), 1856-1859.

22. S. H. Kim, S. Y. Lee, G. R. Yi, D. J. Pine, S. M. Yang. Microwave-assisted self-organization of colloidal particles in confining aqueous droplets. *Journal of the American Chemical Society*, (2006), **128** (33), 10897-10904.

23. D. M. Kuncicky, K. Bose, K. D. Costa, O. D. Velev. Sessile droplet templating of miniature porous hemispheres from colloid crystals. *Chemistry of Materials*, (2007), **19** (2), 141-143.

24. D. M. Kuncicky, O. D. Velev. Surface-guided templating of particle assemblies inside drying sessile droplets. *Langmuir*, (2008), **24** (4), 1371-1380.

25. J. Park, J. Moon, H. Shin, D. Wang, M. Park. Direct-write fabrication of colloidal photonic crystal microarrays by ink-jet printing. *Journal of Colloid and Interface Science*, (2006), **298** (2), 713-719.

26. V. Rastogi, S. Melle, O. G. Calderón, A. A. García, M. Marquez, O. D. Velev. Synthesis of Light-Diffracting Assemblies from Microspheres and Nanoparticles in Droplets on a Superhydrophobic Surface. *Advanced Materials*, (2008), **20** (22), 4263-4268.

27. N. Neamati, J. J. Barchi. New Paradigms in Drug Design and Discovery. *Current Topics in Medicinal Chemistry*, (2002), **2** (3), 211.

28. K. Pancholi, E. Stride, M. Edirisinghe. In Vitro Method to Characterize Diffusion of Dye from Polymeric Particles: A Model for Drug Release. *Langmuir*, (2009), **25** (17), 10007-10013.

29. P. S. Dittrich, A. Manz. Lab-on-a-chip: microfluidics in drug discovery. *Nat Rev Drug Discov*, (2006), **5** (3), 210-218.

30. C. J. Geankoplis, *Transport Processes and Unit Operations*. (Prentice-Hall PTR, Upper Saddle River, NJ, ed. 3, 1993), pp. 444-449.

31. R. S. Harland, C. Dubernet, J. P. Benoit, N. A. Peppas. A Model of Dissolution-controlled, Diffusional Drug Release from Non-swellable Polymeric Microspheres. *Journal of Controlled Release*, (1988), **7** (3), 207-215.

32. A. Egatz-Gómez, J. Schneider, P. Aella, D. Yang, P. Domínguez-García, S. Lindsay, S. T. Picraux, M. A. Rubio, S. Melle, M. Marquez, A. A. García. Silicon nanowire and polyethylene superhydrophobic surfaces for discrete magnetic microfluidics. *Applied Surface Science*, (2007), **254** (1), 330-334.

33. H. M. Princen, in *Surface and Colloid Science,* E. Matijevic, Ed. (Wiley, New York, 1969), vol. 2, pp. 1-84.

34. R. D. Deegan, O. Bakajin, T. F. Dupont, G. Huber, S. R. Nagel, T. A. Witten. Capillary flow as the cause of ring stains from dried liquid drops. *Nature*, (1997), **389** (6653), 827-829.

35. A. A. Noyes, W. R. Whitney. The Rate of Solution of Solid Substances in their own Solutions. *Journal of the American Chemical Society*, (1897), **19** (12), 930-934.

36. J. Smith, *Food additive user's handbook*. (1991).

Chapter 6.

Summary and Outlook

6.1 Summary

The aim of my thesis research has been to perform laboratory operations inside microliter size droplets and exploit them as addressable sites for the development of bioassays or for the synthesis of materials with novel photonic and anisotropic properties. Execution of procedures inside droplets allowed us to overcome the challenges incurred in conventional channel based microfluidic techniques.

During the first project we developed and simultaneously performed bioassays in microliter-sized droplets freely suspended on the surface of high density fluorinated oil and immobilized using a dielectrophoretic chip. These assays enabled optical detection of various analytes based on particle microseparations inside evaporating container droplets. We developed and characterized the bioassays based on their 'limit of detection (LOD)', 'results read-out time' and 'sample volume'. The droplet bioassays were also constructed with latex and ricin simulants immobilized onto the surface of gold nanoparticles and their performance was compared with hand held assays (HHA) obtained from United States Department of Defense (DOD). The droplet microbioassays were found to be 10 times better in terms of lower LOD and 100 times more efficient in terms of 'sample volume'. A kinetic agglutination model was developed for the system based on incubation time and analyte concentration. The results for correlation between theory and experimental outcomes allow generalization of the model to almost any droplet-particle assembly process. This research can also be extended for the fabrication of point-of-care microfluidic device where nanoliter volumes of multiple samples can be injected and results are read out directly.

The second project was focused on the formation of meniscus-directed three-dimensional assemblies of micro and nanoscale particles inside droplet templates dispensed on solid surfaces. We used drying sessile droplets, which assume spherical shape when dispensed on superhydrophobic substrates, as templates for assembling latex microspheres and gold nanoparticles into close packed structures due to restricted free volume. Since the hierarchical structures are ready to use after drying of droplets, this novel method of fabrication has been termed dry self assembly (DSA). Spherical opals of 1 – 2 mm in size could be easily produced within an hour in large quantities by this very simple and efficient process. Upon illumination with collimated light, the dried spherical supraparticles display discrete colored ring diffraction patterns created by the periodic arrangement of latex particles in the surface layer. The physical origin of the colored patterns was investigated and the relationship between the size of colored rings generated by incident light, corresponding wavelength and nanoparticle diameter was established. A series of systematic experiments were conducted to conclude that ring size decreases as the latex particle diameter in the opals increases. This trend was quantified using Bragg's law of diffraction.

In the next stage we explored, understood and explained the application of DSA in producing various types of anisotropies (composition and shape) in the supraparticles. Variation in system parameters including microsphere type, initial particle volume fractions and controlled pinning of the droplet templates allowed synthesis of nanoparticle assemblies of more complex shape and composition. Shape anisotropy is demonstrated by fabricating doughnut assemblies, whereas composition anisotropy is demonstrated by constructing

patchy (mono, bi-, tri-) magnetic supraparticles. These supraparticles have a unique feature of well defined pores wherein drug/materials can be entrained for sustained release. This research will allow the development of micro-scale drug (or any substance which can be contained in the particle matrix) carriers which can be remotely manipulated using magnetic fields.

The final stage of this thesis dissertation research comprised of the development of microfluidic channel based procedure to analyze and evaluate the release rate of materials from dye infused latex matrices fabricated using DSA and colloidal nutrient carriers. The research involved design and fabrication of microchannel networks using soft lithography techniques for analyzing the physical effects taking place in colloidal suspensions. We also established the potential of the novel microchip based evaluation procedure to perform real time observations and characterize the dye (drug simulant) release rate from supraparticles.

6.2 Outlook

The applicability of my graduate research is inherent in the versatility of microdroplets, which serve as individually addressable sites to perform biodetection and materials synthesis operations. Our droplet system introduces the discrete element in biodetection methods wherein multiple samples can be compartmentalized and simultaneously processed. The physical parameters of the droplet containers such as volume, shape and concentrations can be precisely defined for system optimization. The sessile spherical droplets on superhydrophobic surfaces can function as lenses for focusing the

incident probe light beams which may find application in the development of inexpensive high sensitivity point of care devices for third world countries. The dry self assembly method can be employed in large scale fabrication of anisotropic assemblies with unique optical and magnetic properties. Microdroplet engineering showcases its potential for generating soft matter with unique properties.